INFORMATION TO USERS

This manuscript has been reproduced from the microfilm master. UMI films the text directly from the original or copy submitted. Thus, some thesis and dissertation copies are in typewriter face, while others may be from any type of computer printer.

The quality of this reproduction is dependent upon the quality of the copy submitted. Broken or indistinct print, colored or poor quality illustrations and photographs, print bleedthrough, substandard margins, and improper alignment can adversely affect reproduction.

In the unlikely event that the author did not send UMI a complete manuscript and there are missing pages, these will be noted. Also, if unauthorized copyright material had to be removed, a note will indicate the deletion.

Oversize materials (e.g., maps, drawings, charts) are reproduced by sectioning the original, beginning at the upper left-hand corner and continuing from left to right in equal sections with small overlaps.

Photographs included in the original manuscript have been reproduced xerographically in this copy. Higher quality 6" x 9" black and white photographic prints are available for any photographs or illustrations appearing in this copy for an additional charge. Contact UMI directly to order.

Bell & Howell Information and Learning
300 North Zeeb Road, Ann Arbor, MI 48106-1346 USA
800-521-0600

UMI®

DISSERTATION

SOLVENT MOTION NEAR PHOSPHOLIPID INTERFACES

Submitted by

Dale M. Willard

Department of Chemistry

In partial fulfillment of the requirements

for the Degree of Doctor of Philosophy

Colorado State University

Fort Collins, Colorado

Summer, 2000

Bell & Howell Information and Learning Company
300 North Zeeb Road
P.O. Box 1346
Ann Arbor, MI 48106-1346

COLORADO STATE UNIVERSITY

November 22, 1999

WE HEREBY RECOMMEND THAT THE DISSERTATION PREPARED UNDER OUR SUPERVISION BY DALE M. WILLARD ENTITLED "SOLVENT MOTION NEAR PHOSPHOLIPID INTERFACES" BE ACCEPTED AS FULFILLING IN PART REQUIREMENTS FOR THE DEGREE OF DOCTOR OF PHILOSOPHY.

Committee on Graduate Work

Adviser

Department Head/Director

ABSTRACT OF DISSERTATION

SOLVENT MOTION NEAR PHOSPHOLIPID INTERFACES

The solvation dynamics near lipid/water interfaces has been determined via ultrafast time-resolved emission spectra (TRES). The lipid interfaces consisted of reverse micelles or vesicles formed with phosphatidylcholine (lecithin). These measurements represent the first determination of solvent motion on a subpicosecond timescale at a lipid interface. Because free water relaxes on a subpicosecond timescale, these measurements provide the most complete picture to date of the solvent motion at a lipid interface.

Using the fluorescent probe Coumarin 343 (C343), solvation dynamics within the aqueous interior of cyclohexane/lecithin/water reverse micelles was measured as a function of hydration. Small additions of water to these reverse micelles produce a viscous gel, otherwise known as organogels or "living polymers". A single relaxation component is observed at the $w = 4.8$ hydration level with a response time much longer than the response of free water. At hydration levels of $w \geq 5.8$, three relaxation times are observed indicating the existence of three water types that change in response to increasing hydration.

To probe other lipid interfaces, a fluorescently-labled lipid (CLPE) was synthesized by covalently attaching C343 to the phosphatidylethanolamine (PE) headgroup. CLPE proved to be a viable solvation dynamics probe, reproducing the

dynamics that were previously observed with C343 in $w = 6.4$ cyclohexane/lecithin/water reverse micelles.

Solvent motion within the aqueous interior of reverse micelles as a function of micelle morphology is also investigated. Spherical reverse micelles formed in benzene are compared to worm-like reverse micelles formed in cyclohexane at the same hydration level. The results demonstrate that the spherical reverse micelles display significantly faster relaxation. It is proposed that spherical reverse micelles allow for the formation of a defined water core that is a prerequisite for free-water type relaxation.

Finally, the solvation dynamics at a vesicle interface is determined with and without 33 mol% cholesterol present. Surprisingly, the dynamics measured at a vesicle interface are very similar to the dynamics measured within $w = 6.4$ cyclohexane/lecithin/water reverse micelles. Cholesterol shows little influence on the types of relaxation at the interface, but does reduce the overall solvent response indicating cholesterol tightens the interface.

Dale M. Willard
Chemistry Department
Colorado State University
Fort Collins, CO 80523
Summer, 2000

"In daylights – In sunsets,
In midnights – In cups of coffee,
In inches – In miles,
In laughter – In strife.

In five hundred twenty-five thousand six hundred minutes,
How do you measure a year in the life?

How about love?
Measure in love."

-Seasons of Love
From the musical, "Rent"

ACKNOWLEDGEMENTS

A single person does not accomplish an achievement such as an advanced degree. In reality, a community accomplishes it. This is because a wise individual does not need to be the brightest mind to achieve success. The individual just needs to surround himself/herself with great minds. To all of you I owe this dissertation. It has been a difficult road to my Ph. D. but the troubles have allowed me to see how blessed I am to have such supportive and concerned family and friends.

I wish to start by thanking my mother and father. Your care has, in large part, made me the person I am today. Your love and support is eternal and I will always be grateful.

Thanks to my siblings: Laurie, Larry, and Dan. I love you dearly. A special thanks needs to be offered to Larry and Lori. You opened your doors to me, figuratively and literally, when I first moved to Colorado. Those doors have remained opened ever since. On several occasions, your love and support kept me plugging away when I needed it most. I have found that there is nothing like a beer and football with my brother to cure the blues.

Thank you Valerie for taking care of me as I put this dissertation together. What better motivation for finishing my dissertation could be offered than a trip to Italy? I will always cherish the love and support you have offered me. You have taught me more about life than I ever could have learned in graduate school. Thank you.

I have to mention the high school buddies: Dave, Greg, John, Loyd, and Tor. You boys really didn't do a damn thing for this dissertation, but I still love you guys anyway. I hope we always stay in contact.

I will end with many thanks to my graduate school cohorts (in no particular order): Brad Luther, Dr. Ruth Riter, Dr. Tom Wynn, Charlie Patrissi, Dr. Neil Mackie, Dr. Pat McCurdy, Lori Wernersbauch, Dr. Kristina Gansle, Paul Gansle, Carmen Butoi, Joe Bullock, Dr. Jeffrey Kahl, and Erik Kuester. You have all taught me the chemistry I know in addition to being great friends. Special thanks goes to Ruth and Tom. Ruth taught me how to be a graduate student while Tom taught me, a physical chemist, how to do synthetic chemistry.

Finally, I need to thank the person to whom I directly owe this dissertation, my advisor, Prof. Nancy E. Levinger. Even in difficult times, you never doubted my abilities as a chemist. Your cheerleading kept me focused when I carried doubts. Together we have solved the mysteries of reverse micelle dynamics. The world may never be the same.

TABLE OF CONTENTS

LIST OF TABLES

LIST OF FIGURES

Chapter 1

Introduction to Solvation Dynamics at Lecithin Interfaces

Welcome to the world of lipid membrane chemistry. Unlock your mind and come along for a journey. You may laugh and you may cry, but you will be surprised at the fascinating chemistry about to be presented. The following chapter introduces the fundamental themes, techniques, and experimental apparatus that unify the subsequent chapters.

1.I. Lecithin Interfaces

Most of the fundamental biochemical functions in cells involve membranes at some point[1]. Cellular tasks performed by membranes include providing the barrier that encloses cellular compartments, actively passing ions or molecules inside and out of compartments, transmitting information through conformational changes induced in membrane components, housing enzymes that catalyze transmembrane reactions, and providing a substrate for membrane-bound reactions. Essentially, membranes consist of lipid bilayers composed of two oppositely aligned phospholipid layers with polar head groups facing towards the polar exterior/interior and nonpolar lipid chains facing inward toward the opposite layer. Living membranes are very complex, composed of various

lipid types and lipid solvated sterols and proteins. Lipids generally add structure while proteins are largely responsible for function. The structural and dynamical properties of membranes are fundamentally linked to the function of the membrane proteins, and hence the overall function of the membrane.

In order to understand the role of lipids in living membranes, researchers typically find that simplified membranes are more easily interrogated. Model membranes consisting of simple one-component or few-component phospholipid aggregates have played a seminal role in the study of membranes[2]. Such a simplistic approach is deemed absolutely necessary in order to take full advantage of modern physical experimental techniques including, magnetic resonance spectroscopy (NMR and ESR), differential-scanning calorimetry, micromechanics, scattering, and diffraction techniques[2]. Figure 1.1 displays the structures of the most commonly used phospholipids. These lipid molecules vary in many ways, for example, the nature of the polar headgroup, the number of and degree of saturation in the hydrophobic tails, the rigidity of the entire or parts of the molecule, to name a few. One of the major differences that is important for the research reported here is the nature of the polar headgroup. The headgroup is generally either zwitterionic, as is the case for, phosphatidylcholine (PC) and phosphatidylethanolamine (PE), or anionic, such as phosphatidylserine (PS).

One of the most important features of lipid molecules found in membranes is their amphiphilicity. These lipid molecules possess well-defined and separated hydrophobic tails and hydrophilic headgroups. This allows the molecules to aggregate and delineate polar and nonpolar regions thereby defining boundaries. When lipids are dispersed in

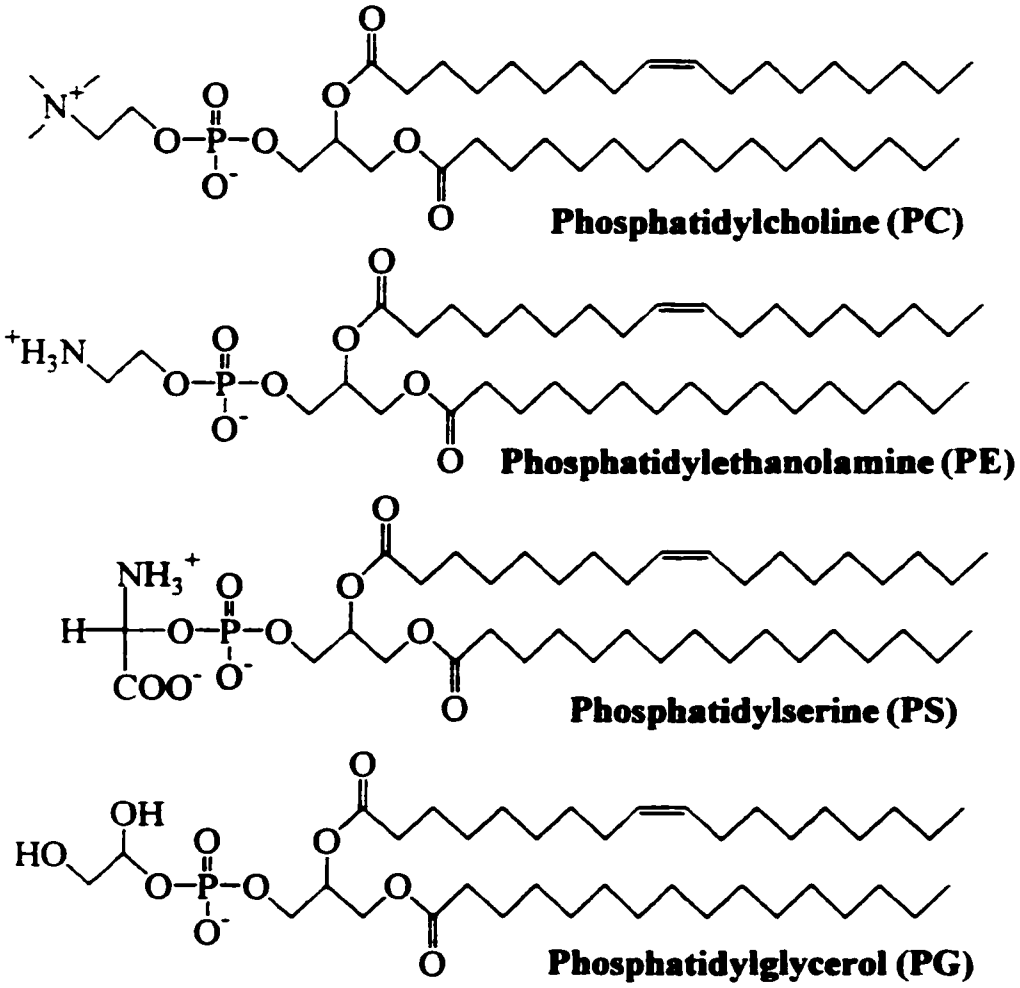

Figure 1.1. Chemical structures of common phospholipids. Although not shown, alkyl chain lengths and degree of unsaturation also vary among phospholipids. Phosphatidylcholine is the most common component of natural membranes.

different solvents, various phases are possible. Some examples of the possible phases include reverse micelles, normal micelles, hexagonal inverted phases, cubic continuous phases, lamellar phases as well as vesicles or liposomes[3]. While some of these phases may seem quite artificial, they are hypothesized to be important in membrane processes such as membrane fusion[4]. In addition to serving as membrane models, lipid aggregates are important to various other applications including, vessels for drug delivery[5], stabilizing biological or organic reactants in synthetic chemistry[6], and as size-controlling microreactors to form solid nanoparticles.

Phospholipids will form different structural phases within a given morphological structure. At different temperatures, membranes can exist in different phases, with each phase showing different order and alkyl chain fluidity[7]. At biological temperatures, the most commonly observed phase transition is the gel to liquid-crystal transition. The gel-state represents a relatively tightly ordered state while the liquid-crystal state is found at higher temperatures with individual molecules possessing higher freedom of movement. The liquid-crystalline state is the more biologically relevant phase and is the only state our research has investigated. Various factors determine a particular membrane's phase transition temperature. Different phospholipids show different transition temperatures. Unsaturation in phospholipid alkyl chains tends to lower the transition temperature. In addition, lipid membrane solutes, such as cholesterol, also affect the transition temperature.

One of the most common lipid sources for model membrane preparation, and the source used for all studies in this text, is lecithin. Lecithin is commercially available (Avanti Polar Lipids & Sigma Aldrich) as a purified product from a variety of biological

sources, such as egg yolk, heart, brain, soybean, etc. Compositions of the lecithin depend on the source. Egg lecithin, the lipid used for the studies reported here, is not a single compound, but contains a mixture of phosphatidylcholines consisting of about 31% saturated fatty acid having a chain length of 16 carbons, 16% saturated fatty acid with 18 carbons, about 48% also with 18 carbons but having at least 1-2 points of unsaturation, and the rest a variety of other fatty acid constituents[8]. Lecithin forms a variety of morphological structures depending on the environment. We have explored three of them: wormlike reverse micelles, spherical reverse micelles, and vesicles (see Figure 1.2). Because we are primarily interested in headgroup/water interactions, we make comparisons to other studies using phosphatidylcholines but not necessarily egg lecithin.

Much is known about the structure of water in the proximity of amphiphiles and their aggregates[9]. Water in these structures is quite different from bulk water. For example, the interaction between neighboring water molecules is less than half that in the bulk, the density of the water is about twice the bulk density, and dielectric relaxation measurements show that the viscosity of bound water is 3 times greater than bulk[9]. Because the lipid-water interaction is so strong and ubiquitous, it affects the structural, dynamic and thermodynamic properties of the interface. A comparison of the solvent motions that are most important for solvation dynamics, rotation and translation, show that motion of interfacial water moves more slowly than the bulk water by at least 1.2 times, and sometimes as much as 4 times[9]. Interfacial water often reveals significant reduction in hydrogen bonding through the display of free OH motions[10]. In addition, and perhaps somewhat surprisingly, the same interfaces also reveal increased amounts of "ice-like" water at the surface[10].

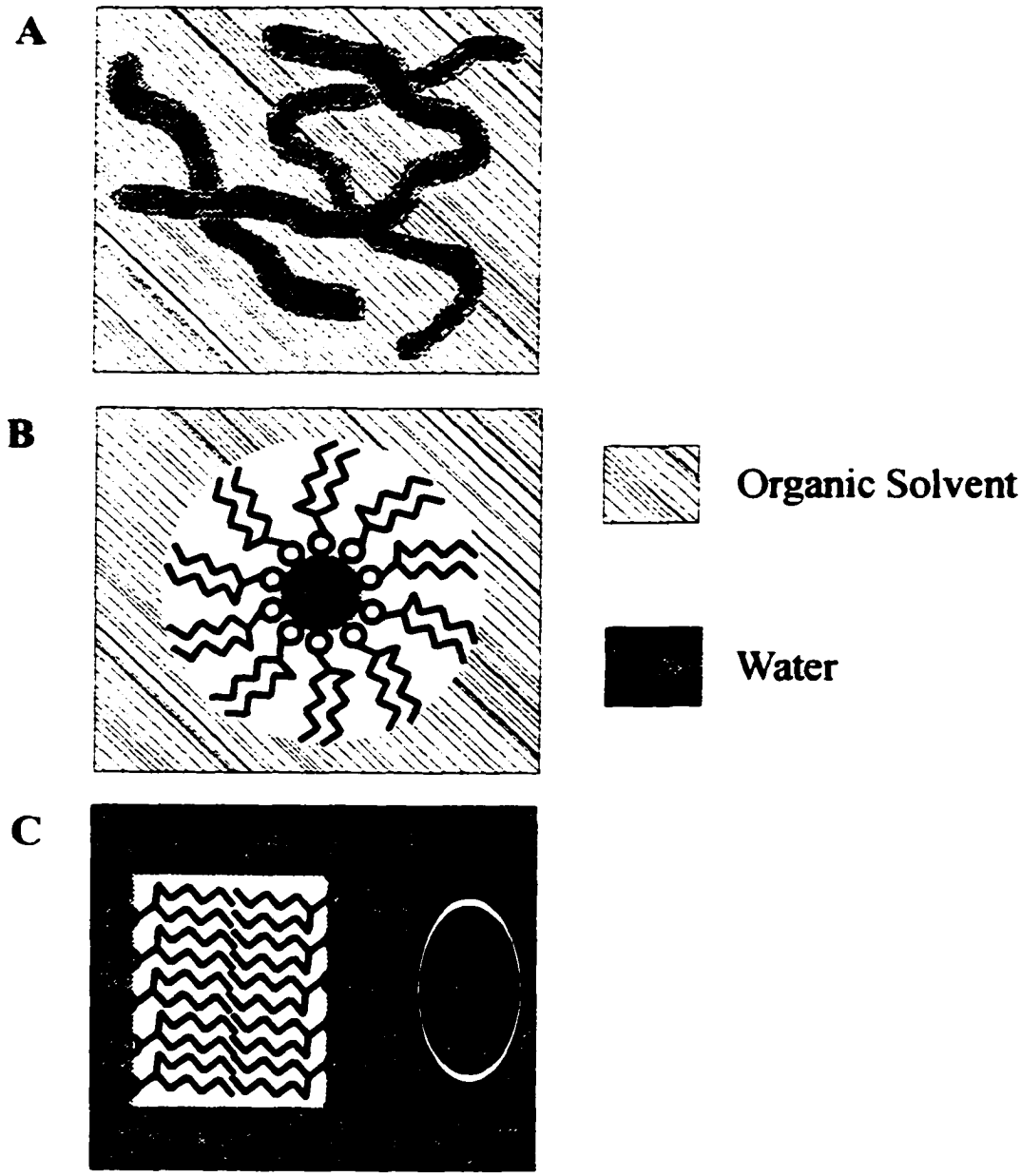

Figure 1.2. Pertinent lecithin aggregate structures: (A) worm-like reverse micelles, (B) spherical reverse micelles, (C) and liposomes. Reverse micelles entrap a small amount of water within a nonpolar organic continuous phase with the phospholipids delineating the boundary. Liposomes are spherical with aqueous solution inside and outside and a phospholipid bilayer forming the boundary.

The structure of solvents plays a large role in their dynamics. Therefore, it is expected that water dynamics will differ for water residing at a membrane surface. There are reports of various experimental measures of water at biological interfaces. Most of the experimental information about water dynamics comes from nuclear magnetic resonance (NMR) measurements. Unfortunately, the time resolution of the experiments cannot probe water motion unless it is significantly slowed down. A related recent review on the dynamics of water-protein interactions[11] reported that the water dynamics at protein surfaces were essentially as fast as bulk water. However, the technique used was not capable of measuring ultrafast motion of water hence was incapable of distinguishing water interacting with the interface unless its dynamical response was slowed by orders of magnitude. Dynamical properties of various phosphatidylcholine lipid-water interfaces have also been studied via spectroscopy of fluorescent probe molecules[12]. These measurements revealed relaxation times for the lipid-water interfaces ranging from 0.6 to 6 ns and showed that variation in the nonpolar parts of the lipid molecules had no effect on the dynamics. Again, the time-resolution of the technique limited the scope of the study.

1.II. Polar Solvation Dynamics

Polar solvation dynamics is the measure of the polar solvent response to an instantaneous change in solute charge distribution. It is highly relevant to fast chemical reactions in solution such as electron transfer since the rate may be limited by the speed with which the surrounding medium can respond[13, 14]. Solvation dynamics have been well studied through experiments, analytical theories and computer modeling[15]. Until

the advent of ultrafast lasers, experiments were limited to highly viscous fluids and glasses. In the past decade, measurements on quickly responding systems, such as acetonitrile and water, have become tenable[16-31]. Time-resolved fluorescence[16, 32, 33], time-resolved optical Kerr effect[23, 34], and photon-echoes[25, 35] have been used to measure the dynamic response of solvent molecules to an instantaneous electric perturbation. Of these methods, time-resolved fluorescence[32, 36] techniques are the oldest thus have more parallels in theory and modeling than do the other more recent techniques. We focus on this technique here.

Time-resolved fluorescence techniques experimentally measure polar solvation dynamics by following the dynamic Stokes shift in fluorescence displayed by a probe molecule[13, 14, 18, 32, 36-41]. Rigid molecular probes ensure that the measured shift in the fluorescence reflects solvation without contributions from solute internal degrees of freedom. Researchers have used time-correlated single photon counting (TCSPC) and fluorescence upconversion (FU) to time-resolve the fluorescence Stokes shift measuring the solvation time, $\langle \tau_S \rangle$, for a wide variety of solvents[13, 14, 17, 18, 32, 33, 36-42]. Data from these experiments are usually analyzed by reconstructing the time-resolved emission spectrum (TRES) over the time period that the dynamic Stokes shift is observed[14, 15, 40, 43]. By marking the shift in the peak of the emission one can obtain an experimental measure of the time-correlation function

$$C(t) = \frac{\nu(t) - \nu(\infty)}{\nu(0) - \nu(\infty)} \qquad (1.1)$$

where $\nu(t)$, $\nu(0)$ and $\nu(\infty)$ are the peak of the TRES at time t, zero and infinity, respectively. $C(t)$ describes the temporal evolution of the solvation free energy in response to a solvent perturbation. The time-correlation function is typically fit with a

sum of exponential decays with each time component corresponding to a particular mode of solvent relaxation. In some situations $\Delta\nu_{max}$ values are reported along with the C(t) function. $\Delta\nu_{max} = \nu(0) - \nu(\infty)$, where ν_{max} refers to the frequency of the fluorescence peak at maximum intensity. $\Delta\nu_{max}$ represents the total energy associated with solvent reorganization. Highly organized as well as most nonpolar environments show little response to a solute perturbation and therefore display low energy responses. $\Delta\nu_{max}$ values quantify the degree of solute solvation.

The theory of solvation dynamics in bulk solution is well developed[14, 15, 43]. Continuum models form the basis for statistical models to generate *C(t)*; the most basic form is the dielectric continuum model. Of the several existing models[15], the simplest is the Debye case. Here *C(t)* is given by:

$$C(t) = \exp-\left(\frac{t}{\tau_l}\right) \qquad (1.2)$$

where τ_l is the longitudinal relaxation time, $\tau_l = \frac{\varepsilon_0}{\varepsilon_\infty}\tau_D$; ε_0 and ε_∞ are the static and infinite frequency dielectric constants and τ_D is the Debye relaxation time. While this treatment is a convenient starting point, it falls short because the observed solvation time, $\langle\tau_S\rangle$ is not well approximated by τ_l, that is, $\tau_S > \tau_l$ and *C(t)* is not well characterized by a single exponential decay. In general, there exist two components to the solvation dynamics: an ultrafast, sub 100 fs inertial component and slower diffusive components[44]. Solvation dynamics of water have been measured[17] and show a large (>50%) sub 50 fs inertial component. Two additional diffusive components comprise the dynamics, with time constants of 120 and 880 fs.

Computer simulations are a relatively new and very powerful part of solvation dynamics research[24, 33, 39, 45-58]. Two basic molecular dynamics techniques exist: equilibrium molecular dynamics in the presence of a solute generate the initial conditions and linear response formalism to relate fluctuations observed at equilibrium to solvation response. Generally, the result of molecular dynamics simulations is that most of the solvation response is generated in a small number of molecules in direct contact with the solute. Unfortunately, molecular dynamics calculations are typically limited to a few hundred picoseconds due to computational time limits. As a result, it is difficult to make direct comparisons with the experimental results to date. However, in subsequent chapters, we will compare our experimental results with various simulations that model lipid interface dynamics because they provide the best insight into ultafast solvent motion.

While the large fraction of past studies has concentrated on dynamics in bulk solutions, a few recent studies have probed solvation dynamics in restricted environments. Yanagimachi et al.[59] measured the dynamics of 1-butanol at a sapphire surface while Bessho et al.[60] studied the fluorescence decays of 1,8-anilino-8-naphthalenesulfonic acid at the water-heptane interface. In both these studies, the polar solvent response observed was slower at the interface than in bulk. Sarkar et al. have probed microemulsion systems with oil-in-water micelles[61] and water-in-oil reverse micelles[62]. Their experiments revealed additional long time, nanosecond components to the water dynamics. In addition, water solvation dynamics in zeolites measured by coumarin 480 has been attributed to the motion of the mobile sodium ions and/or the motion of the probe molecules and is similar to ionic solvation dynamics significantly

slower than bulk water[63]. While the observed dynamics in all these studies were attributed to solvation dynamics, the time resolution was >50 ps, hence the normal ultrafast water response would not be observable. However, Vajda et al. have measured the dynamics of water solvation within cyclodextrin cavities using subpicosecond resolution[64]. At short times, < 0.2 ps, the solvation dynamics in the cyclodextrin cavity is similar to that in bulk water. At longer times, ≥ 0.2 ps, the solvation dynamics in the cyclodextrin cavity is observed to be significantly slower compared to bulk water displaying additional long time components to the relaxation. These were attributed to probe molecule motion in and out of the cavity as well as water molecules constrained by binding to the cyclodextrin[64, 65]. Pierce and Boxer[66] and Chattoraj and Boxer[67] attempted to measure dynamics of water motion in a protein matrix. However, results from the observed relaxation were not interpretable due to the high degree of heterogeneity in the system.

Relative to the more common bulk solvent measurements, investigating solvation dynamics in heterogeneous systems is more complicated. As we will discuss in subsequent chapters, solvated probes need to be localized within the regions of interest. Heterogeneous systems provide a variety of positions a probe molecule may reside. If probes reside in a distribution of environments, not only will the data contain noise from unwanted environments but also the dynamics will be more difficult to interpret. In this thesis, we will spend a significant amount of intellectual energy ensuring that our probe molecule resides at the lipid/water interface.

1.III. Goals and Significance

While there is an enormous amount of information about the structure of lipid/water interfaces, comparatively little is known about the dynamics at the interface. Many NMR as well as a few solvation dynamics studies have measured dynamics at lipid interfaces. However, the time resolution of these studies is never less than 50ps. Water is obviously an integral part of the lipid interface, yet because bulk water relaxes on a subpicosecond timescale, the ultrafast response remains undetected by previous studies unless the water is slowed by orders of magnitude. Therefore, we must employ a analytical method that has subpicosecond time resolution in order to obtain the full picture of solvent motion at a lipid interface. In the following chapters, we present solvation dynamics results obtained at various lecithin interfaces using TRES. Because we employ a ultrafast laser system, these measurements are able to observe bulk water relaxation, and therefore, represent the first picture of fast solvent motion at phospholipid interfaces.

Because our probe molecule was easily confined within this particular system, we initially interrogated the aqueous interior of worm-like reverse micelles (see Chapter 2). After covalently attaching our probe molecule to a phospholipid headgroup (see Chapter 3), we were then able to interrogate the lipid/water interface of spherical reverse micelles (see Chapter 4), and liposomes (see Chapter 5). We attempt to address several unanswered questions concerning lipid interfaces. First, to what degree do the dynamics at a lipid interface differ from dynamics in bulk water? As we discussed previously, studies suggest that the structure of water at membrane surfaces differs significantly from

the bulk. We attempt to find to what degree the lipid interface restricts solvent motion. Second, we attempt to determine what effects aggregate morphology has on the observed dynamics. Although all interfaces will be formed by lecithin aggregates, we expected to observe very different dynamics depending on the shape of interface. Would worm-like reverse micelles show different dynamics than spherical reverse micelles? In addition, would reverse micelles show more restricted motion than the more planar liposome interfaces? Finally, we wished to correlate the dynamics we observe with interface structure. For reverse micelles, we observed the dynamics as a function of reverse micelle hydration. We attempted to find if greater hydrated lipids would show faster dynamics. For liposomes, we observed the dynamics with and without cholesterol incorporated into the lipid bilayer. Both lipid hydration and cholesterol have been shown to alter the lipid chain structure.

The ultimate goal of our research is to better understand biochemical processes occurring at membrane interfaces. Any process near a lipid interface will require solvent reorganization in order to occur. With our results, other studies will have a greater ability to accurately model the process. A large fraction of cellular processes, such as electron, ion, and molecular transport, enzymatic reactions, and electron transfer reactions occur at membrane interfaces. The solvent mobility is known to enhance the rates of these processes in bulk solution, especially electron transfer reactions[68, 69]. Therefore, the motion of water in and at a lipid interface will undoubtedly play a role when the processes span a living membrane.

1.IV. Fluorescence Upconversion Spectroscopy

The femtosecond fluorescence-upconversion spectrometer used to collect time-resolved fluorescence signals (see Figure 1.3) is similar to the apparatus designed by Fleming and coworkers[57]. The excitation source is a modelocked Ti:sapphire laser (NJA-3, Clark) pumped by all lines of an Ar^+ laser (Innova 310, Coherent) at 6.5 W. The Ti:sapphire laser produces output pulses with 80 fs duration (FWHM assuming $sech^2$ pulse shape) at a 100 MHz repetition rate and with energies of 5-6 nJ/pulse. The spectrum of the pulses is centered at about 810±10 nm depending on the laser alignment. Divergence of the output is corrected using a 1.5-m focal length lens (fused silica) and a telescope consisting of a 15-cm negative lens and a 20-cm positive lens (both AR-coated). The resulting collimated beam has a diameter of 2-5 mm. The collimated beam is then frequency doubled in a 1-mm barium-borate crystal (BBO, Type I, INRAD). Frequency doubled pulses measure about 480 ± 50 pJ/pulse. The frequency-doubled pulses are separated from the fundamental using a dielectric beamsplitter (CVI). These pulses are sent through an optical delay line equipped with a motorized delay stage (Parker-Daedl delay stage, American Precision step motor), passed through a λ/2 plate (400-nm center wavelength, Meadowlark Optics), and focused by a 10-cm lens into a 1-mm quartz flowing sample cell. A small cone of the forward fluorescence is collected and focused with an ellipsoidal rhodium reflector (Melles Griot) into a nonlinear crystal (BBO, Type I, 0.5-mm thick, Casix). The fluorescence is upconverted with the residual fundamental pulses that have been passed through a λ/2 plate (780-nm center wavelength, Meadowlark Optics) and focused onto the BBO upconversion crystal with a

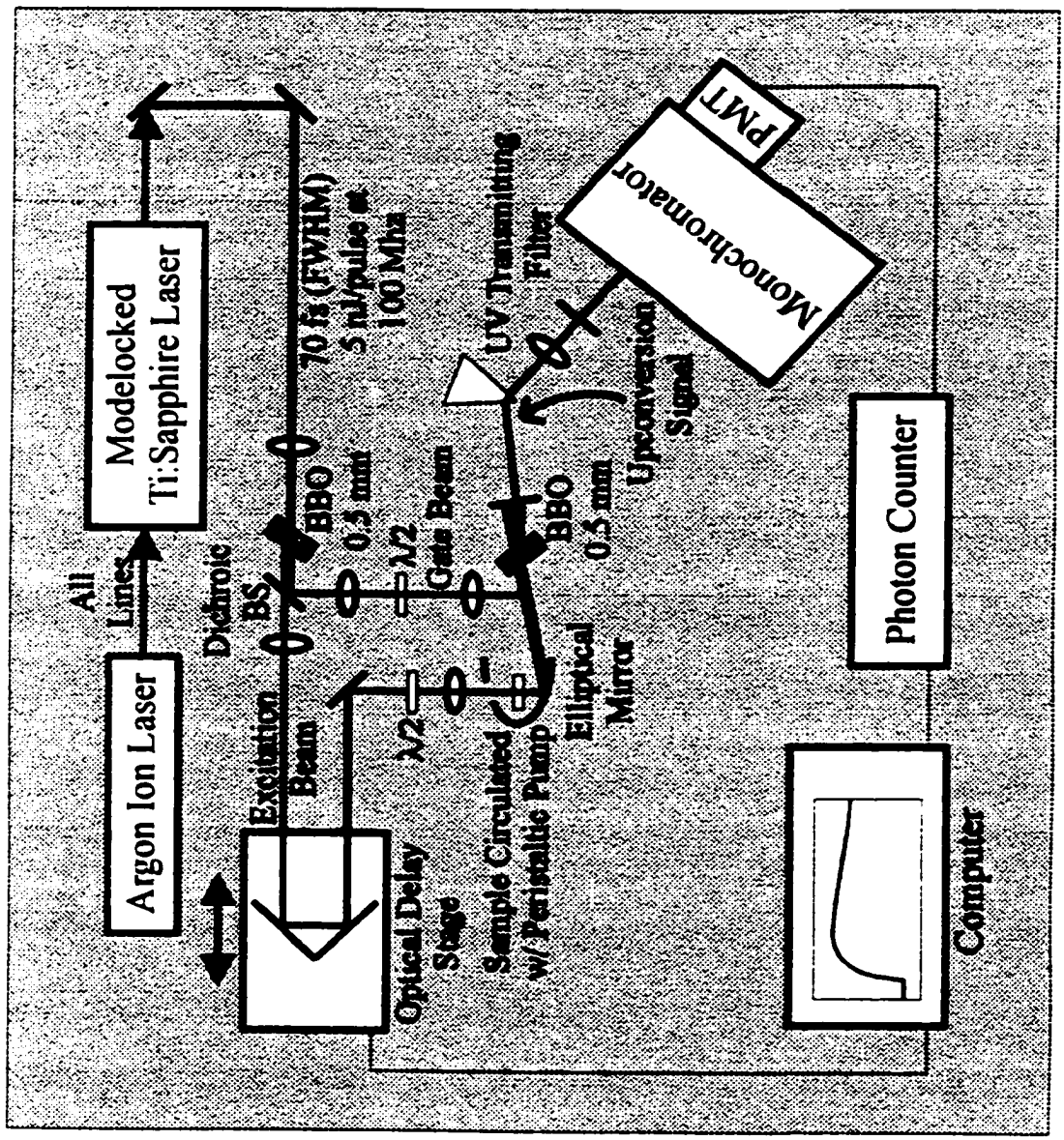

Figure 1.3. Fluorescence upconversion experimental setup.

10-cm lens. Initial solvation dynamics measurements (see Chapter 2) were made with the excitation and gate beams having parallel polarization with respect to each other. All subsequent solvation dynamics measurements are made with the excitation beam at magic angle (54.7°) with respect to the gate beam. Magic angle polarization eliminates any rotational relaxation of the probe molecule that may obscure solvation dynamics measurements[70]. The upconverted light was collimated by a 10-cm lens (2" diameter, fused silica), isolated from the gate and fundamental beams using an iris, and dispersed by a Brewster prism (fused-silica, CVI). The upconverted beam is then focused with a 12.8-cm lens (fused silica) through a UV transmitting filter (340 nm, Opto-Sigma) into a 0.33-m single monochromator (HR320, ISA) equipped with a 2400 g/mm grating blazed at 400 nm. The bandwidth of the fluorescence detected at a single wavelength is on the order of 8 nm. The overall instrument response was determined from the cross correlation of the excitation and gate pulses in the BBO crystal, typically measuring 180 ± 50 fs (FWHM, assuming a Gaussian line shape). Pulse duration and pulse energy are variable quantities that depend on the specific alignment of the Ti:sapphire laser. The upconverted photons are detected using a photomultiplier tube (PMT, R1527P, Hamamatsu) in a cooled housing (TE177RF, Products for Research). The signal is then amplified using two video amplifiers (CLC100, Comlinear Corporation) in series, and digitized by a two channel photon counter (SR400, Stanford Research Systems). A personal computer using LabVIEW (National Instruments) routines collects the photon counter signals as a function of optical delay between the excitation and gate pulses. Fluorescence-upconversion measurements are obtained by counting for 1 second at each

delay. Each transient is the average of 3 to 16 scans, depending on the signal to noise ratio.

For all fluorescence-upconversion measurements, samples (~10 mL volumes) are circulated with a peristaltic pump (Masterflex, Model 7553-70) fitted with PTFE tubing to ensure the integrity of the samples. Samples are typically submerged in a water bath reservoir kept at 21.5±0.5°C. Samples typically have an absorbance of 0.12–0.8 at 400 nm, as measured in a 1–mm quartz cuvette.

1.V. Data Analysis

The spectral reconstruction method is employed to determine the time-correlation functions *C(t)* for the various environments[14, 15]. The time-resolved fluorescence-upconversion transients are fit to multiexponential functions. The longest transient scans are fit with a long time offset that corresponds to the fluorescence lifetime of the probe. We determined fluorescence lifetimes by time-correlation single-photon counting (TCSPC) measurements using either one of two home-built instruments. The first instrument had excitation pulses centered at 315 nm[71] (Prof. Kelley Laboratory), while the second instrument had excitation pulses centered at 425 nm (Biochemistry Laboratory), with both instruments having 50-100 ps (fwhm) response time. Only a single fluorescence lifetime per sample was measured. However, because the fluorescence lifetime is expected to be proportional to the ν^{-3} of the emitted light, the offset used to fit individual wavelength transients is adjusted accordingly[72, 73]. For the shortest scans, 2ps, the instrument response must be accounted for because components of the solvent response occur on a time scale similar to the laser pulse

duration. This was accomplished using an iterative reconvolution analysis program. A Gaussian function fit to the cross-correlation signal of the pump and gate pulses was used as the instrument response function. The resulting deconvolved functions for given fluorescence wavelengths were normalized at long time delay (typically 500 ps) to the corresponding steady-state fluorescence-emission spectrum. The time-resolved fluorescence transients obtained over shorter periods of time were normalized to reconstructed fluorescence spectra obtained from the next longest transient set.

We then construct the TRES from the normalized fits of the fluorescence-upconversion signals. The resulting spectra are parameterized in terms of the peak maximum ($\nu(t)$), spectral width ($\Delta\nu(t)$), and a factor to account for the asymmetry of the line shape (ρ) by fitting the spectra to log-normal line shapes[74]. The time correlation function, $C(t)$ (see eqn 1.1), is calculated with the peak maximum at various gate delays $\nu(t)$; $\nu(0)$ is the peak of the reconstructed fluorescence-emission spectrum at 0-fs delay and $\nu(\infty)$ is the peak of the steady-state fluorescence emission spectrum. $C(t)$ is fit with a multiexponential decay function. The number of exponential components used to fit $C(t)$ is determined by the χ^2 value of the fit. In other words, if an additional exponential decay is used to fit $C(t)$ but no significant decrease in χ^2 results, the additional decay is not included.

1.VI. Solvation Dynamics Probes

The requirements of a probe molecule used for solvation dynamics experiments are multifold. First, the molecule must possess a small or no dipole moment in the electronic ground state and a much larger dipole in the excited state. In this way we can

experimentally "turn on" a new electronic configuration instantaneously and watch the water respond to it. Second, the probe molecule must be quite rigid to avoid complications of intramolecular relaxation in the measured dynamics. Third, while not imperative, it is advantageous for us to use a molecule that matches the wavelength characteristics of our laser system well so that we avoid pumping the dye into nearby excited electronic states that would complicate the measured dynamics.

Coumarin molecules have been used very successfully in experimental solvation dynamics measurements for the past decade[15]. They easily fulfill all of the prerequisites listed above. In addition, there are a wide variety of different substitutions on the basic probe that make it possible to probe different chemical systems. For the initial solvation dynamics studies, we made use of the anionic coumarin probe, Coumarin 343 (C343). The structure of the neutral molecule is shown below in Figure 1.4. C343 is particularly advantageous to our research because it is soluble in water and insoluble in alkane solvents. As will be discussed in Chapter 2, this made it possible for us to specifically probe the polar phase within reverse micelles. Most important for us is the fact that the C343 carboxylic acid group is not associated with the electronic transitions of the molecule. Therefore, changes in this group do not significantly affect the spectroscopy of the molecule. As described in Chapter 3, we successfully formed a covalent bond between the C343 carboxylic acid carbonyl and a phospholipid amine.

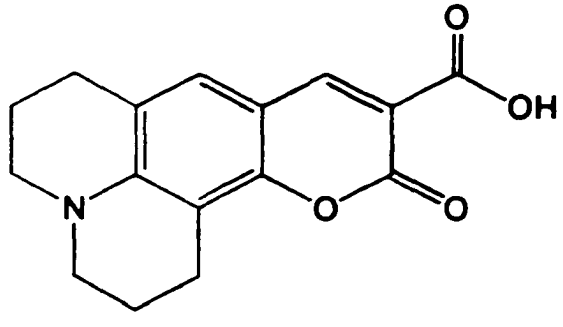

Figure 1.4. Structure of Coumarin 343 (C343)

1.VII. Determining Probe Location

Because we wish to probe a specific region in an inhomogeneous system, namely the lipid/water interface, we spend considerable effort assuring that our solvation dynamics probe resides at the interface. In the subsequent chapters, we utilize steady-state spectroscopy and time-resolved fluorescence anisotropy of the probe molecule in order to identify its position within the system of interest.

An ideal solvation dynamics probe should exhibit a solvent dependence of the fluorescence Stokes shift[14]. In other words, in polar solvents the fluorescence spectrum of a solvated probe should shift to longer wavelengths because the solvent has a greater capacity to stabilize an excited probe molecule via reorganization[14, 15]. Although not as important, the absorption spectra should show similar polarity dependence. Previous studies have shown that C343 dissolved in various solvents displays the expected spectral shifting as a function of solvent polarity[42, 69, 75, 76]. We have also shown that C343 dissolved in AOT reverse micelles shows a continuous spectral shift to longer wavelengths as hydration is increased, indicating the probe responds to the increased micelle polarity as the water content increases[77]. We conclude that C343 is within the aqueous interior of the AOT reverse micelles. In a similar fashion, we will use the polarity dependence of C343 to indicate its position in other systems. Absorption spectra are recorded with a Cary 2400 UV-vis-NIR spectrophotometer. Fluorescence spectra are collected with a home-built fluorometer[78].

Time-dependent anisotropy measures rotation of solvated probes by detecting the depolarization of emitted light as a function of time[1]. The key to the depolarization technique is that the probability of light absorption and of emission is directional. Light polarized along a given axis will preferentially excite molecules oriented with their transition dipole moment along the same axis. Assuming the electronic excitation is a linear transition, light emitted by a molecule will be polarized in the same direction as the dipole moment. Therefore, rotating molecules that are excited along a given axis will emit light along that same axis at early times but will show depolarized emission at late times as rotational motion randomizes the distribution. The emitted light is monitored by using polarizers to quantify the intensity of the components parallel ($I_{\|}$) and perpendicular ($I_{\perp}$) to the original direction of polarization. The values $I_{\|}$ and $I_{\perp}$ are used to obtain the anisotropy, r:

$$r(t) = \frac{I_{\|}(t) - I_{\perp}(t)}{I_{\|}(t) + 2I_{\perp}(t)} \qquad (1.3)$$

Assuming no molecular rotation occurs, the initial value of r has a maximum of 0.4. If the excitation and emission dipoles are not colinear, polarization of emitted light will be scrambled, resulting in an initial r value smaller than 0.4. The anisotropy is measured as a function of time, resulting in a decay curve that is subsequently fit with multi-exponential decays. Each time component determined from the fit represents a rotational mode of relaxation. Fluorescence probes dissolved in bulk solvents typically display single exponential decays with a time component of tens to hundreds of picoseconds.

In subsequent chapters, we measure the anisotropy of the probe molecule in various systems. We find that in some situations a fraction of the probe molecules are

solvated in bulk solvents away from the lipid/water interface. In these situations, the anisotropy is biexponential with a <100ps component and a nanosecond component. The longer time component represents the probes that are embedded in the lipid interface and unable to freely rotate much faster than the interface rotates collectively. The faster component represents the freely rotating probes dissolved in the bulk solvent. By comparing the amplitudes associated with each time component, we can determine what fraction of probes resides detached from the interface.

In some situations, however, all probes may reside in one type of environment but still show multi-component rotational relaxation. This occurs in heterogeneous environments such as lipid membranes where probes may experience greater rotational friction along one axis more than another axis. This is true in general when probe molecules are either anchored in some fashion to the lipid/water interface or are embedded in the lipid membrane and have an extended asymmetrical shape. For example, the lipid probe TMA-DPH is oblong shaped and has a positively charged ammonium group at one end that effectively anchors it to the headgroup region. Therefore, rotational relaxation of TMA-DPH shows a component corresponding to a wobbling motion along the longitudinal bilayer axis that never decays to zero because it is unable to randomize along the lateral bilayer axis[79].

Others have measured the time dependent anisotropy of covalently attached lipid probes within membranes. They have used the wobble component to indicate surface structure[80]. The amplitude of the wobble has been interpreted as the degree to which the fluorophore samples a conical region. The associated time component is the rate at which the fluorophore samples the possible configurations within the cone. Several

models exist that determine the wobble cone angle based on the measured amplitudes. We use the wobble in a cone model presented in Lakowicz[70]:

$$r_\infty/r_0 = [1/2\ (3\ \cos^2\ (\theta_c) - 1)]^2 \qquad (1.4)$$

where r_∞ represents the long time amplitude, r_0 represents the initial amplitude at time zero, and θ_c represents the wobble cone angle.

Time-resolved anisotropy measurements are made with the same upconversion apparatus as the solvation dynamics experiments. Because the gate pulses only upconvert photons with similar polarization, the upconversion crystal essentially acts as a polarization detector. In other words, if the excitation and gate beams are set with parallel polarization, immediately after excitation, the emitted light maintains the same polarization and is therefore upconverted by the gate pulse of similar polarization. However, in time, the polarization of the emitted light will become scrambled and because of this fewer fluorescence photons will have polarization similar to the gate polarization and the upconversion intensity will decrease. Therefore, we determine $I_{||}$ by measuring the fluorescence upconversion intensity in time with the polarizations of the excitation and gate beams parallel and $I_\perp$ with beams perpendicular. Typical transients are taken over 100 ps.

1.VIII. Sample Characterization

A commonly used instrument we use to characterize reverse micelles and liposomes is Dynamic Light Scattering (DLS, DynaPro-801MS-MSTC40, Protein Solutions). The instrument correlates scattered light in time to measure the velocity of

dissolved particles. Using the Stokes-Einstein equation velocities are translated into particle sizes. The instrument includes software packages that determine the polydispersity as well as the corresponding particle sizes of a given sample.

References for Chapter 1

1. Gennis, R.B., *Biomembranes: Molecular Structure and Function*. Springer Advanced Texts in Chemistry, ed. C.R. Cantor. 1989, New York: Springer-Verlag. 533.

2. Jorgensen, K., J.H. Ipsen, and O.G. Mouritsen, *Lipid-Bilayer Heterogeneity*, in *Membranes and Cell Signaling*. 1997, JAI Press, Inc. p. 19-38.

3. Fendler, J., *Microemulsions, micelles, and vesicles as media for membrane mimetic photochemistry*. J. Phys. Chem., 1980. **84**(12): p. 1485-1491.

4. Jones, M.N. and D. Chapman, *Micelles, Monolayers, and Biomembranes*. 1995, New York: John Wiley and Sons.

5. Walde, P., *et al.*, *Phospholipid-based reverse micelles*. Chem. Phys. Lipids, 1990. **53**: p. 265-88.

6. Luisi, P.L. and B.E. Straub, eds. *Reverse Micelles: Biological and Technological Relevance of Amphiphilic Structures in Apolar Media*. . 1984, Plenum Press: New York.

7. New, R.R.C., ed. *Liposomes: A Practical Approach*. The Practical Approach Series, ed. D. Rickwood and B.D. Hames. 1990, IRL Press: New York. 301.

8. Hermanson, G.T., *Bioconjugate Techniques*. 1996, San Diego: Academic Press, Inc.

9. Cevc, G., *Lipid Hydration*, in *Hydration of Macromolecules*, E. Westhof, Editor. 1992, MacMillan Press: New York. p. 338-390.

10. Gragson, D.E., B.M. McCarty, and G.L. Richmond, *Ordering of interfacial water molecules at the charged air/water interface observed by vibrational sum frequency generation*. J. Am. Chem. Soc., 1997. **119**(26): p. 6144-6152.

11. Bryant, R.G., *The dynamics of water-protein interactions*. Ann. Rev. Biophys. Biomol. Struct., 1996. **25**: p. 29-53.

12. Lakowicz, J.R. and D. Hogen, *Dynamic properties of the lipid-water interface of model membranes as revealed by lifetime-resolved fluorescence emission spectra*. Biochemistry, 1981. **20**: p. 1366-1373.

13. Maroncelli, M., J. MacInnis, and G.R. Fleming, *Polar Solvent Dynamics and Electron-Transfer Reactions*. Science, 1989. **243**: p. 1674-1681.

14. Barbara, P.F. and W. Jarzeba, *Ultrafast Photochemical Intramolecular Charge and Excited State Solvation*, in *Advances in Photochemistry*, D.H. Volman, G.S. Hammond, and K. Gollnick, Editors. 1990, John Wiley & Sons, Inc. p. 1-68.

15. Maroncelli, M., *The Dynamics of Solvation in Polar Liquids.* J. Mol. Liq., 1993. **57**: p. 1-37.

16. Kahlow, M.A., *et al.*, *Femtosecond Resolved Solvation Dynamics in Polar Solvents.* J. Chem. Phys., 1989. **90**(1): p. 151-158.

17. Jimenez, R., *et al.*, *Femtosecond solvation dynamics of water.* Nature, 1994. **369**(6480): p. 471-473.

18. Jarzeba, W., *et al.*, *Femtosecond Microscopic Solvation Dynamics of Aqueous Solutions.* J. Phys. Chem., 1988. **92**: p. 7039-7041.

19. Gardecki, J., *et al.*, *Ultrafast measurements of the dynamics of solvation in polar and non-dipolar solvents.* J Mol Liq, 1995. **65-6**: p. 49-57.

20. McMorrow, D. and W.T. Lotshaw, *Intermolecular Dynamics in Acetonitrile Probed with Femtosecond Fourier Transform Raman Spectroscopy.* J. Phys. Chem., 1991. **95**: p. 10395-10406.

21. McMorrow, D., *et al.*, *Probing the microscopic molecular environment in liquids: Intermolecular dynamics of CS_2 in alkane solvents.* J Phys Chem, 1996. **100**(24): p. 10389-10399.

22. Rosenthal, S.J., *et al.*, *Femtosecond Solvation Dynamics in Acetonitrile: Observation of the Inertial Contribution to the Solvent Response.* J. Chem. Phys., 1991. **95**(6): p. 4715-4718.

23. Cho, M., *et al.*, *Ultrafast Solvent Dynamics: Connection Between Time Resolved Fluorescence and Optical Kerr Measurements.* J. Chem. Phys., 1992. **96**(7): p. 5033-5038.

24. Cho, M.H., *et al.*, *The integrated photon echo and solvation dynamics.* J Phys Chem, 1996. **100**(29): p. 11944-11953.

25. Joo, T.H., *et al.*, *Third-order nonlinear time domain probes of solvation dynamics.* J. Chem. Phys., 1996. **104**(16): p. 6089-6108.

26. Scherer, N.F., *et al.*, *Interferometric and Coherence Studies of Liquids and Chemical Processes.* Abstracts of the 208th ACS National Meeting, 1994: p. paper 28.

27. van den Bout, D. and M. Berg, *Ultrafast Raman echo experiments in liquids.* J Raman Spectrosc, 1995. **26**(7): p. 503-511.

28. Nibbering, E.T.J., D.A. Wiersma, and K. Duppen, *Ultrafast Electronic Fluctuation and Solvation in Liquids.* Chem Phys, 1994. **183**(2-3): p. 167-185.

29. Nishiyama, K., *et al., Solvation dynamics of dye molecules in polar solvents studied by time resolved hole burning spectroscopy.* J Mol Liq, 1995. **65-6**: p. 41-48.

30. Pshenichnikov, M.S., K. Duppen, and D.A. Wiersma, *Time-resolved femtosecond photon echo probes bimodal solvent dynamics.* Phys Rev Lett, 1995. **74**(5): p. 674-677.

31. Bingemann, D. and N.P. Ernsting, *Femtosecond solvation dynamics determining the band shape of stimulated emission from a polar styryl dye.* J. Chem. Phys., 1995. **102**(7): p. 2691-2700.

32. Castner Jr., E.W., M. Maroncelli, and G.R. Fleming, *Subpicosecond Resolution Studies of Solvation Dynamics in Polar Aprotic and Alcohol Solvents.* J. Chem. Phys., 1987. **86**(3): p. 1090-1097.

33. Horng, M.L., *et al., Subpicosecond measurements of polar solvation dynamics: Coumarin 153 revisited.* J. Phys. Chem., 1995. **99**(48): p. 17311-17337.

34. Chang, Y.J. and E.W. Castner, Jr., *Femtosecond dynamics of hydrogen-bonding solvents. Formamide and N-methylformamide in acetonitrile, DMF, and water.* J. Chem. Phys., 1993. **99**(1): p. 113-125.

35. Yang, T.S., *et al., The solvent spectral density and vibrational multimode approach to optical dephasing: Two-pulse photon echo response.* J Chem Phys, 1995. **103**(19): p. 8346-8359.

36. Kahlow, M.A., *et al., Ultrafast Emission Spectroscopy in the Ultraviolet by Time-Gated Upconversion.* Rev. Sci. Instrum., 1988. **59**(7): p. 1098-1109.

37. Kahlow, M.A., T.J. Kang, and P.F. Barbara, *Transient Solvation of Polar Dye Molecules in Polar Aprotic Solvents.* J. Chem. Phys., 1988. **88**(4): p. 2372-2378.

38. Kahlow, M.A., T.J. Kang, and P.F. Barbara, *Electron-Transfer Times Are Not Equal to Longitudinal Relaxation Times in Polar Aprotic Solvents.* J. Phys. Chem., 1987. **91**: p. 6452-6455.

39. Maroncelli, M., *Computer Simulations of Solvation Dynamics in Acetonitrile.* J. Chem. Phys., 1991. **94**(3): p. 2084-2103.

40. Maroncelli, M. and G.R. Fleming, *Picosecond Solvation Dynamics of Coumarin 153: The Importance of Molecular Aspects of Solvation.* J. Chem. Phys., 1987. **86**(11): p. 6221-6239.

41. Simon, J.D., *Time-Resolved Studies of Solvation in Polar Media.* Acc. Chem. Res., 1988. **21**: p. 128-134.

42. Tominaga, K. and G.C. Walker, *Femtosecond experiments on solvation dynamics of an anionic probe molecule in methanol.* J. Photochem. Photobiol., A, 1995. **87**(2): p. 192-196.

43. Stratt, R.M. and M. Maroncelli, *Nonreactive dynamics in solution: The emerging molecular view of solvation dynamics and vibrational relaxation.* J. Phys. Chem., 1996. **100**: p. 12981-12996.

44. Maroncelli, M., *et al.*, *Studies of the Inertial Component of Polar Solvation Dynamics*, in *Ultrafast Reaction Dynamics and Solvent Effects*, Y. Gauduel and P.J. Rossky, Editors. 1994, American Institute of Physics. p. 310-333.

45. Schwartz, B.J. and P.J. Rossky, *Aqueous solvation dynamics with a quantum mechanical solute: Computer simulation studies of the photoexcited hydrated electron.* J. Chem. Phys., 1994. **101**(8): p. 6902-6916.

46. Schwartz, B.J. and P.J. Rossky, *An exploration of the relationship between solvation dynamics and spectrally determined solvent response functions by computer simulation.* J. Phys. Chem., 1995. **99**(10): p. 2953-2958.

47. Schwartz, B.J. and P.J. Rossky, *The interplay of dielectric and mechanical relaxation in solvation dynamics.* J. Mol. Liq., 1995. **65-6**: p. 23-30.

48. Brown, R., *Molecular dynamics modeling of time-resolved fluorescence shifts in liquid solution.* J. Chem. Phys., 1995. **102**(22): p. 9059-9068.

49. Lin, Y. and C.D. Jonah, *Computer simulation of solvation dynamics in several model solvents.* Chem. Phys. Lett., 1995. **233**(1-2): p. 138-144.

50. Baranyai, A. and G. Toth, *Solvation dynamics from nonequilibrium molecular dynamics simulation.* Mol Simulat, 1995. **14**(6): p. 403-407.

51. Kumar, P.V. and M. Maroncelli, *Polar solvation dynamics of polyatomic solutes: Simulation studies in acetonitrile and methanol.* J Chem Phys, 1995. **103**(8): p. 3038-3060.

52. Maroncelli, M. and G.R. Fleming, *Computer Simulation of the Dynamics of Aqueous Solvation.* J. Chem. Phys., 1988. **89**(8): p. 5044-5069.

53. Nandi, N. and B. Bagchi, *Ultrafast solvation dynamics of an ion in a restricted environment.* Indian J Chem Sect A, 1995. **34**(11): p. 845-849.

54. Neria, E. and A. Nitzan, *Simulations of Solvation Dynamics in Simple Polar Solvents.* J. Chem. Phys., 1992. **96**(7): p. 5433-5440.

55. Olender, R. and A. Nitzan, *Solvation dynamics in dielectric solvents with restricted molecular rotations: Polyethers.* J. Chem. Phys., 1995. **102**(18): p. 7180-7196.

56. Rips, I., *Electron solvation dynamics in polar liquids.* Chem Phys Lett, 1995. **245**(1): p. 79-84.

57. Rosenthal, S.J., *et al.*, *Solvation dynamics in methanol: Experimental and molecular dynamics simulation studies.* J. Mol. Liq., 1994. **60**(1-3): p. 25-56.

58. Ladanyi, B.M. and S. Klein, *Contributions of rotation and translation to polarizability anisotropy and solvation dynamics in acetonitrile.* J Chem Phys, 1996. **105**(4): p. 1552-1561.

59. Yanagimachi, M., N. Tamai, and H. Masuhara, *Solvation Dynamics of a Coumarin Dye at Liquid-Solid Interface Layer. Picosecond Total Internal Reflection Fluorescence Spectroscopic Study.* Chem. Phys. Lett., 1992. **200**(5): p. 469-474.

60. Bessho, K., *et al.*, *Microenvironments of 8-anilino-1-naphthalenesulfonate at the heptane-water interface: Time-resolved total internal reflection fluorescence spectroscopy.* Chem Phys Lett, 1997. **264**(3-4): p. 381-386.

61. Sarkar, N., *et al.*, *Solvation dynamics of coumarin 480 in micelles.* J Phys Chem, 1996. **100**(38): p. 15483-15486.

62. Sarkar, N., *et al.*, *Solvation dynamics of coumarin 480 in reverse micelles. Slow relaxation of water molecules.* J. Phys. Chem., 1996. **100**(25): p. 100523-100527.

63. Das, K., *et al.*, *Solvation dynamics in a solid host. Coumarin 480 in zeolite 13X.* Chem Phys Lett, 1996. **249**(5-6): p. 323-328.

64. Vajda, S., *et al.*, *Femtosecond to nanosecond solvation dynamics in pure water and inside the γ-cyclodextrin cavity.* J. Chem. Soc. Faraday Trans., 1995. **91**(5): p. 867-873.

65. Nandi, N. and B. Bagchi, *Ultrafast solvation dynamics of an ion in the gamma-cyclodextrin cavity: The role of restricted environment.* J Phys Chem, 1996. **100**(33): p. 13914-13919.

66. Pierce, D.W. and S.G. Boxer, *Dielectric relaxation in a protein matrix.* J. Phys. Chem., 1992. **96**(13): p. 5560-5566.

67. Chattoraj, M. and S.G. Boxer, *personal communication*, . 1994.

68. Reid, P.J. and P.F. Barbara, *Dynamic solvent effect on Betaine-30 electron-transfer kinetics in alcohols.* J. Phys. Chem., 1995. **99**(11): p. 3554-3565.

69. Walker, G.C., *et al.*, *Interplay of Solvent Motion and Vibrational Excitation in Electron-Transfer Kinetics: Experiment and Theory.* J. Phys. Chem., 1992. **96**: p. 3728-3736.

70. Lakowicz, J.R., *Principles of Fluroescence Spectroscopy*. 1983, New York: Plenum Press.

71. Parsapour, F. and D.F. Kelley, *Torsional and Proton Transfer Dynamics in Substituted 3-Hydroxyflavones.* J. Phys. Chem., 1996. **100**: p. 2791-2798.

72. Birks, J.B., *Chapter 4*, in *Photophysics of Aromatic Molecules*. 1970, Wiley: New York.

73. Fee, R.S., J.A. Milsom, and M. Maroncelli, *Inhomogeneous decay kinetics and apparent solvent relaxation at low temperatures.* J. Phys. Chem., 1991. **95**(13): p. 5170-81.

74. Siano, D.B. and D.E. Metzler, *Band shapes of the electronic spectra of complex molecules.* J. Chem. Phys., 1969. **51**(5): p. 1856-61.

75. Riter, R.E., *et al.*, *Novel reverse micelles partitioning nonaqueous polar solvents in a hydrocarbon continuous phase.* J. Phys. Chem. B, 1997. **101**(41): p. 8292-8297.

76. Drexhage, K.H., *et al.*, *Water-soluble Coumarin Dyes for Flashlamp-pumped Dye Lasers.* Opt. Comm., 1975. **15**(3): p. 399-403.

77. Riter, R.E., D.M. Willard, and N.E. Levinger, *Water immobilization at surfactant interfaces in reverse micelles.* J. Chem. Phys. B, 1998. **102**(5): p. 2705-14.

78. Brucker, G.A. and D.F. Kelley, *Proton transfer in matrix-isolated 3-hydroxyflavone and 3-hydroxyflavone complexes.* J. Phys. Chem., 1987. **91**: p. 2856-2861.

79. Lakowicz, J.R., ed. *Topics in Fluorescence Spectroscopy: Biochemical Applications*. Topics in Fluorescence Spectroscopy, ed. J.R. Lakowicz. Vol. 3. 1992, Plenum Press: New York. 390.

80. Kimura, Y. and A. Ikegami, *Local dielectric properities around polar region of lipid bilayer membranes.* J. Membrane Biol., 1985. **85**: p. 225-31.

Chapter 2

Dynamics of Polar Solvation in Lecithin/Water/Cyclohexane Reverse Micelles

2.I. Introduction

When surfactants are dispersed in nonpolar solvents, reverse (or inverted) micelles can form spontaneously[1]. If water is present, the inverted portion of the micelle can swell, creating dispersed water droplets delineated by the layer of surrounding surfactant molecules[2]. The polar end of the surfactant, or head group, points into the aqueous pool, while the hydrophobic alkyl chains are directed into the continuous organic phase. These aqueous pools are thermodynamically stable, and their sizes and shapes can often be controlled[3]. The micellar matrix can be controlled by adjusting variables such as water content, surfactant concentration, and temperature. Reverse micelles can deliver polar solutes to nonpolar solutes present in the organic phase allowing cosolvation of both polar and nonpolar reactants in a single macroscopic phase[4]. Molecules trapped in the reverse micelles have shown enhanced behavior. For example, pharmaceuticals have displayed

enhanced structural and conformational stability and slow diffusivity, and certain enzymes manifest enhanced activity at certain hydration levels[5].

Reverse micelles have been used as biological membrane models to aid in understanding membrane chemistry[2]. Biomembranes are composed, in part, of lipid bilayers that consist of two sheets of aggregated lipids arranged so that the polar head groups face out into the aqueous environment while the hydrophobic alkyl chains face into one another. Reverse micelles, therefore, represent a simplified lipid membrane containing only one water/lipid interface. At the same time, some features of the interfaces bear resemblance to biological membranes. For instance, water solubilized in reverse micelles has restricted mobility, a depressed freezing point, and lacks the normal hydrogen-bonded structure present in bulk water[6]. Because interfacial interactions should be similar for both reverse micelles and lipid bilayers, studies of one system are frequently compared to studies of the other[7].

The water solubilized within reverse micelles influences micelle radius, shape, and polar head group packing[2]. As a result, micelle properties are often characterized using w_0,

$$w_0 = \frac{[H_2O]}{[surfactant]} \qquad (2.1)$$

the ratio of the water concentration to the surfactant concentration. The lipid interface influences the water sequestered in the micellar interior. A variety of methods have been used to interrogate this perturbed water structure[8]. Vibrational and NMR spectroscopy have revealed distinct water environments based on their proximity to the surfactant interface. Finer[9] formally proposed that water shells are sequentially filled as hydration

of lipid bilayers increases. Each shell contains a water type that becomes progressively more bulk-like as hydration increases. The first water type is considered to be strongly bound to the surfactant head group, while the final type is considered to be bulk-like. Although details vary, several studies have proposed the existence of three water types in various reverse micellar systems[6, 10].

Two very different surfactants commonly used in the formation of reverse micelles, Aerosol OT (AOT) and lecithin, have been used in this study. The chemical structures of each are displayed in Figure 2.1. AOT is a synthetic anionic surfactant that forms spherical micelles and can solubilize large amounts of water, as high as $w_0 = 60$[8, 11]. On the other hand, lecithin is a naturally occurring phospholipid that can be purified from cellular membranes. Figure 1 shows the phosphatidylcholine which is the main component of lecithin. Unlike AOT, lecithin has a zwitterionic head group.

Lecithin reverse micelles in many nonpolar solvents possess the unusual property of forming cylindrical tubes when small amounts of water are added to the microemulsion. At a constant surfactant concentration with increasing water loading, these tubular reverse micelles extend into worm-like structures crossing one another and forming a transient entangled network[12, 13]. Macroscopically, the system appears as a viscous gel, often termed an organogel[14]. The gel is thermostable, thermoreversible, and isotropic[13]. If viscosity of a lecithin/organic solvent sample is measured vs. water addition, a maximum viscosity is reached at a given hydration level, sometimes called the percolation threshold. Further hydration results in a gradual decrease in viscosity until a phase separation point is reached[13]. While organogels may be formed in many organic solvents, cyclohexane

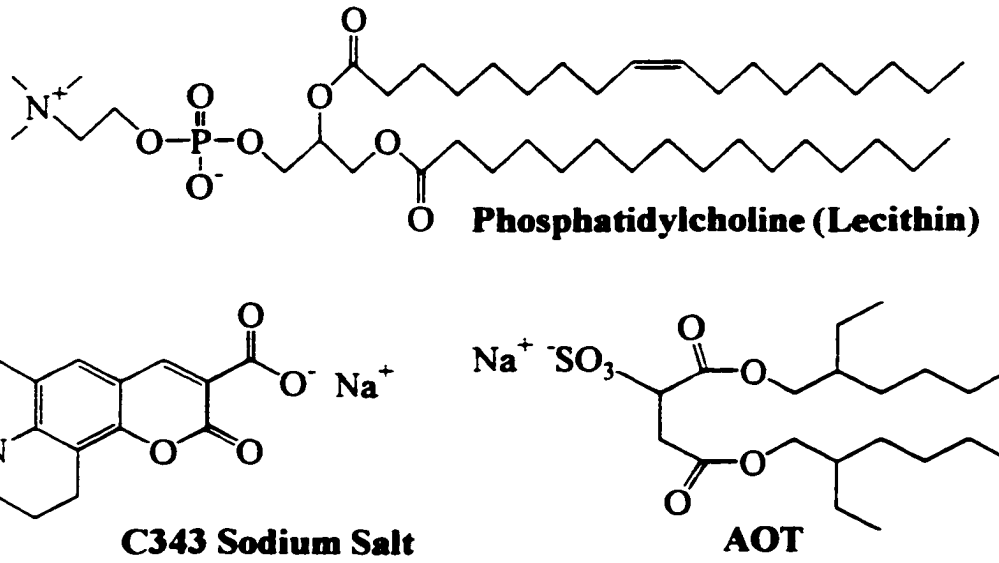

Figure 2.1. Chemical structures of the two surfactants and solvation dynamics fluorescent probe molecule used in this chapter.

allows greater hydration of the lecithin micelles before phase separation occurs than either linear or branched alkanes[4].

Lecithin organogels have recently attracted attention for several reasons. Because lecithin is a natural phospholipid, it can be used in biological applications. In this role, it can be used to deliver pharmaceuticals and cosmetics and is preferable to bioincompatible surfactants such as AOT[2]. Direct comparison between lecithin reverse micelles and lipid bilayers can be drawn since the water-head group interactions should be very similar[15]. Furthermore, the role of molecular structure in macroscopic gel formation remains a particularly challenging question[2, 16]. Current theory juxtaposes the static properties of the transient network to semidilute solutions of flexible polymers[17, 18], hence the term "living polymers". However, details of the microscopic interactions of the cylindrical micelles remain a point of contention[16, 19].

The role of water in organogel formation is not well understood. Indeed, lecithin hydration has been studied via a variety of techniques. It is well known that the structure of water at phospholipid interfaces differs significantly from bulk water. In addition, the dynamics of water also differ from bulk water. Several studies have investigated the dynamical nature of the water/lecithin interface. For example, using ^{2}H-NMR, several groups have probed the mobility of water at phosphatidylcholine bilayer surfaces[20, 21]. Whaley Hodges et al. investigated the relaxation of water in aqueous palmitoyloleoylphosphatidylcholine vesicles using proton NMR with nitroxide spin labels[22]. Enders and Nimtz[23] and Klosgen et al.[24] probed the dielectric relaxation of lecithin bilayers at microwave frequencies. Dynamical properties of various phosphatidylcholine lipid-water interfaces have also been studied via spectroscopy of

fluorescent probe molecules[25]. The major finding of all these studies is that water mobility is reduced at the lipid interface but increases with increasing hydration. However, none of these techniques is capable of measuring the ultrafast motion of water hence they are incapable of distinguishing water interacting with the interface unless its dynamical response is slowed by orders of magnitude. In addition, water mobility seems to have little correlation with the percolation threshold.

Of particular relevance to these studies are recent investigations into solvation dynamics in AOT reverse micelles. We have used ultrafast time-resolved fluorescence techniques to probe the motion of water and formamide in AOT reverse micelles[26-28]. These experiments show that the water inside the reverse micelles is significantly immobilized compared to the bulk solvents. Mittleman et al.[29] have probed the dielectric properties of water in Aerosol OT reverse micelles using subpicosecond terahertz spectroscopy. Both the timescale and amplitude of the relaxation they observed had significantly smaller amplitude than bulk water and was attributed to reduced long-range collective behavior resulting from the small water pool in the reverse micelles.

In this chapter, we report the first ultrafast measurements of the aqueous solvation dynamics in lecithin reverse micelles using the fluorescence upconversion technique. By comparing the dynamics within reverse micelles comprised of surfactants of different molecular structures, that is lecithin and AOT, we probe the surfactant interactions that dictate the dynamics of the solubilized water. In addition, we probe the dynamics of lecithin reverse micelles as a function of hydration. The dynamics are correlated with present knowledge of water structure in micelles based primarily on FTIR and NMR techniques. We also explore the relation between the aqueous dynamics and lecithin

organogel formation. Finally, we compare our results for water dynamics within lecithin reverse micelles to studies of aqueous structure and dynamics near phospholipid bilayers.

2.II. Experimental

2.II.A. Sample Preparation

Lyophilized egg phosphatidylcholine (lecithin) was purchased from Avanti Polar Lipids, Inc. A typical lecithin structure is shown in Figure 2.1. Samples were stored at -10°C prior to use and were used without further purification. Lecithin samples were always prepared from newly opened bottles to minimize water adsorption. Using the method of standard additions, ^{1}H-NMR analysis (Bruker AM•500 MHz Spectrometer) revealed 1.8 ± 0.2 mol H_2O per mol lecithin. Aerosol-OT (AOT, sodium bis-(2-ethylhexyl)sulfosuccinate, Aldrich) was dried over molecular sieves (Grade 522 5Å, Mallinckrodt) in diethyl ether, filtered, and stored as a precipitate under nitrogen gas. Analysis by Karl-Fisher titration showed the dried AOT contained 0.037 ± 0.002 mol H_2O per mol AOT. All reported w_0 values for both lecithin and AOT samples include this intrinsic water, that is, a $w_0 = 0$ value refers to completely dry surfactant. Lecithin micelles were prepared with cyclohexane (spectrophotometric grade, 99+%, Acros), while AOT micelles were prepared with isooctane (2,2,4-trimethylpentane, HPLC grade, Aldrich). Cyclohexane and isooctane were used without further purification. Added water was of high purity (Milli-Q filtered, 18.2MΩ/cm^2 resistivity).

Coumarin 343 (C343, Exciton, Inc.) was used as the fluorescent probe molecule. We use C343, in particular, because it is more readily solvated in aqueous environments

than other dyes. The aqueous solubility of C343 was enhanced via the sodium salt, shown in Figure 2.1, prepared by titrating an aqueous solution of C343 with sodium hydroxide to pH = 7, evaporating the excess water, and storing under nitrogen. When placed in either a pure cyclohexane or water/cyclohexane biphasic solution, the sodium salt form of C343 showed no detectable UV/vis absorbance or fluorescence in cyclohexane.

Reverse micellar samples were prepared as follows: lecithin was weighed into 10 ml of cyclohexane to make 5% (w/v) solutions. Assuming a lecithin density of 0.95 g/cm^3,[30] this corresponds to a volume fraction of ca. $\phi = 0.047$[31]. Water was added with a microliter syringe (Hamilton) to make a $w_0 = 3.8$ solution. Next, excess C343 sodium salt was added to the prepared solutions. Samples were briefly sonicated, and then shaken for at least 12 hours. Samples were then heated to 35°C and subsequently filtered through 0.1 μm syringe filters (PTFE, Whatman). Differing quantities of water were added to the samples with the microliter syringe to create the final samples. Samples were again shaken for at least 12 hours before use. The AOT $w_0 = 5$ sample was prepared in a similar fashion except the AOT was weighed into isooctane to create 10% (w/v) solutions, corresponding to a volume fraction of ca. $\phi = 0.10$[27].

2.II.B. Sample Characterization

Samples exhibited absorbances between 0.22 and 0.35 at 410 nm, measured in a 1 mm quartz cell. While the absorbance of the C343 dye in the samples dropped as much as 46% during the course of upconversion measurements, no shift of the absorbance or fluorescence spectra was observed indicating that the chromophore of the dye was unchanged.

Using $\varepsilon_{C343} = 1.99\times10^{-4}$ L/mol·cm[32] and $N_{agg} = 3000$ as the average micellar aggregation number of $w_0 = 4.8$ lecithin micelles,[33] we estimate that there are seven C343 molecules per micelle. This would correspond to an aqueous concentration of about 3 mM within the micellar interior. At this concentration, it is conceivable that C343 could aggregate. However, there are no reports of coumarin aggregation in the literature. Moreover, absorption spectra for C343 sodium salt in bulk water over a concentration range from 0.025 mM to 2.5 mM revealed no evidence of aggregating species. Therefore, we believe C343 exists as monomers in the micelles.

Because dryness, purity, and temperature are variables that can influence the point at which gel formation is seen from researcher to researcher, we performed viscosity measurements on the different lecithin samples for comparison. Viscosity measurements were made with a home-built viscometer. Depending on the sample's viscosity, stainless steel or glass balls were timed as they dropped down a glass tube filled with a given sample. Time measurements were converted to viscosity by calibrating the apparatus with solvents of known viscosity[34]. At 25°C, steel balls were calibrated with glycerol, while glass balls were calibrated with cyclohexane. Sample measurements were performed at 21.5°C. The viscosity of the different samples we analyzed were as follows: $w_0 = 4.8$ measured 0.1 cP, $w_0 = 5.8$ measured 5000 cP, and $w_0 = 6.8$ measured 20,000 cP. In comparison, lecithin in isooctane is reported to produce an organogel with a viscosity of 10^6 cP[35] while the viscosity of pure cyclohexane is 0.09 cP[34]. These measurements clearly show that macroscopically the samples change from a very fluid like state at $w_0 = 4.8$ to a viscous gel state at $w_0 = 6.8$.

When placed on a glass slide and observed through a Zeiss Axiophot compound microscope fitted with cross polarizers, samples showed no birefringence. The isotropic nature of these reverse micelles is in accord with previous characterizations[13, 36].

2.III. Analysis & Results

Before presenting solvation dynamics results, we first ascertained that C343 would perform as a viable reverse micelle probe. For several reasons we conclude C343 is within the reverse micelle aqueous interior. First, we have shown that C343 sodium salt has negligible solubility in cyclohexane. Therefore, we can conclude any solvated C343 is associated with the reverse micelles. Figure 2.2 reports the absorption and emission of C343 in the lecithin micelles as a function of hydration in comparison to C343 solvated in bulk water. As seen with AOT, the absorption and emission both shift to longer wavelengths with increasing hydration. Because the emission spectrum shifts with hydration, we conclude that C343 probes the aqueous interior of the lecithin reverse micelles and is, therefore, sensitive to the aqueous dynamics within them. In addition, no isosbestic point is observed in either the absorption or the emission spectra, suggesting that different populations of C343 do not exist inside and outside the aqueous interior. Finally, time-resolved anisotropy measurements revealed that C343 has a single rotational relaxation of several nanoseconds at the $w_0 = 5.8$ hydration level. If C343 was solvated in the aqueous interior, we would expect a less than 100 ps time component as we have seen with AOT reverse micelles at elevated hydrations[27]. Therefore, we conclude that C343 is probably solvated within the lipid headgroups, in contact with the aqueous interior but not freely rotating within it.

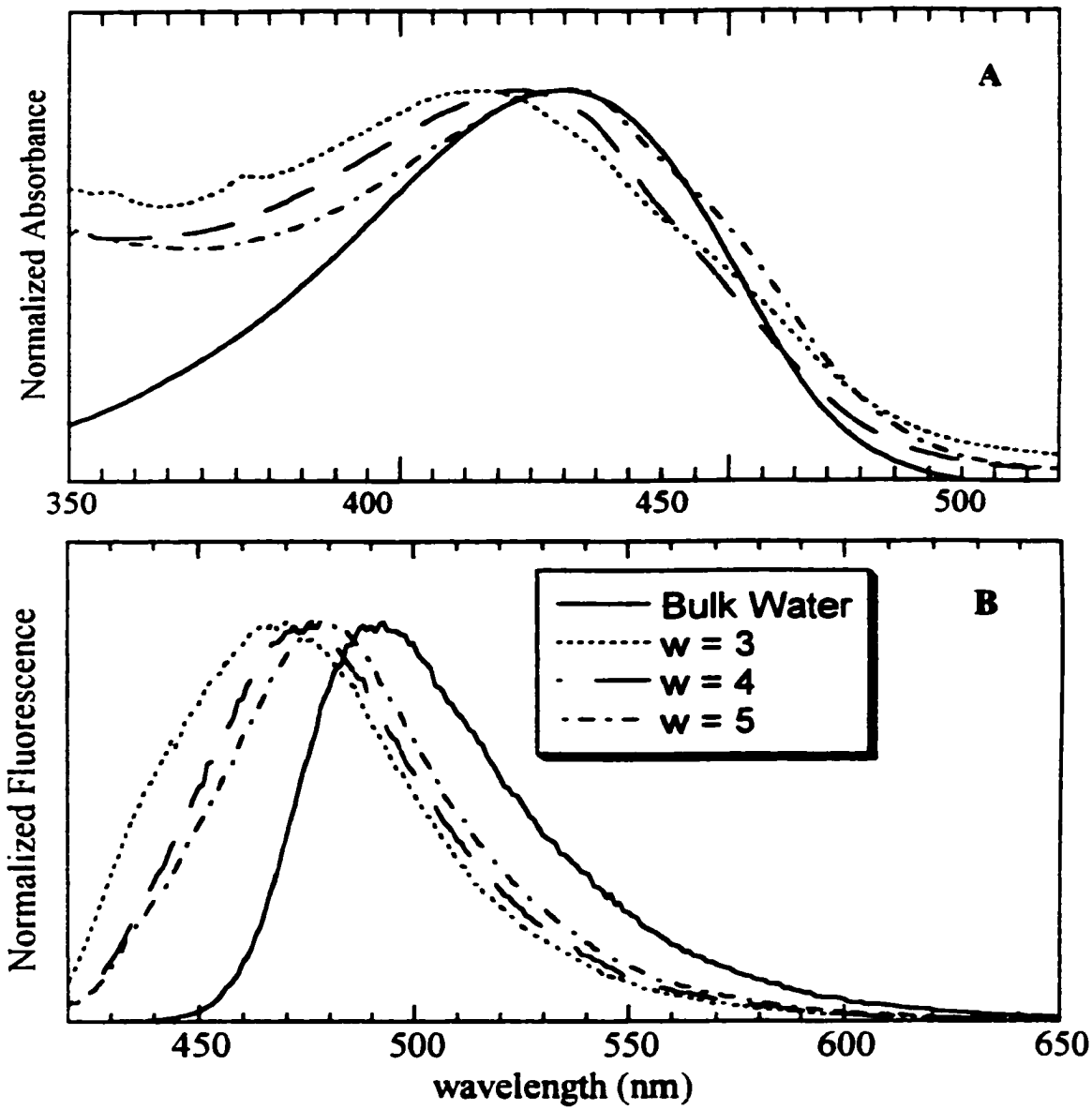

Figure 2.2. Absorption (A) and emission (B) spectra of coumarin 343 sodium salt in lecithin reverse micelles and bulk water.

The solvation dynamics for water in $w_0 = 4.8$, $w_0 = 5.8$, and $w_0 = 6.8$ lecithin in cyclohexane reverse micelles and $w_0 = 5$ AOT in isooctane reverse micelles are reported here. We obtained single-wavelength fluorescence transients over a wavelength range from roughly 440 nm to 530 nm in 10 nm increments. These decays were acquired over various time periods, that is, 2 ps and 477 ps. The time step size was adjusted to total approximately 250 time steps per scan. Thirty-three ps scans were alsc acquired for selected wavelengths of $w_0 = 6.8$ lecithin and $w_0 = 5$ AOT micelles in order to resolve dynamics on the 2 - 15 ps timescale. Figure 2.3 shows 2 ps fluorescence transients at selected wavelengths for each micellar sample. The responses for $w_0 = 4.8$ lecithin micelles are flat, revealing no solvent relaxation processes over this time period. In contrast, the transients for the AOT sample, and to a lesser extent the $w_0 = 5.8$ and $w_0 = 6.8$ lecithin samples, show significant relaxation on this time scale.

Figure 2.4 shows the C(t) points fit with multiexponential decays for cyclohexane/lecithin/water reverse micelles at three hydration levels: $w_0 = 4.8$, 5.8, and 6.8. The insets display the corresponding TRES from which C(t) was determined. Table 2.1 summarizes the numerical results of the fits displayed in Figure 2.4. For comparison, Table 2.1 also displays the spectral response of C343 in bulk water that we have previously obtained[27].

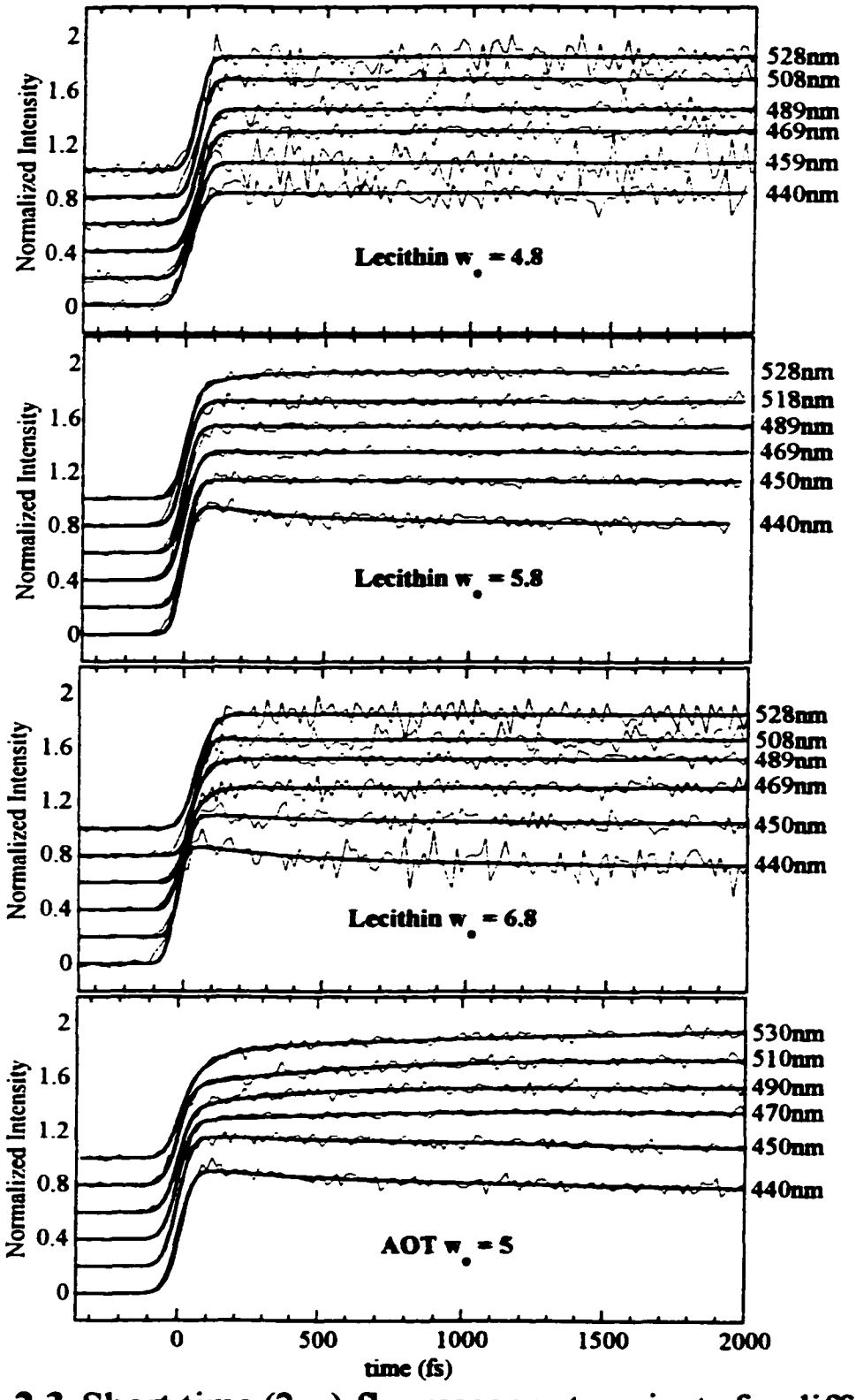

Figure 2.3. Short time (2ps) fluorescence transients for different reverse micellar environments with multiexponential fits.

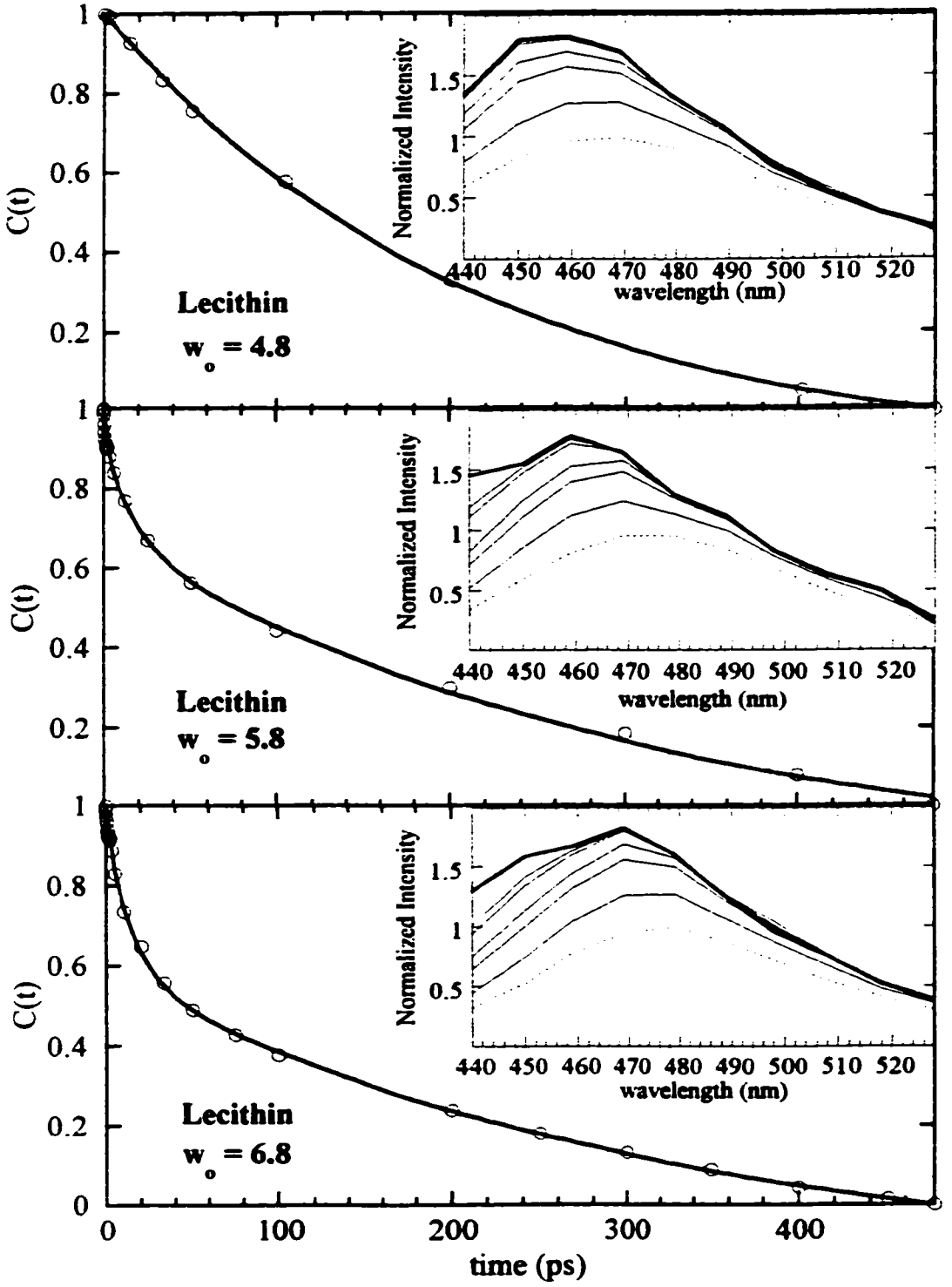

Figure 2.4. Time-correlation functions, C(t), for the different lecithin samples. Insets: TRES spectra for each lecithin sample. Dashed lines represent steady-state spectra.

Table 2.1. Multiexponential fits of the time correlation functions, C(t), for Coumarin 343 solubilized in various aqueous environments[a].

Sample[b]	a_1	τ_1 (ps)	a_2	τ_2 (ps)	a_3	τ_3 (ps)
Bulk water[c]	0.3 ± 0.3	0.2 ± 0.1	0.7 ± 0.3	0.6 ± 0.1	-	-
AOT $w_0 = 5$[c]	0.19 ± 0.03	0.3 ± 0.1	0.19 ± 0.03	6 ± 2	0.63 ± 0.02	130 ± 10
Lecithin $w_0 = 4.8$[d]	1.00 ± 0.01	219 ± 7	-	-	-	-
Lecithin $w_0 = 5.8$[d]	0.100 ± 0.003	0.42 ± 0.03	0.17 ± 0.03	17 ± 7	0.74 ± 0.07	340 ± 100
Lecithin $w_0 = 6.8$[d]	0.13 ± 0.01	0.57 ± 0.07	0.25 ± 0.01	14 ± 1	0.62 ± 0.02	320 ± 40

[a] $C(t) = \sum_i a_i \exp(-t/\tau_i)$. [b] Uncertainties refer to standard error associated with each parameter obtained from a single multiexponential fit of the time correlation function. [c] Results taken from ref [27]. [d] Longest relaxations were not fully complete by 477 ps. The amplitudes have been normalized by taking this into account.

The results from the solvation dynamics experiments show a number of interesting features. First, as the hydration of the lecithin micelles increases, the number of distinct decay components increases. For $w_0 = 4.8$ lecithin micelles, there exists only a single relaxation. In contrast, both $w_0 = 5.8$ and $w_0 = 6.8$ lecithin micelles display three components to the decay. Second, while the amplitudes for each decay component change with hydration, the time-constants remain largely constant. Third, the relative relaxation for similarly hydrated lecithin and AOT micelles reveal significant departure from each other. Finally, all micellar samples show additional relaxation components with longer time-constants that are not present in bulk water. Each of these points is discussed and interpreted in detail in the following section.

2.IV. Discussion

2.IV.A. Lecithin Hydration

While a variety of techniques have been used to correlate microscopic structure with macroscopic viscosity associated with organogel formation, several questions remain

unanswered[37]. The experiments reported here present a unique perspective on the mechanism of the organogel formation. However, while we employ a unique technique, we make several direct comparisons to the current view of organogel structure and dynamics. Before comparing our results to previous studies, we review the most applicable points.

Many studies have attempted to correlate properties of phospholipid components with the onset of organogel formation. While the choline moiety of the head group shows insignificant changes upon hydration[38], the properties of the phosphate groups, carbonyl groups, and alkyl chains have shown progressive trends correlating with organogel formation. The phosphate atom NMR linewidth has been shown to reach a maximum at the percolation threshold[37, 38]. Similarly, the frequency of the P=O stretching vibration, measured using FTIR, shifts to lower energies until the percolation threshold is reached and then levels off[19, 39]. These findings have been interpreted as the phosphate moiety becoming increasingly hydrogen bonded with increased hydration that culminates in a decrease in local motion at the percolation point. In contrast, the carbonyl moiety seems to only show water interactions at elevated hydration levels. Like P=O, the frequency of the C=O stretching vibration also shifts to lower energies, but only at hydration levels higher than the percolation threshold[39]. The lipid chain C-H symmetric and antisymmetric stretching vibrations display evidence of increased lateral packing order with increasing hydration. However, the increasing order shows no correlation with gel formation[40].

Previous studies have explored the behavior of water at the various hydration stages leading to organogel formation using NMR and FTIR techniques[37, 38, 40, 41].

While these studies reveal the expected trend that water becomes less restricted with increasing hydration, they do not correlate with organogel formation. These studies suggest that the first 1-2 water molecules added to the system become strongly coordinated to the phosphate moiety. Further hydration, even past the percolation threshold, results in the aqueous environment becoming progressively more bulk-like in nature. While there is evidence for the existence of three water types in the spherical non-organogel forming lecithin/benzene reverse micelles[10], studies of lecithin/cyclohexane reverse micelles detect only two types, strongly bound and free. In contrast, by accounting for solvated monomers, Maitra et al.[41] find that for micelles between w_0 = 4.8 to 6.8, the hydration range we have studied, half the water population is bound and the other half free. From these studies it is clear that (1) two water types are detected for the entire hydration level we have probed, and (2) the water structure shows no correlation with the onset of organogel formation.

While there are several microscopic trends that coincide with the formation of the organogel, there is little proof for tubular micelle crossover or branch points that should be prevalent at the percolation threshold[16, 19]. According to the organogel model proposed by Schurtenberger et al. [35, 42], upon increasing hydration, the mean length of the worm-like micelles should reach a threshold value at which a transient network is formed and the system undergoes a macroscopic phase transition to the gel-like form. It is hypothesized that at the percolation threshold, worm-like micelles pass through each other, creating structural anomalies at crossover points not seen at lower hydration levels. These crossover points should be evident in the motion of the CH_2 groups of the lipid tails. However, Arcoleo et al. argue that no discontinuity in the CH_2 region of the FTIR

spectrum is observed and question whether crossover points are the source of the increased viscosity of the lecithin system[16]. We note that microscopic anomalies have been seen at the percolation threshold in a series of papers by Kumar et al. [43-46]. However, since their organogel was described as anisotropic while our organogel and all others reported in this chapter have been shown to be isotropic, direct comparisons are not warranted.

In comparison to the current structural view of organogel formation, our results reveal some interesting points. From our dynamical results, we find that faster relaxation processes appear sequentially with increasing hydration in the same manner different water types appear structurally from FTIR and NMR techniques. We therefore attribute the different time constants to different water types and the relative amplitudes of the components to the amount of each water type. While previous studies have detected only strongly bound and free water in water/lecithin/cyclohexane reverse micelles, our results clearly show the existence of three distinct water types. We attribute the three relaxation times to strongly bound, bound, and free states. The single 220 ps relaxation that we observe for $w_0 = 4.8$ is attributed to very slow, hindered water relaxation. In contrast, diffusive relaxation in bulk water occurs on the 0.2 and 0.6 ps time scales (See Table 2.1). Since this 200 ps relaxation is so much slower than free water, it is unlikely to be due exclusively to water motion. Furthermore, because there are 4.8 water molecules per head group, it is just as unlikely that the observed dynamics arise exclusively from head group motion. Rather, the observed dynamics most likely reflect coupled motion of the water and head group. We therefore assign the water populations with relaxation time components longer than 200 ps to strongly bound water. At hydration levels above $w_0 =$

4.8, we observe additional relaxation components. For the $w_0 = 5.8$ and $w_0 = 6.8$ micelles, we see two additional relaxation processes with time constants of about 15 ps and 0.5 ps. We attribute the 15 ps population to bound water because it displays intermediate relaxation between strongly bound and free water. We attribute the 0.5 ps population to free water since the relaxation time is similar to bulk water (See Table 2.1).

Although the relative amplitudes can be thought of as indicating ratios of the different water populations, they do not necessarily reflect the *actual* ratios at a given hydration level for a number of reasons. First, the presence of the probe molecule perturbs the environment. This is significant because our results are compared to FTIR and NMR techniques that do not require a probe molecule. Furthermore, some solutes present in the micellar interior have been shown to redistribute water organization[15]. However, C343 and related coumarins are not reported to have specific interactions with water[47]. Therefore, while the probe may perturb the aqueous environment to some degree, it is unlikely that this perturbation approaches that of the lecithin head group. Second, the position of the individual probe molecules within the micelles is not well defined; most likely, the molecules span a distribution of locations with preference near the interface. Time-resolved fluorescence anisotropy measurements of C343 in AOT reverse micelles shows that the probe is preferentially located at the lipid interface[27]. While time constants are not influenced, it is probable that the spatial location of the probe molecules in the lecithin micelles influences the relative relaxation amplitudes. However, it is unlikely that the spatial distribution varies over the hydration range we have studied. Therefore, we are justified in comparing the relative amplitudes from one hydration level to the next. In Table 2.1, we see that the populations of both bound and free water

increase while the relative population of the strongly bound water decreases as hydration goes from $w_0 = 5.8$ to 6.8. As we would expect, the dynamics of the micellar interior become less restricted and more bulk-like in nature as hydration increases.

It is possible C343 interacts with components of the surfactant head groups such as the Na^+ counterion in AOT or the cationic quaternary ammonium on lecithin. Such interactions could conceivably account for relaxations that proceed in the picosecond regime. We have observed a 100 ps relaxation component for C343 in 1 M aqueous Na_2SO_4[27]. If the 15 ps component appearing at $w_0 \geq 5.8$ is due to such interaction, then it should be manifest at every hydration level decreasing in amplitude as the hydration increases. To the contrary, the 15 ps component appears only above $w_0 = 4.8$ and *grows* with increasing hydration. One could also argue that the 200 ps component observed arises exclusively from dye-headgroup interactions. Again this seems unlikely because that would preclude any aqueous dynamics in micelles containing 4.8 water molecules per headgroup.

The three distinct water types seen in these studies are not only a noteworthy finding in comparison to organogel hydration studies, but also with respect to reverse micellar and lipid bilayer studies in general. The relaxation times reported here associated with strongly bound, bound, and free water vary little with changing hydration, while their relative populations do. This provides strong evidence that distinct water types exist and remain invariant as micelle hydration level changes. This is an important finding because there has been considerable debate over whether distinct water types actually exist since the model was formally introduced by Finer[9] in 1973. Several studies have interpreted

results to conclude that the water properties evolve smoothly, or at least quasi-continuously, as hydration of a lipid bilayer[21, 23, 48, 49] or reverse micelles[7, 50] increases. If there truly is a quasi-continuous water organization, our data would show gradual shifting of relaxation times as hydration is increased. However, we see the *same* relaxation times at all hydration levels with only relative *amplitudes* changing.

The hydration levels at which the different water types appear in our studies disagree with previous lecithin organogel studies. We find that all water is strongly bound in the $w_0 = 4.8$ micelles. Furthermore, while we do observe free water in $w_0 = 5.8$ and $w_0 = 6.8$ micelles, it represents a relatively small population. Based on the relative amplitude of the free water signal, we estimate that the free water population in the $w_0 = 6.8$ micelles is, at most, one water per head group. Since the addition of the first few water molecules induces the tubular micelle structure, previous researchers have assumed these water molecules are incorporated into the lipid head group[35, 36, 51-53]. However, FTIR and NMR studies, suggest that all further water addition is bulk-like in nature. Clearly, our results reveal the aqueous interior of the lecithin organogel contains much less free water than has previously been predicted. As will be discussed in the next section, we believe this arises due to the lipid head groups sequestering water to a greater extent than predicted from static studies.

We find that at least 4.8 water molecules per head group are strongly bound, while predictions state that only 1 - 2 water molecules are strongly bound. While it is possible that the first 1 - 2 water molecules are more strongly coordinated than the subsequent 3 - 4 water molecules comprising $w_0 = 4.8$, the time correlation function shows no evidence that part of the water is substantially more immobilized than the rest. Furthermore, the

200 ps relaxation observed is very slow for aqueous motion indicating that all water at w_0 = 4.8 is strongly bound. The apparent discrepancy between previous work indicating 1 - 2 strongly bound water molecules per lecithin headgroup and the work reported here most likely stems from the fact that structure and dynamics are not equivalent[28]. A significant water population may appear bulk-like in FTIR and NMR studies but at the same time have hindered solvation dynamics due to its position, for example, intercalated between lipid head groups. We have observed a similar effect for formamide sequestered in AOT reverse micelles [28]. In this case, the static structure indicated by FTIR studies reveals essentially bulk-like characteristics while dynamical measurements show that the solvent is completely immobilized. In addition, the lack of agreement can be attributed to the sensitivities of the detection method. FTIR analysis involves deconvolution of the different water types from a single peak[10]. If relative populations are small, as our results suggest for both bound and free water, analysis becomes difficult. Dielectric studies suffer a similar drawback requiring deconvolution of a small perturbation from a single spectroscopic anomaly[19, 23]. Proton and deuterium NMR identify different types by deconvolving the separate time constants from a single T_1 relaxation study[54]. If different types have similar time constants, deconvolution becomes challenging. Moreover, if exchange between different types occurs on a timescale faster than the experiment, a single weighted average relaxation will be observed. The time-resolved fluorescence experiments reported here follow motion on a much faster timescale than diffusional exchange processes. Therefore, water populations are essentially frozen on the timescale of the experiment. Also, the technique is sensitive to motion of small populations as long as the relaxation is significantly different from others.

Finally, like previous studies, we find no evidence for crossover point anomalies as the percolation threshold is approached. It is likely that our $w_0 = 6.8$ micelles are not quite at the percolation threshold. We anticipate our samples would reach maximum viscosity at about $w_0 = 8$. Therefore these results only show the aqueous dynamics as hydration *approaches* the percolation threshold. As can be seen in Table 2.1, less restricted water types appear with increasing hydration in a very predictable way with relaxation times remaining constant while the relative amplitudes change. The formation of crossover points at higher hydration levels should result in new and shifting relaxation processes. We see no evidence for this and conclude that macroscopic rheological properties have no apparent correlation with aqueous dynamics in agreement with others[37, 38, 40, 41].

2.IV.B. Lecithin vs. AOT Hydration

Comparison of relaxation in AOT and lecithin micelles shows that water in AOT reverse micelles approaches bulk-like dynamics at significantly lower hydration levels than lecithin reverse micelles. Our previous work has shown a growing population of free water with increasing hydration of AOT micelles[27]. Although the degree of hydration possible in AOT micelles is significantly greater than lecithin, we observed the same general trend of increasing bulk-like dynamics with hydration. However, the first appearance of free water in lecithin micelles appears as a faint relaxation at $w_0 = 5.8$, while in AOT micelles we detect a significant free water relaxation at $w_0 = 5$. As Table 2.1 indicates, even the dynamics of the $w_0 = 6.8$ lecithin micelles are slower than the dynamics of $w_0 = 5$ AOT micelles.

The relative increased water mobility in the AOT micelles over the lecithin micelles is, at first glance, counterintuitive. AOT should perturb the water strongly from ion-dipole interactions with the SO_3^- and Na^+ head group ions. In comparison, interactions with the phosphate and choline moieties of the zwitterionic lecithin head group should present a much softer ion-dipole interaction. FTIR and NMR studies suggest that the AOT head group should require a greater hydration to stabilize lipid-lipid interactions than the lecithin head group. Studies of AOT have concluded that 3 - 4 water molecules are strongly bound to the sulfate moiety[55-57]. In contrast, lecithin studies have found only 1 - 2 water molecules strongly bound to the phosphate moiety[37, 38, 40, 41].

To explain the discrepancy between our results and what would be expected, we propose that, at least at low hydration levels, lecithin does not form well defined core water pools to the same extent AOT does. For AOT, the first few water molecules bind to the sulfonate and sodium ions[56, 57]. FTIR studies have shown that the AOT carbonyl groups show no shifting attributed to water interactions as hydration increases[56, 57]. After the first few water molecules pack around the sulfonate, additional water molecules become localized in core water pools rather than interacting with the AOT carbonyl groups or between the alkyl chains. Conversely for lecithin micelles, we propose that, at low hydration levels ($w_0 \leq 4.8$), water associates with the phosphate group and becomes sequestered in the head group region, unable to coalesce into core pools. Like the sulfonate group of AOT, the phosphate group is the initial site of hydration. However, the lecithin head group occupies significantly more volume than the AOT head group (see Figure 2.1). Therefore, water added once the phosphate group is hydrated can still hydrate the head group without coalescing to form core pools. Using

FTIR, Maitra et al.[41] have shown that with increasing hydration, the frequency of the P=O stretching vibration shifts up to hydration levels of about $w_0 = 4 - 5$. Further evidence suggesting that the hydration of the lecithin head group is more extensive than AOT comes from the behavior of the ester groups. Unlike AOT,[56, 57] Maitra et al. also find that the C=O frequency shifts above hydration levels $w_0 = 4$, suggesting that the carbonyl moieties interact with the water.

Geometrical arguments based on small-angle neutron scattering (SANS) and dynamic light scattering (DLS) also suggest that lecithin lacks a defined water core at low hydration levels, while AOT does not. Drawing from SANS data of $w_0 = 1$ AOT micelles, Kotlarchyk et al. [58] find the micelle dimensions allow for the existence of a water core of one water molecule per head group. Additionally, Gorski et al. [59, 60], also interpreting SANS data, have found that AOT micelles in benzene and decane have spherical radii that are larger than would be expected based on accepted volumes of water and AOT molecules. They show that only at substantial hydration levels ($w_0 \geq 20$) do the measured and predicted radii agree. DLS data show the spherical radius of AOT micelles increases linearly with increasing hydration, even below $w_0 = 5$; the micellar radii increase from 15 Å at $w_0 = 0$ to ca. 100 Å at $w_0 = 50$[11, 31]. These results show AOT micelles have a substantial aqueous core. In direct contrast, dimensions of lecithin reverse micelles suggest a lack of available space to form a defined aqueous core. SANS data of $w_0 = 1 - 3$ lecithin micelles in isooctane has shown that the cross-sectional radius is constant over this hydration range (ca. 30 Å). This led Schurtenberger et al. [13] to suggest that added water distributes radially throughout a very extended head group region. SANS data of

lecithin in cyclohexane at higher hydration levels ($w_0 \geq 6$) revealed similar evidence that there is considerable penetration of the water molecules into the interfacial region, although a defined water core did seem evident at these hydration levels[61]. Wachtel et al. [36] have used DLS to investigate lecithin in cyclohexane reverse micelles. Assuming a uniform cylindrical reverse micelle shape, their data showed modest cross-sectional radius increases from $w_0 = 1$ to $w_0 = 5.4$ (ca. 110%)[36]. [While Wachtel et al. report hydration levels excluding the intrinsic one water molecule per lecithin molecule, we add this to the w_0 value listed here to make direct comparison with our work possible.] To further illustrate, assuming the water molecular volume is about 30 $Å^3$, 1.7 lecithin molecules per angstrom align along the micellar contour[61], and 1 water molecule per lecithin becomes bound to the phosphate moiety of the head group, we estimate the radius of Wachtel's cylindrical micelles[36] would increase 340% at the $w_0 = 5.4$ hydration level if the remaining 4.4 water molecules formed an aqueous core instead of incorporating into the head groups.

In addition to experimental evidence, there is also a theoretical basis supporting the interpretation that a significant population of water exists radially distributed in the head group without forming a bulk-like core pool. It has been established that lecithin micelles are transformed from spherical micelles to long cylindrical aggregates with small additions of water[13, 35]. According to the theory of lipid packing parameters developed by Israelachvili et al. [3, 62] in order for micelles to transform from spherical to cylindrical the phospholipid head group area must increase or the chain volume must decrease. Because water addition initiates the transformation, we can assume that the head group

area increases due to water incorporation. If lecithin forms planar sheets, such as lipid bilayers, even greater head group hydration should be detected than in reverse micelles. While FTIR and NMR studies of lecithin reverse micelles find 1 - 2 bound water molecules, similar studies of lecithin in lipid bilayers suggest at least 6 and as many as 11 water molecules per head group are incorporated into the head group[9, 63, 64]. Also, simulations of lipid bilayers conclude that significant water populations become trapped within the head group region[65, 66]. Koga et al. have argued this point suggesting that head group surface area of lecithin in small micelles in isooctane increases from 30 $Å^2$ to 61-74 $Å^2$ when compared to the head group area of bilayer vesicles[67]. Because lipid morphology seems to control hydration, this analysis suggests that water incorporation into the lecithin head group region is thermodynamically driven by lipid chain interactions rather than specific water-head group interactions. In contrast, AOT reverse micelles show no morphological changes, remaining spherical at all hydration levels below w_0 = 60[11]. We argue that there is no thermodynamic driving force to incorporate water into the head group past 3 - 4 strongly bound water molecules. Therefore as would be expected, AOT shows only modest head group surface area increases as hydration increases[68].

While there is ample evidence, there is no definitive proof that the lecithin head group is hydrated to a greater extent than the AOT head group. However, our results coupled with the supporting evidence make a strong case. We find that even though the AOT head group should have stronger water interactions than the lecithin, the water dynamics in AOT micelles become more bulk-like at lower hydration levels. Therefore,

the extent that surfactant head groups perturb interfacial water depends not only on specific water-head group interactions, but also on the interfacial interactions as a whole. In the case of lecithin, we suggest a greater population of water is perturbed because lipid chain interactions encourage increased hydration. This conclusion is not very surprising if we consider that previous studies have already concluded that the hydration capacities of phospholipids depend on the state of their lipid chains[63]. Whether the 4.8 strongly bound water molecules per head group are actually immobilized with specific head group interactions remains unanswered. It may be that the strongly bound water actually has loose head group interactions. But, because the water is incorporated between head groups, the water is effectively hidden from the probe molecule. In any case, we conclude a solvated molecule will experience no solvation dynamics faster than 200 ps in a $w_0 = 4.8$ lecithin micelle. We also conclude that while techniques assessing the structural aspects of water intercalated into the head group region, i.e. FTIR and NMR, reveal only minor perturbations, our dynamical measurements show water motion is significantly impacted.

2.IV.C. Implications

While many studies have probed the dynamics of water at lecithin interfaces in lipid bilayers, the results reported here are unique in that we probe the interface in reverse micelles. Unfortunately, there are no experiments with which we can compare our dynamics results directly. However, there are a plethora of computer simulations predicting the structure and dynamical behavior of water at a variety of lecithin interfaces. The bulk of these studies have focused on the structure of the model membrane, bilayer or lamellar interfaces[69-71]. A handful of reports discuss the dynamics of water at bilayer

or lamellar interfaces. We are unaware of any simulations, structure or dynamics, of lecithin reversed micellar organogels. Again, the morphology difference between our micelles and the calculated lipid bilayers makes direct comparison of the results reported here with the computer simulations unclear. However, because the same water head group interactions persist, we can still mark the predicted trends to learn whether our observations are supported by the predictions.

The major finding of the computer simulations is similar to the predictions one would make from structural studies, that is, the water molecules bound to the surfactant interface suffer significant reduction in their mobility[72-75]. However, many details differ from our findings. For example, both Klose et al.[74] and Damodaran et al.[72, 73] have predicted two hydration shells for water near phosphatidylcholine and phosphatidylethanolamine bilayers on the basis of calculated radial distribution functions. The dynamics of the water in each shell differs from bulk water. However, Damodaran et al. predict the water orientational correlation time, which is longer than measured solvation dynamics[76], are ~12 ps for "bound" water and ~4 ps for "bulk" water. Klose et al. predict motion on the picosecond timescale due to an oscillation of water molecules about the preferred hydration site. The times reported for bound water in these simulations are significantly faster than motion we observe. However, the structure predicted in both these simulations entails two hydration shells, bound and free, differing from our interpretation of strongly bound, bound and free water. Raghavan et al.[75] have modeled reorientation times for water between phosphatidylethanolamine bilayers including no "bound" water. While their reorientation times are slightly slower for water molecules close to the bilayer surface, they are faster than bulk water in the middle of the

bilayers. In molecular dynamics simulations of dimyristoylphosphatidylcholine monolayers, Alper et al.[77, 78] have predicted three hydration shells about the lipid head groups. They predict that the motion of the hydrating, or bound, water is about ten times slower than bulk water. Often direct comparison between experiment and simulation is difficult or impossible because simulations cannot run long enough to model the observed dynamics. In our case, the timescale for our experiment is short enough to preclude this problem so it should be possible for structural molecular dynamics simulations to propagate dynamical information about the water motion for a direct comparison with our results. We find that, while these simulations do predict the general trends that motion of water near interfaces is reduced, the simulations do not seem to either agree on the timescale of bound water motion or predict the reorientation times even close to those that we observe. There exist several reasons for this discrepancy. First, lecithin is a mixture of a variety of phospholipid molecules with differing hydrophobic regions. Therefore, the mixture that we use may preclude direct comparison. Second, the morphology of our systems ranges from small quasispherical droplets to long tubular chains. All the simulations look at planar interfaces. So, while there exists hydrating water in both systems, the curvature of the micellar interface may impact the water dynamics. Finally, we note that our experiments might preclude observation of water that is sequestered in a cavity located some distance from the probe molecule. That is, our experiments might not reveal mobile water hidden deep within the alkyl chains.

One important application of lecithin reverse micelles is in the study of enzyme activity. There have been many studies done following the activity of enzymes sequestered in the interior of reverse micelles. These studies have shown that the enzymes

show activity in these synthetic environments[79-81]. Interestingly, some enzymes display maximal activity at a relatively low water hydration level, with activity dropping for increasing hydration levels. For example, in the case of trypsin and α-chymotrypsin in lecithin reverse micelles, the optimal hydration level for maximal enzyme activity was found between $w_0 = 7$ and 10. Perhaps even more importantly, some enzymes display enhanced activity over the native state[82]. Hence, the reverse micellar organogels studied here could serve as excellent alternative environments for biocatalysis. In a theoretical study, Bru et al. suggest that bound water may be important to activate catalytic activity of enzymes in reverse micelles[83]. Luisi et al. have hypothesized that 1-2 molecules of the water available in a reverse micellar lecithin organogel are tightly bound to the phosphate moiety[84]. We find that at least 4.8 water molecules are involved in head group hydration. Clearly, to understand the observed super-activity of enzymes in micellar environments and tailor systems for biocatalysis, requires an improved understanding of water dynamics in these reverse micellar systems.

2.V. Conclusions

This chapter reports the first ultrafast aqueous dynamics measured near a phospholipid interface. By comparing the dynamics of sequential hydration levels, our results provide a unique perspective of the water structure and mobility within the lecithin organogel. Dynamics reveal three distinct water types that appear with increasing hydration. We show that the dynamics are much more restricted than has previously been predicted by FTIR and NMR spectroscopic investigations. More specifically, we find no

free water at the $w_0 = 4.8$ hydration level and not more than one free water molecule per lecithin molecule at the $w_0 = 6.8$ hydration level. We also see no evidence for crossover or branch points in the measured aqueous dynamics, even though the sample exists macroscopically as a viscous gel. We find that lecithin perturbs the water core to a much greater extent than similar AOT reverse micelles. We explain these findings by proposing that lecithin, unlike AOT, sequesters water to a much greater degree than has previously been predicted.

Although we examined the dynamics within reverse micelles, our results also have significance for understanding the aqueous structure and dynamics near other lipid interfaces. For example, we have related the water that is incorporated into the head groups to the water that others have concluded as trapped within the phospholipid interface. Comparison of our dynamical results to dynamics determined by computer simulations at lipid surfaces show that while the trends observed agree, the timescales we measure for water motion are substantially longer than what the simulations predict. We hope that our dynamical results of motion within reverse micelles can be used as a first approximation to predicting dynamics near a lipid interface.

2.VI. Acknowledgments

We greatly appreciate advice from Prof. Peter Schurtenberger during the course of this work.

References for Chapter 2

1. Luisi, P.L. and B.E. Straub, eds. *Reverse Micelles. Biological and Technological Relevance of Amphiphilic Structures in Apolar Media.* . 1987, Plenum Press: New York.

2. Walde, P., *et al.*, *Phospholipid-based reverse micelles.* Chem. Phys. Lipids, 1990. **53**: p. 265-88.

3. Israelachvili, J.N., *Intermolecular & Surface Forces*. 2nd ed. 1991, San Diego: Academic Press, Inc.

4. Luisi, P.L., *et al.*, *Reverse micelles as hosts for proteins and small molecules.* Biochim. Biophys. Acta., 1988. **947**: p. 209-46.

5. Maestro, M., *Enzymatic activity in reverse micelles-some moldellistic considerations on bell-shaped curves.* J. Molec. Liq., 1989. **42**: p. 71-82.

6. Jain, T.D., M. Varshney, and A. Maitra, *Structural studies of Aerosol OT reverse micellar aggregates by FT-IR spectroscopy.* J. Phys. Chem., 1989. **93**: p. 7409-16.

7. Grdadolnik, J., J. Kidric, and D. Hadzi, *An FT-IR study of water hydrating dipalmitoylphosphatidylcholine multibilayers and reversed micelles.* J. Molec. Struc., 1994. **322**: p. 93-103.

8. De, T. and A. Maitra, *Solution behavior of Aerosol OT in non-polar solvents.* Adv. Colloid Interface Sci., 1995. **59**: p. 95-193.

9. Finer, E.G., *Interpretation of deuteron magnetic resonance spectroscopic studies of the hydration of macromolecules.* J. Chem. Soc. Faraday Trans. II, 1973. **69**: p. 1590-1600.

10. Boicelli, C.A., M. Giomini, and A.M. Giuliani, *Infrared characterization of different water types inside reverse micelles.* Appl. Spec., 1984. **38**(4): p. 537-9.

11. Zulauf, M. and H.F. Eicke, *Inverted micelles and microemulsions in the ternary system H2O/Aerosol-OT/Isooctane as studied by photon correlation spectroscopy.* J. Phys. Chem., 1979. **83**(4): p. 480-6.

12. Schurtenberger, P., *et al.*, *Cylindrical structure and flexibility of polymerlike lecithin reverse micelles.* J. Phys. Chem., 1991. **95**(11): p. 4173-6.

13. Schurtenberger, P., *et al.*, *Structural and dynamic properties of polymer-like reverse micelles.* J. Phys. Chem., 1990. **94**(9): p. 3695-701.

14. Scartazzini, R. and P.L. Luisi, *Organogels from lecithins.* J. Phys. Chem., 1988. **92**(3): p. 829-833.

15. Boicelli, C.A., *et al.*, *Water organization in reversed micelles.*, in *Physical Methods on Biological Membranes and Their Model Systems*, F.B. Conti, W. E.; de Gier, J.; Pocchiari, F., Editor. 1985, Plenum Press: New York.

16. Arcoleo, V., *et al.*, *Study of lecithin reverse micelles by FT-IR spectroscopy.* Prog. Colloid Polym. Sci., 1997. **105**: p. 220-3.

17. Schurtenberger, P., *Structure and dynamics of viscoelastic surfactant solutions-an application of concepts from polymer science.* Chimia, 1994. **48**: p. 72-8.

18. Cates, M.E. and S.J. Candau, *Statics and dynamics of worm-like surfactant micelles.* J. Phys.: Condens. Matter, 1990. **2**: p. 6869-92.

19. Cirkel, P.A., J.P.M. van der Ploeg, and G.J.M. Koper, *Headgroup mobility in lecithin inverse worm-like micelles.* Prog. Colloid Polym. Sci., 1997. **105**: p. 204-8.

20. Takahashi, A., T. Takizawa, and Y. Nakata, *A deuteron NMR study of the dynamics of water molecules bound tightly to the phosphate group in dipalmitoyl-phosphatidylcholine-D2O system.* J. Phys. Soc. Jpn., 1996. **65**(2): p. 635-642.

21. Volke, F., *et al.*, *Dynamic properties of water at phosphatidylcholine lipid-bilayer surfaces as seen by deuterium and pulsed field gradient proton NMR.* Chem. Phys. Lipids, 1994. **70**: p. 121-31.

22. Whaley Hodges, M., *et al.*, *Water translational motion at the bilayer interface: An NMR relaxation dispersion measurement.* Biophys. J., 1997. **73**(5): p. 2575-2579.

23. Enders, A. and G. Nimtz, *Dielectric relaxation study of dynamic properties of hydrated phospholipid bilayers.* Ber. Bunsenges. Phys. Chem., 1984. **88**: p. 512-7.

24. Klosgen, B., *et al.*, *Dielectric spectroscopy as a sensor of membrane headgroup mobility and hydration.* Biophys. J., 1996. **71**(6): p. 3251-3260.

25. Lakowicz, J.R. and D. Hogen, *Dynamic properties of the lipid-water interface of model membranes as revealed by lifetime-resolved fluorescence emission spectra.* Biochemistry, 1981. **20**: p. 1366-1373.

26. Riter, R.E., E.P. Undiks, and N.E. Levinger, *The impact of the counterion on water motion in Aerosol OT reverse micelles.* J. Am. Chem. Soc., 1998. **120**(24): p. 6062-7.

27. Riter, R.E., D.M. Willard, and N.E. Levinger, *Water immobilization at surfactant interfaces in reverse micelles.* J. Phys. Chem. B, 1998. **102**(15): p. 2705-14.

28. Riter, R.E., *et al.*, *Formamide in reverse micelles: restricted environments effects on molecular motion.* J. Phys. Chem. B, 1998. **102**(41): p. 7931-8.

29. Mittleman, D.M., M.C. Nuss, and V.L. Colvin, *Teraherz spectroscopy of water in inverse micelles.* Chem. Phys. Lett., 1997. **275**: p. 332-338.

30. Aliotta, F., *et al.*, *Hyperacoustic properties and percolation effects in polymer-like lecithin reverse micelles.* J. Phys. Chem., 1993. **97**(24): p. 6541-5.

31. Riter, R.E., *et al.*, *Novel reverse micelles partitioning nonaqueous polar solvents in a hydrocarbon continuous phase.* J. Phys. Chem. B, 1997. **101**(41): p. 8292-7.

32. Brackmann, U., *Lambdachrome Laser Dyes Data Sheets.* 2nd revised ed. 1994, Gottingen, Germany: Lambda Physik GmbH.

33. Schurtenberger, P. and C. Cavaco, *Polymer-like lecithin reverse micelles. 1. A light scattering study.* Langmuir, 1994. **10**: p. 100-8.

34. Riddick, J.A., W.B. Bunger, and T.K. Sakano, *Organic Solvents.* 4 ed. Techniques of Chemistry, ed. A. Weissberger. Vol. II. 1986, New York: John Wiley and Sons. 1325.

35. Luisi, P.L., *et al.*, *Organogels from water-in-oil microemulsions.* Colloid Polym. Sci., 1990. **268**: p. 356-74.

36. Wachtel, E., S. Federman, and N. Greenspoon, *Interaction of carbohydrates with phosphatidylcholine inverse micelles.* Israel J. Chem., 1992. **32**: p. 113-9.

37. Capitani, D., E. Rossi, and A.L. Segre, *Lecithin microemulsion gels: an NMR study.* Langmuir, 1993. **9**: p. 685-9.

38. Capitani, D., A.L. Segre, and R. Sparapani, *Lecithin microemulsion gels: a NMR study of molecular mobility based on line widths.* Langmuir, 1991. **7**: p. 250-3.

39. Shervani, Z., T.K. Jain, and A. Maitra, *Nonconventional lecithin gels in hydrocarbon oils.* Colloid Polym. Sci., 1991. **269**: p. 720-6.

40. Cavallaro, G., *et al.*, *Structural investigation of water/lecithin/cyclohexane microemulsions by FT-IR spectroscopy.* J. Colloid Inter. Sci., 1995. **176**: p. 281-5.

41. Maitra, A., T.K. Jain, and Z. Shervani, *Interfacial water structure in lecithin-oil-water reverse micelles.* Colloid Surf., 1990. **47**: p. 255-67.

42. Schurtenberger, P., *et al.*, *Structure and phase behavior of lecithin-based microemulsions: a study of the chain length dependence.* Colloid Inter. Sci., 1993. **156**: p. 43-51.

43. Kumar, V.V., P.T. Manoharan, and P. Raghunathan, *31P NMR spin lattice relaxation in lecithin reverse micelles.* J. Biosci., 1982. **4**(4): p. 449-54.

44. Kumar, V.V., C. Kumar, and P. Raghunathan, *Studies on licithin reverse micelles: optical birefringence, viscosity, light scattering, electrical conductivity, and electron microscopy.* J. Colloid Inter. Sci., 1984. **99**(2): p. 315-23.

45. Kumar, V.V. and P. Raghunathan, *Proton NMR studies of the interaction of water with lecithin in non-polar organic media.* Chem. Phys. Lipids, 1986. **41**: p. 159-71.

46. Kumar, V.V. and P. Raghunathan, *Spectroscopic investigations of the water pool in lecithin reverse micelles.* Lipids, 1986. **21**(12): p. 764-68.

47. Barbara, P.F. and W. Jarzeba, *Ultrafast Photochemical Intramolecular Charge and Excited State Solvation*, in *Advances in Photochemistry*, D.H. Volman, G.S. Hammond, and K. Gollnick, Editors. 1990, John Wiley & Sons, Inc. p. 1-68.

48. Lis, L.J., *et al.*, *Interactions between neutral phospholipid bilayer membranes.* Biophys. J., 1982. **37**: p. 657-66.

49. Ulrich, A.S. and A. Watts, *Molecular response of the lipid headgroup to bilayer hydration monitored by D-NMR.* Biophys. J., 1994. **66**: p. 1441-9.

50. Davenport, J.B. and L.R. Fisher, *Interaction of water with egg lecithin in benzene solution.* Chem. Phys. Lipids, 1975. **14**: p. 275-90.

51. Shchipunov, Y.A. and E.V. Shumilina, *Lecithin bridging by hydrogen bonds in the organogel.* Mater. Sci. Eng. C, 1995. **3**(1): p. 43-50.

52. Shchipunov, Y.A. and E.V. Shumilina, *Lecithin organogels: role of polar solvent and nature of intermolecular interactions.* Colloid J., 1996. **58**(1): p. 117-25.

53. Shumilina, E.V., Y.L. Khromova, and Y.A. Shchipunov, *Lecithin organogels: the effect of phosphatidylethanolamine additives.* Colloid J., 1997. **59**(4): p. 514-8.

54. Boicelli, C.A., *et al.*, *Interactions of small molecules with phospholipids in inverted micelles.* Chem. Phys. Lett., 1982. **89**(6): p. 490-5.

55. Llor, A. and P. Rigny, *Some tentative models of molecular motion applied to water in small reversed micelles.* J. Am. Chem. Soc., 1986. **108**(24): p. 7533-41.

56. Christopher, D.J., *et al., A Fourier Transform Infrared study of water-head group interactions in reversed micelles containing sodium bis(2-ethylhexyl) sulfosuccinate (AOT).* J. Colloid Inter. Sci., 1992. **152**(2): p. 465-72.

57. Moran, P.D., *et al., Vibrational spectroscopic study of the structure of sodium bis(2-ethylhexyl)sulfosuccinate reverse micelles and water-in-oil microemulsions.* Langmuir, 1995. **11**(3): p. 738-43.

58. Kotlarchyk, M., J.S. Huang, and S.H. Chen, *Structure of AOT reversed micelles determined by small-angle neutron scattering.* J. Phys. Chem., 1985. **89**(20): p. 4382-6.

59. Gorski, N. and Y.M. Ostanevich, *Small-angle neutron scattering (SANS) determination of the volume occupied by a single water molecule in the inverted micellar systems AOT + $X(H,D)_2O$ + $C_{10}D_{22}$ by internal contrast variation technique.* J. Phys. IV (France), 1993. **3**: p. 149-52.

60. Gorski, N. and Y.M. Ostanevich, *Inverted micelles in a ternary system AOT-water-benzene as studied by small-angle neutron scattering.* Ber. Bunsenges. Phys. Chem., 1990. **94**: p. 737-41.

61. Schurtenberger, P., *et al., Cross-section structure of cylindrical and polymer-like micelles from small-angle scattering data.* Langmuir, 1996. **12**(10): p. 2433-40.

62. Israelachvili, J.N., D.J. Mitchell, and B.W. Ninham, *Theory of self-assembly of hydrocarbon amphiphiles into micelles and bilayers.* J. Chem. Soc. Faraday Trans. 2, 1976. **72**(9): p. 1525-68.

63. Klose, G. and K. Gawrisch, *Lipid-water interaction in model membranes.* Studia Biophys., 1981. **84**: p. 21-2.

64. Finer, E.G. and A. Darke, *Phospholipid hydration studied by deuteron magnetic resonance spectroscopy.* Chem. Phys. Lipids, 1974. **12**: p. 1-16.

65. Huang, P., J.J. Perez, and G.H. Loew, *Molecular dynamics simulations of phospholipid bilayers.* J. Biomolec. Struc. Dyn., 1994. **11**(5): p. 927-56.

66. Perera, L., U. Essmann, and M.L. Berkowitz, *The role of water in the hydration force-molecular dynamics simulations.* Progr. Colloid Polym. Sci., 1997. **103**: p. 107-15.

67. Koga, K. and Y. Kanazawa, *Head group interaction in phosphatidylcholine micelles studied by 14N-nuclear magnetic resonance.* Chem. Phys. Lipids, 1984. **36**: p. 153-67.

68. Lang, J., A. Jada, and A. Malliaris, *Structure and dynamics of water-in-oil droplets stabilized by sodium bis(2-ethylhexyl) sulfosuccinate.* J. Phys. Chem., 1988. **92**(7): p. 1946-53.

69. Cevc, G., *Lipid Hydration*, in *Hydration of Macromolecules*, E. Westhof, Editor. 1992, MacMillan Press: New York. p. 338-390.

70. Kothekar, V., *Molecular dynamics simulation of hydrated phospholipid bilayers.* Indian J. Biochem. Biophys., 1996. **33**(6): p. 431-447.

71. Merz, K.M., Jr., *Molecular dynamics simulations of lipid bilayers.* Curr. Opin. Struct. Biol., 1997. **7**(4): p. 511-517.

72. Damodaran, K.V., K.M. Merz, Jr., and B.P. Gaber, *Structure and dynamics of the dilauroylphosphatidylethanolamine lipid bilayer.* Biochemistry, 1992. **31**(33): p. 7656-7664.

73. Damodaran, K.V. and K.M. Merz, Jr., *A comparison of DMPC- and DLPE-based lipid bilayers.* Biophys. J., 1994. **66**: p. 1076-1087.

74. Klose, G., *et al.*, *The structure and dynamics of water near membrane surfaces.* Colloids and Surfaces, 1985. **14**: p. 21-30.

75. Raghavan, K., M. Rami Reddy, and M.L. Berkowitz, *A molecular dynamics study of the structure and dynamics of water between dilauroylphosphatidylethanolamine bilayers.* Langmuir, 1992. **8**(1): p. 233-240.

76. Maroncelli, M., V.P. Kumar, and A. Papazyan, *A Simple Interpretation of Polar Solvation Dynamics.* J. Phys. Chem., 1993. **97**(1): p. 13-17.

77. Alper, H.E., D. Bassolino, and T.R. Stouch, *Computer simulation of a phospholipid monolayer-water system: The influence of long range forces on water structure and dynamics.* J. Chem. Phys., 1993. **98**(12): p. 9798-9807.

78. Alper, H.E., D. Bassolino-Klimas, and T.R. Stouch, *The limiting behavior of water hydrating a phospholipid monolayer: A computer simulation study.* J. Chem. Phys., 1993. **99**(7): p. 5547-5559.

79. Pileni, M.P., ed. *Structure and Reactivity in Reverse Micelles.* Studies in Physical and Theoretical Chemistry. Vol. 65. 1989, Elsevier: Amsterdam.

80. Martinek, K., *et al.*, *Micellar enzymology.* Eur. J. Biochem., 1986. **155**: p. 453-468.

81. Luisi, P.L. and L. Magid, *Solubilization of enzymes and nucleic acids in hydrocarbon micellar solutions.* CRC Crit. Rev. Biochem., 1986. **20**: p. 409-474.

82. Garti, N., D. Lichtenberg, and T. Silberstein, *The hydrolysis of phosphatidylcholine by phospholipase A2 in microemulsion as microreactor.* Colloids and Surfaces A, 1997. **128**(1): p. 17-25.

83. Bru, R., A. Sanchez-Ferrer, and F. Garcia-Carmona, *A theoretical study on the expression of enzymatic activity in reverse micelles.* Biochem. J., 1989. **259**: p. 355-361.

84. Luisi, P.L., *et al.*, *Organogels from water-in-oil microemulsions.* Colliod Polym. Sci., 1990. **268**: p. 356-374.

Chapter 3

Synthesis of Coumarin Labeled Phosphatidylethanolamine

3.I. Introduction

Our goal for all the studies reported here was to determine solvation dynamics near lecithin interfaces. As we discussed in Chapter 1, a variety of structures can be formed using phospholipids. Unfortunately, due to its solubility C343 is only effective as a reverse micelle probe with a saturated hydrocarbon solvent as the continuous phase. Lecithin reverse micelles made in these solvents have worm-like morphology (see Chapter 2). Only in these systems can we be confident C343 is at or near the lipid/water interface because of C343's low solubility in saturated hydrocarbon solvents. We wished to interrogate spherical reverse micelles. However, lecithin only forms micelles with this morphology when the continuous organic phase is chloroform, methylene chloride, carbon tetrachloride, or benzene[1]. C343 has significant solubility in all of these solvents. As will be discussed in Chapter 4, time-resolved anisotropy of C343 in benzene/lecithin/water reverse micelles revealed 63% of C343 molecules was solvated in the continuous organic phase. We also wished to interrogate vesicle interfaces. Again,

as will be discussed in Chapter 5, time-resolved anisotropy of C343 revealed 74% of C343 molecules was solvated in the aqueous continuous phase.

To probe lecithin interfaces other than worm-like reverse micelles, we needed to find a probe molecule that would be confined to the lipid/water interface. We determined that one way to accomplish this would be to covalently attach a probe molecule to a phospholipid headgroup. The dye-labeled lipid could then be added to other lipid aggregates such as reverse micelles and vesicles in dilute amounts. Unlike C343 that most likely occupied a distribution of positions within reverse micelles, a dye labeled lipid would have a much better defined location simplifying interpretation of the results. Most importantly, a dye-labeled lipid would allow us to interrogate any lipid aggregate, for example spherical reverse micelles and vesicles. Although unrealized to this point, we also envisioned the possibility of synthesizing hydrophilic peptide spacers between the phospholipid headgroup and dye. In effect, we could observe the solvent motion as a function of distance from a lipid interface. Petrossian et al. have already shown how a fluorescent dye may be covalently attached to a phosphatidylethanolamine by variable length peptide spacers[2].

Fluorescent probes are commonly attached to lipid headgroups for a variety of reasons[3]. Probes are usually attached through a primary amine of a phospholipid headgroup, typically phosphatidylethanolamine (PE). Various dye-labeled lipids are commercially available through Avanti Polar Lipids, Inc. and Molecular Probes, Inc. Molecular Probes offers several succinimide derivatives of selected dyes that can be readily attached to a PE of choice. Dye-labeled headgroups are used in a variety of applications in cellular research such as[4]: visualizing spatial relationships of lipid

populations by resonance energy transfer microscopy, lateral diffusion in membranes using fluorescence recovery after photobleaching measurements, cell-surface pH indicators, and detecting cell surface binding of antibodies. To our knowledge, we know of only one solvation dynamics experiment that has utilized a fluorescently labeled lipid to probe membrane interfaces[5].

Unfortunately, we were unable to locate a commercially available dye-labeled lipid that met our experimental requirements. However, we found that covalently attaching C343 to a PE would be a relatively simple synthesis. Because C343 was already our probe molecule of choice, it obviously met our experimental requirements. More importantly, C343 contains a carboxylic acid substituent that could easily be coupled to a PE headgroup amine via peptide bond formation.

Although covalently attaching C343 to PE would seem to meet our experimental requirements, we had several concerns that we needed to address once the synthesis was completed. First, derivatizing C343 could alter the electronic structure, reducing the dye's effectiveness as a solvation dynamics probe. Derivatizing the C343's carboxylic acid could alter the electronic structure. We could find that the derivatized C343 had a shifted absorption spectra relative to C343, possibly reducing our ability to excite the probe with our laser system. Also, the substantial dipole change that occurs when C343 is electronically excited from its ground state to its first excited state (see Chapter 1) may be reduced or eliminated for the derivatized C343. Second, the derivatization could enhance the intramolecular vibrational relaxation (IVR). As discussed in Chapter 1, we assume the IVR occurs on a much shorter timescale than we measure in solvation dynamics experiments. Structurally rigid fluorescent dyes are typically employed to

ensure IVR is not a factor in solvation dynamics measurements. Adding a non-rigid phospholipid to the structure of C343 could reduce the fluorescence quantum yield and/or add longer time IVR that could be misinterpreted as solvent relaxation. Third, we were concerned the reduced polarity of the C343-PE final product structure would alter its effectiveness as a lipid/water interface probe. We found C343 to be a less than ideal probe for a lipid interface. Ideally, the probe molecule would extend into the polar headgroup/water interface. C343 is significantly soluble in aqueous solutions but the solubility is primarily derived from the carboxylic acid substituent. Replacing the carboxylic acid with an amide bond could reduce its water solubility. Therefore, the C343 may bury itself within the headgroup region. The C343-PE final product would also lack the ammonium positive charge that is present in PE. We were concerned that the reduced polarity of the headgroup and dye could result in a population of the C343-labeled lipids that would either not align with other phospholipids correctly or not aggregate at all.

There are many strategies for coupling a carboxylic acid to a primary amine. In the typical synthesis, the final product is synthesized in two steps. The first step involves reacting the carboxylic acid with an activating reagent that converts one of the carbonyl oxygens into a better leaving group. At this point the converted carboxylic acid starting material is termed the activated complex. The second step is N-acylation and involves nucleophilic attack by the primary amine at the activated complex carbonyl followed by departure of the leaving group. The final product is an amide. The overall reaction consumes a water molecule.

There are many different activating reagents that may be employed. To optimize the yield, we attempted to activate C343 with three different reagents that are readily available and commonly used in amide syntheses: triphenylphosphine/2,2'-dipyridyl disulfide (TPP/DPDS), 1,1'-carbonyldiimidazole (CDI), and 1-[3-(dimethylamino)propyl]-3-ethylcarboiimide hydrochloride (EDCI). In addition, we also attempted to couple C343 to two different primary amine containing compounds: PE and 4-chloroaniline. Of course, C343-labeled phosphatidylethanolamine (CLPE) was the target synthesis. But first, we coupled C343 to chloroaniline as a model synthesis. The model synthesis served as a practice coupling that was relatively easy to perform and allowed us to determine what effects an amide coupling of C343 had on its spectroscopy.

Figure 3.1 displays the relevant structures and mechanisms for all three activating agents. The presumed mechanisms have been taken from reference [6]. Notice that the EDCI activation requires a base to deprotonate the carboxylic acid in the initiation step, while the TPP/DPDS and CDI activations do not. Also, if PE is left in its zwitterionic form, the ammonium substituent will be unable to nucleophilically attack the activated C343. Therefore, when PE is added an equivalent of base is needed to promote the acylation of PE due to its zwitterionic character.

This chapter describes the methods we used to synthesize CLPE and C343-chloroaniline. We compare and contrast the effectiveness of the different reagents in activating C343. Also, we discuss the various methods we used to identify the final products as CLPE and C343-chloroaniline. We determine the effect N-acylation of C343 has on the electronic structure of the fluorophore for both CLPE and C343-chloroaniline.

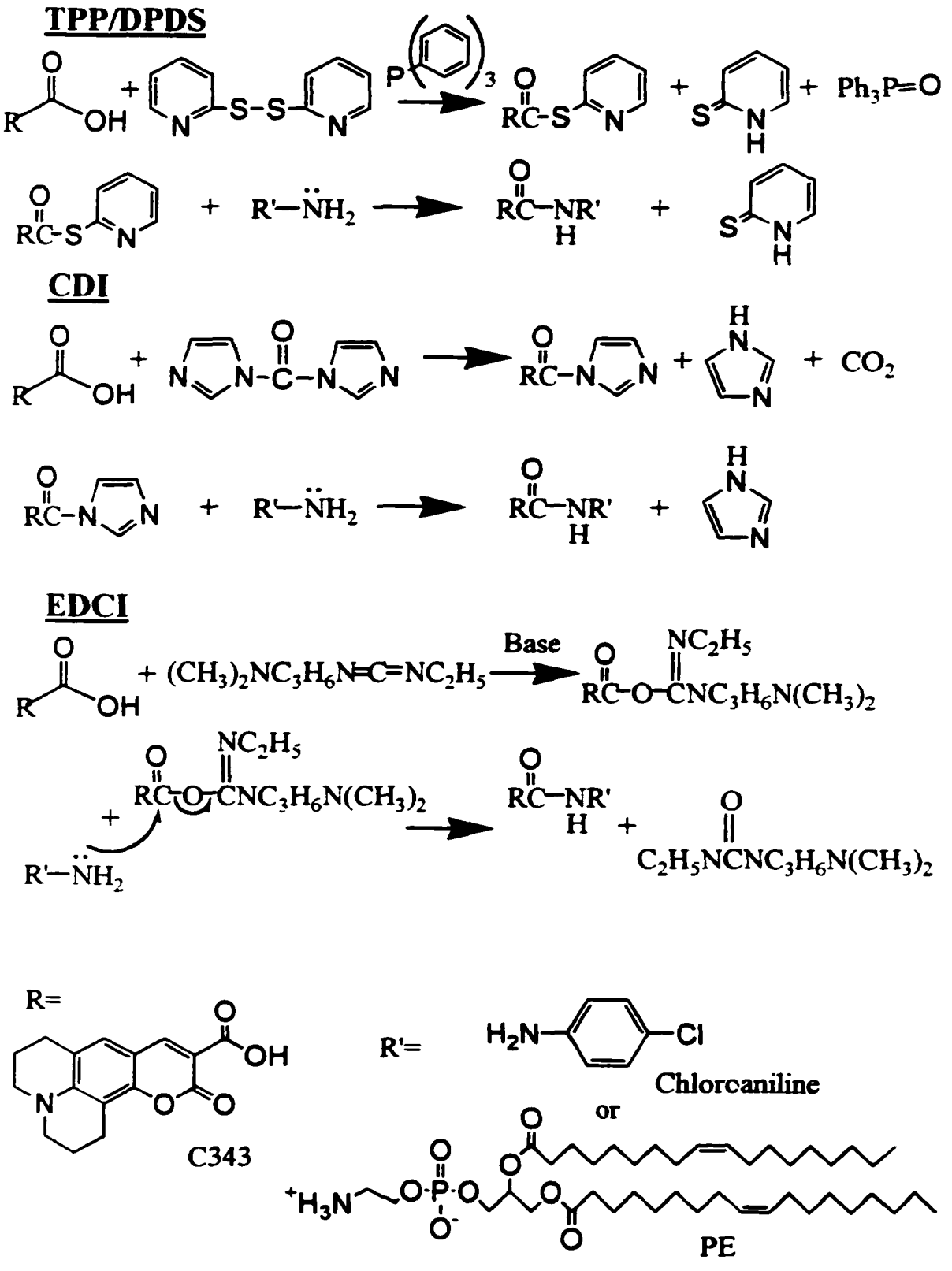

Figure 3.1. Mechanisms and Structures.

Finally, we incorporate CLPE into lecithin reverse micelles to evaluate its effectiveness as a solvation dynamics probe at lipid/water interfaces.

3.II. Experimental Methods

3.II.A. Raw Materials

Solvents were used as received except when used in the reaction. Reaction solvents were distilled over calcium hydride to remove water impurities. The following solvents were employed: chloroform (Fisher, ACS certified), methylene chloride (Fisher, ACS certified), methanol (Fisher, ACS certified), acetic acid (Aldrich, 99.8+%), and 1,2-dichloroethane (Fisher, ACS certified). Water used in the synthesis as well as in reverse micelle preparation was of high purity (Milli-Q filtered, 18.2MΩ/cm^2 resistivity). Deuterated solvents for NMR analysis were obtained from Cambridge Isotope Laboratories, Inc.

Starting materials were used as received. Coumarin 343 (C343, Exciton, Inc.) was our fluorescent probe molecule. We coupled C343 to both 4-chloroaniline (chloroaniline, Aldrich, 99+%) and 1,2-dioleoyl-sn-glycero-3-phosphoethanolamine (PE, Avanti Polor Lipids, Inc., 99+%, lyophilized powder). PE contains two cis double bonds at the ninth carbon position of both chains (see Figure 3.1). We chose this particular phosphoethanolamine because the double bonds tend to reduce the gel to liquid-crystalline phase transition of lipid membranes. As discussed in Chapter 1, we chose to use lipids with transition temperatures below room temperature so that we would determine dynamics near lipid aggregates that are in the biologically relevant liquid-crystalline phase.

We activated the C343 with the following activating agents: Triphenylphosphine (TPP, Aldrich, 99%), 2,2'-dipyridyl disulfide (DPDS, Aldrithiol-2, Aldrich, 98%), 1,1'-carbonyldiimidazole (CDI, Aldrich), and 1-[3-(dimethylamino)propyl]-3-ethylcarboiimide hydrochloride (EDCI, Aldrich, 98+%). All were used as received. CDI is especially prone to degradation. ^{1}H-NMR of several year old bottles found that almost 50% had degraded to imidazole. While all the activating agents degrade over time, their degradation products are inert when added to the reaction vessel. However, in order to obtain a good yield, care should be taken to ensure reagents have not decomposed.

We used both triethylamine (TEA, Fisher, HPLC grade) and 4-(dimethylamino)pyridine (DMAP, Aldrich, 99+%) as the organic solvent base. Either can be used with the same success. We found DMAP easier to use because it exists as a solid at room temperature and can be easily weighed. TEA is a liquid at room temperature and should be distilled and placed over molecular sieves to avoid atmospheric water contamination.

Reverse micelles were prepared with lyophilized egg yolk L-α-lecithin-phosphotidylcholine (lecithin, Avanti Polar Lipids, Inc.). Reverse micelles were dissolved in cyclohexane (Acros, spectrophotometric grade, 99+%).

3.II.B. Physical Measurements

The synthetic final products were identified by a variety of methods. Elemental analysis for carbon, hydrogen, nitrogen, and phosphorous was performed by M-H-W Laboratories (P.O. Box 15149, Phoenix, AZ 85060). We attempted elemental analysis of sodium and phosphorous using an inductively coupled plasma-atomic emission spectrometer (ICP-AES, Perkin-Elmer P400 spectrometer). ^{1}H and ^{13}C Nuclear magnetic

resonance (NMR) analyses were performed on either a Varian Mercury-Inova 300 MHz or a Varian Inova 300 MHz spectrometer. The instruments are identical except only the Varian Inova allows for temperature variation experiments. Fourier transform infrared (FTIR) were taken on one of two spectrometers: Nicolet Magna-IR 760 spectrometer or Nicolet-5PC-FTIR. Positive-ion fast atom bombardment (FAB+) mass spectra were obtained on a Fisons VG AutoSpec, calibrated with PPG. Electrospray mass spectra were obtained on a Fisons VG Quattro-SQ. Absorption spectra, emission spectra, time-resolved anisotropy, and TRES spectra were performed on instrumentation described in Chapter 1.

3.II.C. Miscellaneous Tools

Plates used for thin layer chromatography (TLC) were coated with silica gel 60 F_{254} (EM Separations Technology, 250 μm layer thickness). Chromatography columns were packed with silica gel (Silicycle, 230-400 mesh). Solvents were removed with a rotary evaporator (Buchi Rotavapor R-1214) with a vacuum created by water aspiration. UV lamps were used to illuminate TLC plates. Short wavelength lamps were effective at identifying aromatic compounds such as TPP, DPDS, chloroaniline, and CDI, while long wavelength lamps identified any C343 or C343-derivatised compound.

TLC stains were very useful in identifying PE and CLPE. Avanti technical support suggested a phosphorous stain[7] and ninhydrin reagent[8] to stain phosphorous and amine containing compounds, respectively. Directions for the preparation of these stains may be found at the Avanti web site (http://www.avantilipids.com) or within the references above. We should note that the phosphate stain is a relatively weak stain and requires a spot of significant phosphate concentration to be observed.

3.II.D. Procedures

C343 Activation

Whether we were coupling PE or chloroaniline to C343, the first step of the reaction sequence involved activation of the C343 carboxylic acid. The goal of this step is to replace the carboxylic hydroxyl group with a more electron-withdrawing group that will open the carbonyl to nucleophilic attack. Only after the activation of C343 is complete, do we add the amine-containing nucleophile. We activated C343 with three different reagents: TPP/DPDS, CDI, and EDCI.

The activation step must proceed under anhydrous conditions because water will tend to act as a nucleophile and convert the activated C343 back to the original C343, consuming the activating reagents in the process. To ensure anhydrous conditions, glassware was oven dried immediately prior to use, solvents were freshly distilled, and solid reagents were placed in the reaction vessel under nitrogen before being dissolved in organic solvent. The organic solvent employed must not react with the reagents and be able to solvate the reagents. Unfortunately, C343 is not highly soluble in many organic solvents. We originally used 1,2-dichloroethane but found C343 was most readily solvated in methylene chloride.

TPP/DPDS. C343 was combined with TPP and DPDS in molar equivalents. However, to ensure all of the PE or chloroaniline to be added in the subsequent step is reacted, we found the C343/TPP/DPDS reagents should be at least twice the molar equivalent of PE or chloroaniline. For example, we typically reacted 100 mg (0.13 mmol) of PE. Therefore, in the activation step, we combined ca. 80 mg of C343 (0.28 mmol) with 60 mg (0.27 mmol) of DPDS and 70 mg (0.27 mmol) of TPP. These

reagents were added to a 25 ml round bottom flask and dissolved in ca. 5 ml of organic solvent. The reaction was stirred at room temperature and kept under nitrogen.

We followed the activation of C343 by TLC analysis. This was accomplished by dipping capillaries through large gauge syringe needle while maintaining a low positive nitrogen pressure inside the reaction vessel. Spotted TLC plates were eluted with a 9:1 methylene chloride:methanol solvent system. C343 has a R_f value of ca. 0.6 in this solvent system. Activated C343 usually appeared with a R_f value of ca. 0.8 and became slightly more intense as the activation progressed. Both spots were most easily viewed with a long wavelength UV lamp. When the plate was illuminated with a short wavelength UV lamp, several spots separate from the activated C343 and C343 spots could be readily seen between $R_f = 0.7$ to 0.9. These corresponded to TPP and DPDS. The activated C343 spot became very intense within a few minutes of combining the reagents. The activation was usually allowed to progress at least 30 minutes, even though, the activated spot would only show a minor gain in intensity. The C343 spot was never more intense than the activated C343 spot.

CDI. Because unreacted CDI can polymerize PE, the C343, CDI, and PE or chloroaniline were reacted in molar equivalents. For example, we combined 40 mg (0.14 mmol) of C343 with 22 mg (0.14 mmol) of CDI that would later be combined with 100 mg PE (0.13 mmol) after the activation step. These reagents were added to a 25 ml round bottom flask and dissolved in ca. 5 ml of organic solvent. The reaction was stirred at room temperature and kept under nitrogen.

The activation was followed with TLC in a similar manner as described above for TPP/DPDS. Activated C343 appeared as two yellow spots with $R_f = 0.8$ and 0.85. We

believe the two spots correspond to C343-imidazole and $(C343)_2C_2O_3$ anhydride that are both reactive to nucleophilic attack. Imidazole which formed as the reaction progressed, appeared as a faint, diffuse spot with a short wavelength UV lamp and had a $R_f = 0.1$. Much like TPP/DPDS activation, the activated C343 appears soon after reagents are combined and only intensifies slightly with time. The C343 spot remains more intense than the activated C343 spots even after the reaction is allowed to proceed overnight. We allowed the activation to proceed at least 1 hr.

EDCI. EDCI was investigated as an activating agent but it was found to not perform as well as TPP/DPDS and CDI in activating C343 and will not be discussed further.

N-acylation of Activated C343

Once C343 was activated, we could then add PE or chloroaniline to complete the synthesis of CLPE or C343-chloroaniline. It is important to note that we did not add PE or chloroaniline at the beginning of the activation step because the activating agents can possibly react with PE or chloroaniline. Therefore, only after the activating reagents have reacted with C343 do we begin the second step. Because water can still act as a nucleophile and deactivate the activated C343, this step must also be run in anhydrous conditions. Therefore, PE or chloroaniline were transferred to the reaction flask within a glove bag filled with nitrogen gas. We also considered the water that is inherent in any phospholipid sample. We originally dried PE over molecular sieves in diethyl ether but found the drying was unnecessary. The small amount of inherent water did not seem to lower the percent yield and dehydrated PE showed reduced solubility in the organic solvent making the transfer to the reaction vessel difficult. Unlike chloroaniline, PE was

added with an equivalent amount of base. For PE to nucleophilically attack the carbonyl, the amine must be in its neutral state. Therefore, we added 17 mg DMAP (0.14 mmol) with 100 mg PE (0.13 mmol) to the reaction vessel, while in the model reaction, we added 17 mg chloroaniline (0.13 mmol) with no base. All these reagents are solids and were typically transferred by dissolving in methylene chloride.

As was the case with the activation step, the progression of the N-acylation was followed with TLC. While chloroaniline may be visualized with a short wavelength UV lamp, PE must be visualized on the TLC plate with ninhydrin and phosphorous stains. Ninhydrin stains primary and, to a lesser extent, secondary amines as light pink. The phosphorous stain reacts with phosphorous containing components and appears blue/black with heating. Because C343-chloroaniline is nonpolar, we used 100% methylene chloride as the TLC solvent system for the model system. The C343-chloroaniline spot is yellow with a $R_f = 0.5$ and only appears after the addition of chloroaniline. Chloroaniline has a $R_f = 0.4$ and seemed to react to quickly to be visualized during the reaction. CLPE is fairly polar because of the charged phosphate group and the zwitterionic PE is even more polar. We found only a relatively polar solvent system of 90:9:1 methylene chloride:methanol:acetic acid can remove CLPE and PE from the baseline. Including acetic acid in the solvent system tends to sharpen acidic components and helped increase the R_f of CLPE. Because of this C343 and activated C343 tighten to almost one spot that has a $R_f = 0.7$. The PE spot appears bright pink after staining with ninhydrin and appears blue after staining with the phosphorous stain. The PE spot appears as a small streak from the baseline with a $R_f = 0.1$. The CLPE spot is yellow with a $Rf = 0.35$ and appears only after the addition of PE. CLPE does not stain

with ninhydrin but does appear black when heated with the phosphorous stain. Completion of the N-acylation step was indicated by the disappearance of the chloroaniline or PE spot. For the TPP/DPDS activation, the disappearance would occur within a few minutes of PE or chloroaniline addition. For the CDI activation, the PE or chloroaniline spots never completely disappeared, but did grow faint within one hour. All N-acylations were allowed to proceed for at least one hour.

Reaction Quench

The reaction was quenched by transferring the contents of the reaction flask to a 125 ml separatory funnel containing ca. 10 ml of saturated sodium bicarbonate solution. The transfer was aided by sequential flask washes of methanol and chloroform. Approximately 10 ml methanol and 20 ml chloroform were added to the separatory funnel. Once the reactants come in contact with water, the reaction should be quenched. As discussed above, water should act as a nucleophile and convert all activated C343 back to C343. In addition, all activating agents are converted to their nonreactive forms. For example, CDI is converted to imidazole and carbon dioxide. The reaction was quenched with a sodium bicarbonate solution to reduce emulsification and to provide a sodium counterion for CLPE.

The organic portion was washed in the separatory funnel with three sequential 10 ml additions of sodium bicarbonate solution. CLPE preferentially partitions into the organic phase. TLC analysis of the aqueous phase revealed a significant concentration of C343 but no CLPE. The washed organic phase was transferred to a 100 ml round bottom flask. The transfer was aided by washing the funnel with chloroform. The emulsion layer that contains a significant amount of sodium bicarbonate and water was also

transferred to the round bottom flask. Using a rotary evaporator, the organic solvent was evaporated at room temperature. We removed residual water by placing the sample under vacuum overnight. The sample would appear dry the next day. While trace amounts of water are inconsequential, removing residual water is important because the water can degrade the silica column used in the next step.

Purification

The final product was purified from all other reagents and starting materials by flash chromatography. Silica gel was packed into a one-inch diameter column to a height of about 8 inches. The mobile phase for the model synthesis was 100% methylene chloride, while the CLPE synthesis used 92:7:1 methylene chloride:methanol:acetic acid. Because both CLPE and C343-chloroaniline are yellow/orange colored molecules, they produce a clearly visible colored band as they elute down the column. C343-chloroaniline is substantially more nonpolar than C343 and the other reagents, therefore, it is the first to elute off the column and can be collected with high purity. For CLPE, the C343 elutes off the column first followed by CLPE that elutes off fairly slowly in about 200 ml of mobile phase. Approximately 5 ml fractions were collected into individual test tubes. The fractions were then recombined into a 100 ml round bottom flask. The mobile phase solvent was evaporated with a rotary evaporator. Then, the flask placed under vacuum for further drying.

Even after being placed under vacuum for several days, the CLPE remained gummy/waxy. We found that repeated solvation and evaporation of CLPE with a methylene chloride/methanol mixture would produce a flaky "dry" product. We believe acetic acid is slow to evaporate and this procedure facilitates its evaporation. For reasons

unknown, the flaky-dry product would be produced whenever a solvation/evaporation cycle ended with a boiling explosion of the last portion of solvent.

Preparation of Lecithin Reverse Micelles Containing CLPE

Once we synthesized CLPE, we needed to prove that CLPE would align correctly within a lipid interface and that the attachment of PE to C343 would not influence the measured solvation dynamics. We knew from Chapter 2 that C343 resides near the lecithin headgroup interface within cyclohexane/lecithin/water reverse micelles in much the same manner as we would expect CLPE to reside if prepared in the same system. By preparing these reverse micelles with CLPE instead of C343, we should observe similar spectroscopic properties as we had observed with C343, i.e. the static absorption and emission should show hydration dependent spectra and the measured solvation dynamics should be similar.

Materials, concentrations, and methods for preparing the cyclohexane/lecithin/water reverse micelles were similar to those outlined in Chapter 2. The major difference was the incorporation of CLPE into the lecithin. For CLPE to be homogeneously distributed within the reverse micelles, both the lecithin and CLPE needed to be dissolved in the same solvent and then dried before being dispersed into cyclohexane. Because CLPE most readily solvates in a 9:1 methylene chloride:methanol solvent, we co-dispersed 500 mg lecithin and 2 mg CLPE in this solvent system. Originally, we attempted evaporating the organic solvent by placing the mixture under vacuum overnight. We found that complete dryness was never met with this method because the reverse micelles never appeared gelatinous at higher hydration levels (see Chapter 2). Instead, the unevaporated methylene chloride/methanol was removed by

three cycles of cyclohexane addition and vacuum evaporation. About 10 ml of cyclohexane was used to dissolve the lipids each cycle and the evaporation would last 1 to 2 hours. The last evaporation was usually done overnight. With this method, the reverse micelles showed the expected viscosity as a function of hydration. After dispersing CLPE into the lecithin, the reverse micelles were prepared as described in Chapter 2 by dissolving in 10 ml of cyclohexane, adding the required amount of water, shaking on a mechanical shaker overnight, and filtering through a 0.1 μm syringe filter (PTFE, Whatman). We found that placing circulated samples in a nitrogen environment could reduce CLPE oxidation. Therefore, samples used in upconversion experiments were placed in a vacuum tight sample holder. Samples were subjected to three freeze-pump-thaw cycles before being placed under nitrogen. These cycles did not disturb the sample viscostiy, and therefore the worm-like reverse micelle structure as well.

Because the methodology for preparation of the reverse micelles was different from those prepared with C343 in Chapter 2, we needed to find the amount of inherent water to expect by this method. In Chapter 2, we found 1.8 molecules of water per molecule of lipid within a freshly opened bottle of lyophilized lecithin. We could expect that some of this inherent water would be evaporated off by the methodology described above. As expected, ^{1}H-NMR analysis revealed only 0.4 inherent water molecules per lipid. The water peak has a chemical shift of about 4.2 ppm and can be discerned from lecithin peaks by either the method of standard water additions or by adjusting the NMR probe temperature.

3.III. Results and Discussion

3.III.A. Model Synthesis

We found that C343 can be coupled to chloroaniline with either TPP/DPDS or CDI as the coupling reagents. With both reagents, we found the reaction to proceed as expected by TLC analysis. In both cases, we observed an activated C343 spot appear in the activation step with a R_f value greater than C343. We expect a greater R_f because the carboxylic acid substituent of C343 is replaced with less polar substituent when activated. Most certainly, C343's carboxylic acid substituent has a large interaction with the polar silica immobile phase which therefore has a large influence on the R_f value. Again in both methods, we observe the final product spot appears only after chloroaniline addition. As expected, a yellow spot appears with a greater R_f value than all the other starting materials and with the same value regardless of the method of preparation. This is because C343-chloroaniline has weak polar interactions with the silica immobile phase while the amine of aniline and the carboxylic acid of C343 has strong polar interactions. The distinctive yellow color of C343 allows us to easily trace its derivatives as the reaction progresses. As we discuss below, derivatizing C343 at the carboxylic acid position does not alter its spectroscopy. Therefore a yellow spot is always indicative of a C343 derivative. With either method of preparation, the C343-chloroaniline final product appeared fluffy, yet grainy, with a uniform yellow/orange hue.

The main goal of attempting to attach C343 to chloroaniline by TPP/DPDS and CDI was to practice the synthesis with an inexpensive starting material (i.e., chloroaniline vs. PE). In light of this, the yields were not considered important and therefore not

determined. However, we believe it is likely one can expect a greater percent yield when TPP/DPDS is used as the activating agent. This is because by TLC analysis, we found that the chloroaniline spot would completely disappear after addition to C343 activated with TPP/DPDS. To the contrary, when chloroaniline was added to C343 activated with CDI, the chloroaniline spot never disappeared. As will be discussed further below, we believe TPP/DPDS allows for a greater percent yield because the activating reagents can be combined at a larger molar equivalent than chloroaniline. This was not the case for CDI activation where all reagents and starting materials must be combined in molar equivalents.

We were encouraged by the synthesis of C343-chloroaniline because chloroaniline was not expected to be a strong nucleophile. Due to the electron withdrawing character of the chlorine substituent, the nitrogen of chloroaniline is predicted to be deactivated relative to aniline. Because PE's amine is not deactivated, we expected the basic form of PE to be a better nucleophile than chloroaniline.

^{1}H-NMR spectra confirmed that the final product's proton structure is the same whether it was made with either TPP/DPDS or CDI. We obtained spectra for both products synthesized with TPP/DPDS and CDI (see Figure 3.2 and 3.3). Both spectra were taken with the final product dissolved in $CDCl_3$ at 25°C. In Figure 3.2, the $CHCl_3$ proton appears at 7.27 ppm and is not resolved from the final product's protons at a similar chemical shift. The final product shows peaks in both spectra that are consistent with C343-chloroaniline: δ 10.96 (s, 1 H), δ 8.65 (s, 1 H), δ 7.65 (m, 2 H), δ 7.27 (m, 2 H), δ 7.02 (s, 1 H), δ 3.33 (m, 4 H), δ 2.89 (m, 2 H), δ 2.77 (m, 2 H), δ 1.98 (m, 4 H). In

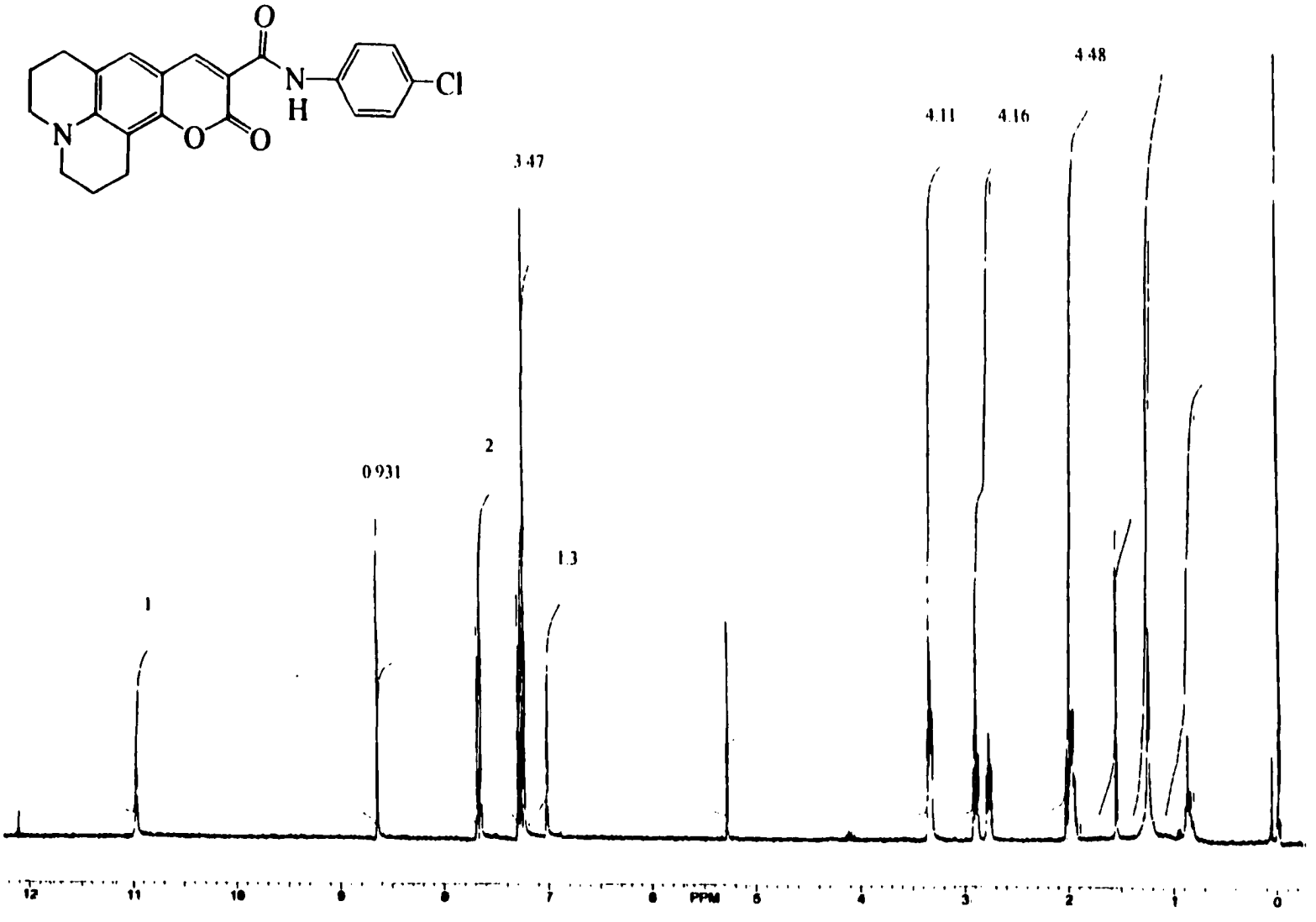

Figure 3.2. ^{1}H-NMR of C343-chloroaniline prepared with TPP/DPDS. Product dissolved in $CDCl_3$.

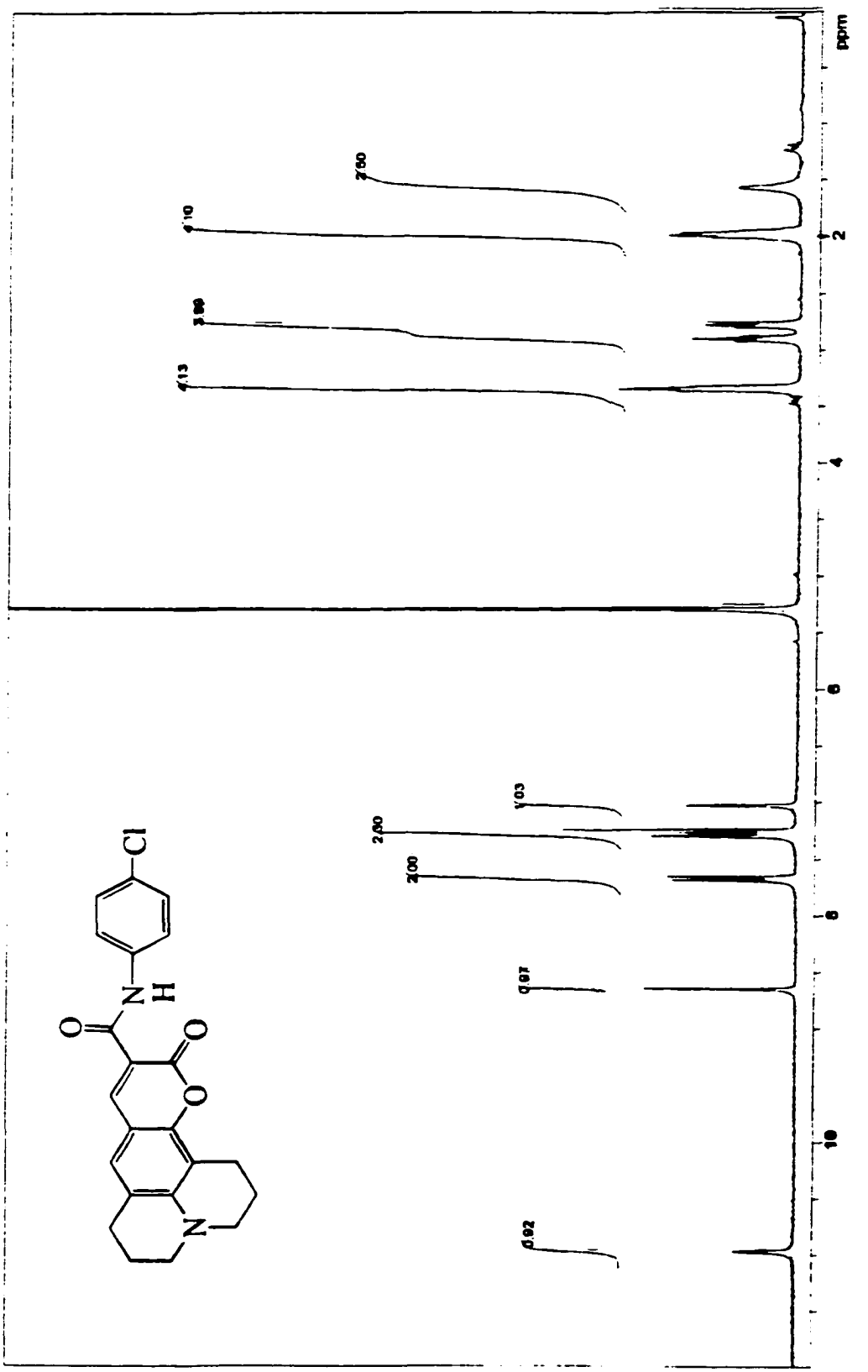

Figure 3.3. ^{1}H-NMR of C343-chloroaniline prepared with CDI. Product dissolved in $CDCl_3$.

both spectra, methylene chloride unevaporated after purification appears as a contaminant, δ 5.27. Water also contaminates the samples with a peak at δ 1.54. Two other unidentified peaks appear in the CDI spectrum at δ 1.24 and δ 0.85. They do not integrate to integers and are assumed to be greasy contaminants.

We compare the NMR spectrum of the final product to spectra of C343 and chloroaniline to conclude the final product is C343-chloroaniline. The ^{1}H-NMR spectrum for C343 dissolved in 9:1 $CDCl_3$:CD_3OD at 25°C is displayed as Figure 3.4: δ 8.47 (s, 1 H), δ 7.08 (s, 1 H), δ 3.41 (m, 4 H), δ 2.88 (m, 2 H), δ 2.78 (m, 2 H), δ 2.02 (m, 4 H). The solvent peaks CHCl3 (δ 7.37), CH3OH (δ 3.90), and TMS (δ 0.00) also appear. Notice that the acidic proton of C343 does not appear in the spectrum, presumably because it has exchanged with the CD_3OD solvent. In another spectrum of C343 without methanol we found the acidic proton at δ 12.45. A previously published spectrum of chloroaniline shows peaks at δ 7.05 (m, 2H), δ 6.45 (m, 2 H), and δ 3.58 (m, 2H)[9]. Clearly, the main protons of C343 and chloroaniline appear in the spectrum of the final product. In addition, the acidic proton of C343 (δ 12.45) and the amine protons of chloroaniline (δ 3.58) disappear in the final product's spectrum, while a new proton at δ 10.96 appears corresponding to the amide proton of the final product.

To further prove the final product is C343-chloroaniline, FT-IR (Nicolet Magna-IR 760 spectrometer) spectra of the final product and C343 were taken (Appendix 3.III). The spectra reveal that the final product is distinctly different from C343. However, appearance and disappearance of specific bands as proof of the final product's structure is difficult. For C343, we detect a low intensity broad peak at 3432 cm^{-1} that we assign as a carboxylic acid vibration. This peak does not seem to be present in the final product, as

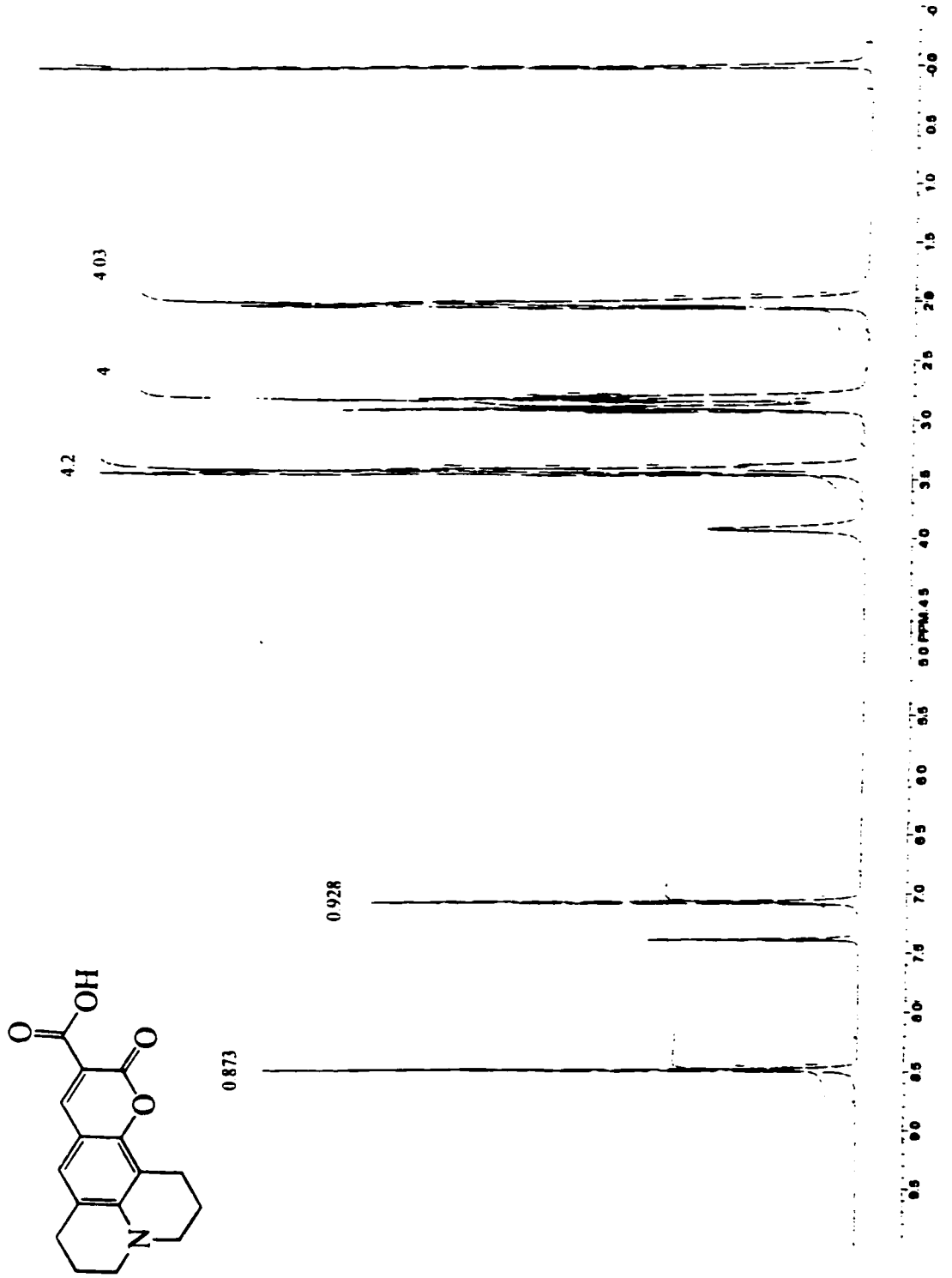

Figure 3.4. ^{1}H-NMR of C343 dissolved in 9:1 $CDCl_3$:CD_3OD.

expected. Further assignments are difficult. We only obtained FT-IR spectra for C343-chloroaniline prepared with TPP/DPDS.

We analyzed the steady-state spectroscopy of C343-chloroaniline and found there is little difference between the C343 and C343-chloroaniline. Figure 3.5 displays the absorption and emission of C343-chloroaniline in comparison to C343. We conclude that N-acylation of C343 has little effect on the first electronic excited state. We expected that this would be the case because the first excited state of C343 is assumed to be a charge transfer state that involves the promotion of a nitrogen lone pair electron to the ring carbonyl. Because the carboxylic acid substituent is not directly bound to the nitrogen or carbonyl nor does it alter the conjugation between them, the caboxylic acid substituent may influence but not alter the charge transfer state. The fact that several coumarin dyes are commercially available that are derivatives of C343 at the carboxylic acid position confirms these assumptions, for example, coumarin 153 ($-CF_3$), coumarin 334 ($-COCH_3$), coumarin 314 ($-CO_2C_2H_5$), and coumarin 102 ($-CH_3$). Also, we find that while the C343 absorption and emission spectra display pH dependent shifts associated with protonation and deprotonation of the carboxylate moiety, the spectral shape, absorption cross section and fluorescence quantum yield remain constant.

In summary, we have shown with the model synthesis that C343 may be N-acylated, even with a relatively weak nucleophile. Furthermore, we have shown C343 may be activated with either TPP/DPDS or CDI and still produce the same final product. We cite the similar behavior of the final product by TLC analysis and the similarity of ^{1}H-NMR spectra as evidence that the final product is the same for either synthesis. In addition, we find that derivatizing the carboxylic acid of C343 does not alter the first

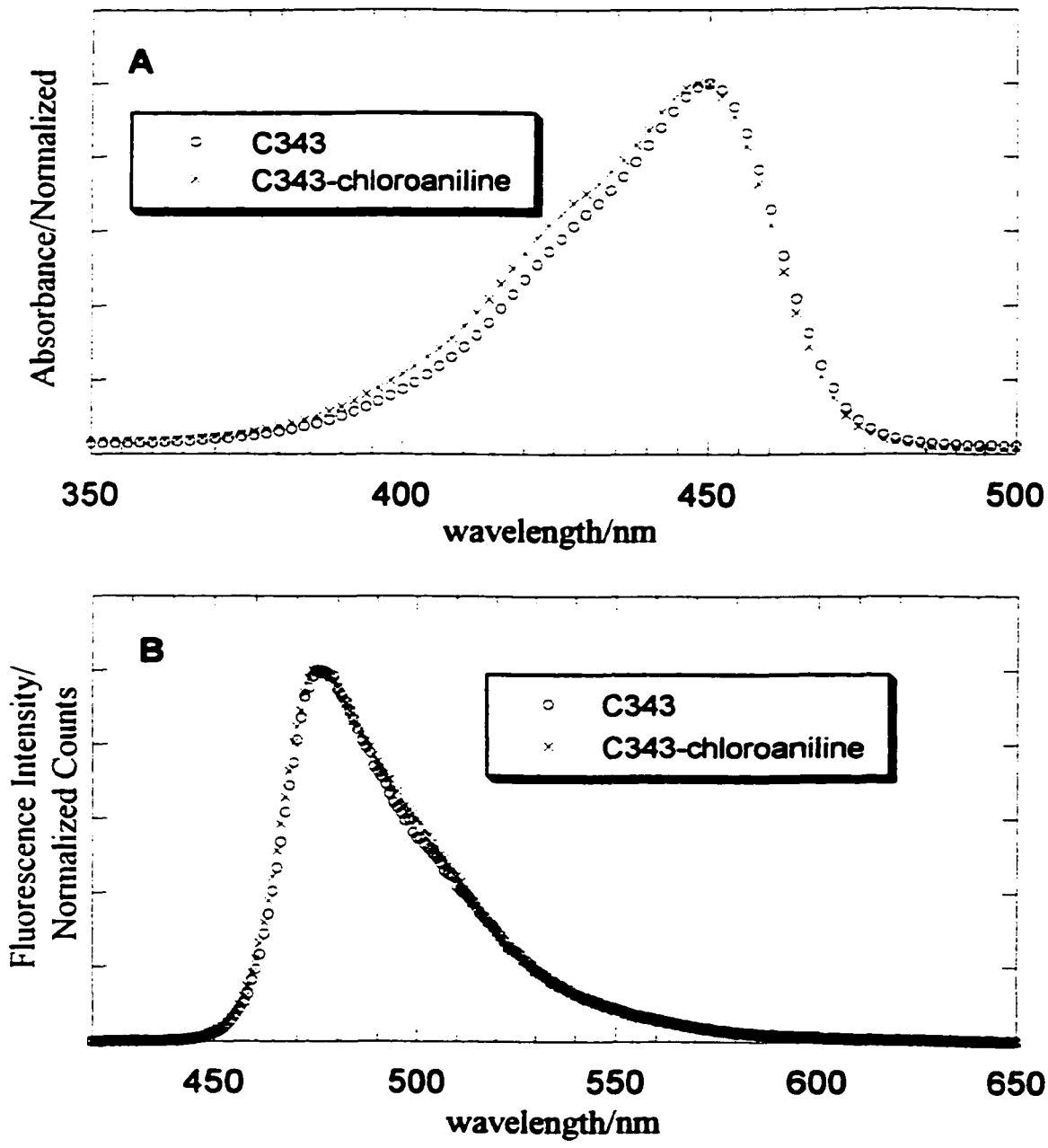

Figure 3.5. Absorption and emission of C343 and C343-chloroaniline dissolved in chloroform.

excited state spectroscopy. This is an important conclusion because our goal of using CLPE as a lecithin interface probe, relies on the spectroscopy of C343.

3.III.B. Target CLPE Synthesis

As with the model synthesis, we were able to synthesize CLPE with either TPP/DPDS or CDI as the activating agents. While we wanted to determine what method would allow for the greatest yield, we also found additional value in synthesizing CLPE by different pathways. As we will present below, positive identification of the final product as CLPE proved difficult. Being able to produce the same final product by two different methods gave us confidence we were synthesizing CLPE at a time when we lacked definitive proof. Recently, we have obtained ^{1}H-NMR and mass spectrometry data for the final product prepared by TPP/DPDS activation that conclusively identifies it as CLPE. We will present further data that supports the identification of CLPE but does not conclusively identify it. The evidence we synthesized CLPE with CDI as the activating agent is more circumstantial.

As was seen with the model synthesis, the reaction progressed as expected when either TPP/DPDS or CDI was used to activate C343. How the reaction progresses during the activation step is discussed for the model synthesis above. By TLC analysis, we found the final product spot to appear only after the addition of PE, with both spots having much smaller R_f values than all other reagents. We expected both PE and CLPE to have small R_f values because of the charged phosphate group. PE has a relatively small R_f value even though the lipid is composed of two-eighteen carbon length alkyl chains. We expect CLPE to be less polar than PE with a charged ammonium substituent being replaced by a peptide bond with C343. However, because CLPE still contains a

charged phosphate, we expect the R_f value to be relatively small but yet larger than PE. As detailed in the experimental, we use a relatively polar mobile phase to remove PE and CLPE from the TLC base line. Even with this solvent system, PE has a R_f value no greater than 0.1, while CLPE is a broader spot with R_f value from 0.3 to 0.4. According to the technical support team at Avanti, the CLPE R_f value we observe is in line with their dye labeled lipids that have similar structures.

We find evidence the final product spot corresponds to CLPE not only by the R_f value, but also by the staining behavior. PE is easily visualized with the ninhydrin stain, while CLPE shows no reaction with ninhydrin. This is to be expected because ninhydrin reacts most vigorously with primary amines and only faintly with secondary. CLPE is a secondary amine but appears as a bright yellow spot that most certainly covers any faint pink stain that may occur from reaction with ninhydrin. When the spots are sprayed with the phosphate stain, both spots become stained. This is expected because, unlike the amine, the phosphate substituent of PE should remain unaffected by the covalent attachment of C343. The phosphate stain turns the PE spot dark blue but the CLPE spot black. Phosphates usually stain dark blue like PE, but because CLPE is a yellow dye, the addition of the two dyes produce a black spot.

According to TLC and staining behavior, the final product behaves the same way we expect CLPE to behave. First, whether C343 was activated with TPP/DPDS or CDI, we observed exactly the same R_f value and staining properties of the final product spot. In addition, especially for the CDI synthesis, the staining behavior is what we would expect for CLPE. Spot assignment is complicated for the TPP/DPDS synthesis because TPP contains a phosphate that stains blue with the phosphate stain. CDI does not contain

a phosphate group and therefore shows no reaction with the phosphate stain. Because we observed a second phosphate stained spot on top of the PE spot for the CDI synthesis, we conclude the spot corresponds to a compound that must be a derivative of PE. In addition, the spot was yellow indicating the compound was also a derivative of C343. Also the final product spot is unreactive with Ninhydrin stain, indicating the primary amine of PE has reacted. Therefore, unless a completely unexpected reaction was taking place, these results certainly suggested the final product spot was CLPE.

For both TPP/DPDS and CDI syntheses, the purified final product appeared flaky with brown and orange specks. The TPP/DPDS synthesis gave the higher percent yield of 98%. We have reservations in quoting this percent yield. As will be discussed below, elemental analysis of the sample suggests the sample is impure, most likely the result of unevaporated solvent. In addition, we are uncertain as to what the counterion of CLPE is. For the percent yield presented above, we assumed sodium is the counterion. The CDI synthesis gave a 57% yield. We will discuss why CDI gave a lower percent yield below.

We found that the activation of C343 was the most important step for obtaining the highest yield of CLPE. Several obstacles arose that seemed to limit the activation of C343 and therefore the yield. First, we found it difficult to dissolve C343 in organic solvents at high concentrations. We found C343 to dissolve to the greatest extent in methylene chloride. However, even with methylene chloride as the solvent, C343 never seemed to completely dissolve during the activation step. We did find that as the reaction progressed, especially after PE addition, the amount of unsolvated C343 would decrease. We also found that C343 is relatively difficult to activate. When we observed the activation of C343 by TLC, we found that the activated C343 spot was never more

intense than the C343 spot. We believe that the carbonyl of the ring system's ester stabilizes the carboxylate proton and makes C343 less susceptible to attack by the activating agents. X-ray crystallography of solid C343 indicates that the carboxylate proton does indeed reside near the ring system carbonyl[10].

In order to obtain the greatest yield, we attempted to activate C343 with several agents: TPP/DPDS, CDI, and EDCI. As a separate experiment, we combined the three different activating agents into three separate containers with molar equivalents of C343. We then watched by TLC analysis which agent produced the brightest activated C343 spot. For all three, we found that the activated spot was never more intense than the C343 spot. TPP/DPDS and CDI gave similar intensities but both seemed more effective than EDCI. Because of this result, we decided not to attempt a CLPE synthesis with EDCI as the activating agent. These results suggest that TPP/DPDS and CDI activate C343 to the same extent. However, we found that the synthesis of CLPE using TPP/DPDS gave a much greater yield. We believe the reason for the greater yield is from the molar equivalents used in each synthesis. According to Avanti technical support, CDI, when in excess, can polymerize phospholipids. Therefore, CDI, C343, and PE need to be combined in molar equivalents. We did not find this to be the case for TPP/DPDS. We did not observed a reaction between TPP, DPDS, and PE when C343 was not present. This allowed us to combine TPP, DPDS, and C343 at twice the molar equivalent as PE and therefore drive the equilibrium of the reaction towards products.

We have found evidence that the CLPE we collect is not completely pure. Elemental analysis performed by M-H-W Laboratories found: Calculated for $NaC_{57}H_{90}PN_2O_{11}$: C, 66.25%; H, 8.78%; P, 3.00%; N, 2.71%. Found: C, 62.06%; H,

8.58%; P, 2.51%; N, 2.48%. Obviously, the CLPE is contaminated. Although the contamination is not significant to our experiments, we believe CLPE may be contaminated to a small extent by unpurified C343, CLPE degradation, the counterion is something other than sodium, or unevaporated solvent.

We are particularly concerned about C343 contamination. The point of synthesizing CLPE is so we can assume that all the collected fluorescence is emitted by CLPE localized at the water/lipid interface. If CLPE is contaminated with C343, a percentage of the collected fluorescence would be from C343 dissolved in an environment removed from the interface. We will address this concern further in Chapters 4 and 5. TLC analysis of CLPE does show a small C343 spot. However, we believe the amount is too small to be a concern because this spot appears by sight as no more than 5% of the CLPE spot. In addition, as we will discuss below, NMR spectra of CLPE show no indication of C343 contamination. Contamination greater than a 10%, and probably greater than a 5%, would be expected to appear in the spectra. While we did not quantify the amount of residual C343 in the CLPE sample, the analysis should be relatively straightforward by high-pressure liquid chromatography (HPLC). Because CLPE is not readily dissolved, we must borrow equipment from other laboratories, and a new column would be relatively expensive, we have been reluctant to attempt the analysis. However, it should be possible to perform using a normal phase column and HPLC equipment with a detector capable of measuring 425nm absorption. We note that C343 can not account for the contamination measured by elemental analysis. The percent mass of carbon, hydrogen, and nitrogen for C343 is as follows: C, 67.35%; H, 5.30%; N, 4.91%. While based on TLC analyis it is obvious some C343 contaminates CLPE, the

addition of C343 to a CLPE sample cannot produce the elemental analysis results. The small amount of C343 contamination should not affect the solvation dynamics experiments we perform in subsequent chapters.

TLC analysis of CLPE has also revealed evidence of CLPE degradation. When a methylene chloride:methanol:acetic acid 90:9:1 solvent system was used to elute CLPE, we observed a brown streak that followed the CLPE spot from the baseline. Two-dimensional TLC analysis with the same solvent both directions, revealed a triangular swath of light brown product with the CLPE spot at the apex. This result suggests that CLPE degrades as it elutes along the plate. Although difficult to identify positively, we believe the brown streak is related to the presence of acetic acid. Without acetic acid in the solvent system, CLPE elutes as a streak from the baseline. However, purification without acetic acid would be difficult. Other solvent systems may perform more effectively although, to this point, we have found none. We do not find this degradation product to be a significant concern. First, the degradation product appears very faint on the TLC plate and therefore should be only a minor contaminant. More importantly, the degradation product is not fluorescent and therefore would not contribute to the solvation dynamics we will ultimately measure. We note that this degradation product could account for the elemental analysis results if the product corresponds to an oxidized derivative of CLPE. Oxygen would lower the measured percent carbon, hydrogen, nitrogen, and phosphorous without being detected itself.

Also, we may be in error for assuming sodium ion is the counterion of CLPE. We have assumed that washing the reaction with sodium bicarbonate in the reaction quench step allowed sodium to serve as the counterion. It may be possible the counterion is

actually a proton or another unforeseen positive ion. Although unlikely, a higher molecular weight counterion without high-mass percentages of carbon and hydrogen could account for the elemental analysis results. Thus we attempted to determine sodium and phosphorous mass percentages of the CLPE sample with ICP-AES. We analyzed for phosphorous because the ICP-AES instrument is more accurate than the techniques used by M-H-W Laboratories. Unfortunately, our results were inconclusive because we found it difficult to digest CLPE with nitric acid. Analysis determined: Calc.: Na, 2.23%; P, 3.00%. Found: Na, 0.53%; P, 0.84%. While we believe these results are in error, they do indicate that the CLPE sample contains a significant amount of sodium and therefore constitutes at least a percentage of the sample. Since this analysis was done, we have found an equal molar ratio of nitric acid and perchloric acid fully digests CLPE.

Although the CLPE sample most likely contains some amount of C343, shows some degradation, and may contain counterions other than sodium, we believe unevaporated solvent is probably the largest contributor to the unpredicted elemental analysis results. Any of the individual solvents employed in the purification step, that is, methylene chloride, methanol, and acetic acid, could account for the elemental analysis results if they remained in the sample. Specifically, including elemental chlorine or oxygen to the sample would raise the overall weight of the sample and reduce the percentage of carbon, hydrogen, nitrogen, and phosphorous. For example although ^{1}H-NMR suggests unlikely, we calculate that if 16% by mass of the CLPE sample were acetic acid, then the elemental analysis would show: C, 62.0%; H, 8.45%; P, 2.52%; N, 2.28%. No matter what the source of contamination is, we do not find it a significant concern as long as the impurity level is small. Typical lecithin samples require 2 mg of

CLPE for a 10 ml sample. A 15% by mass impurity would correspond to 30 ppm. At this concentration, the effect would be undetectable in a lecithin interface prepared at a concentration of about 50 mM phospholipids.

^{1}H-NMR and mass spectroscopy positively identified the final product as CLPE. We first present NMR data followed by mass spectroscopy data. Initial ^{1}H-NMR of the final product displayed broad peaks with many of the single proton peaks completely missing. To sharpen peak widths, we attempted to solvate CLPE in several deuterated solvents including chloroform, methylene chloride, toluene, and pyridine with little success. In addition, we attempted taking the spectrum at elevated temperatures. Toluene has an elevated boiling point and is commonly used for variable temperature NMR. We obtained the spectrum of the final product in toluene at 75°C but found very little change of the peak widths. In the end, we determined that the final product was not dissolved at a high enough concentration. These solvents were effective in solvating up to about 10 - 20 mg of final product per milliliter. By using a 9:1 deuterated-methylene chloride:methanol solvent system, we could dissolve greater than 50 mg of final product per milliliter. As a result, spectra resolution greatly improved. Unfortunately as discussed below, deuterated-methanol exchanges with acidic protons of the final product obscuring the identification.

Figure 3.6 displays the ^{1}H-NMR spectrum of the final product in 9:1 CD_2Cl_2:CD_3OD at 25°C. Of the many spectra of the final product we have obtained, this spectrum most clearly displays all the proton peaks associated with CLPE. The spectrum contains no solvent or TMS peaks to reference. Instead, we have referenced the δ 7.04

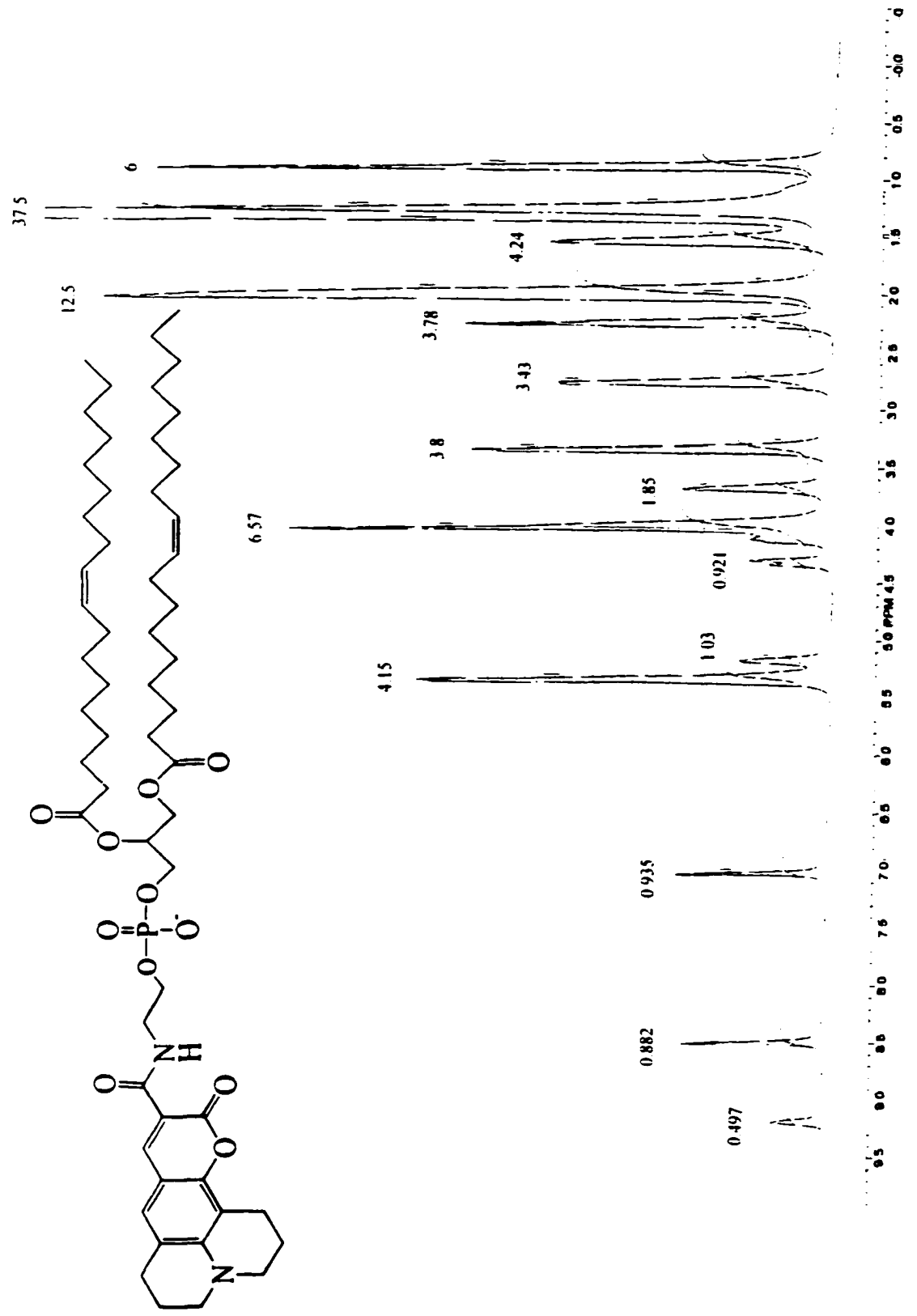

Figure 3.6. ^{1}H-NMR of CLPE prepared with TPP/DPDS. Product dissolved in 9:1 CD_2Cl_2:CD_3OD.

peak to the corresponding peak of another final product spectrum that was referenced with TMS (see Appendix 3.I). We find peaks at: δ 9.20 (s, 1 H), δ 8.51 (s, 1 H), δ 7.04 (s, 1 H), δ 5.35 (m, 4 H), δ 5.20 (m, 1 H), δ 4.32 (m, 1 H), δ 4.00 (m, 5 H), δ 3.68 (m, 2 H), δ 3.36 (m, 4 H), δ 2.77 (m, 4 H), δ 2.26 (m, 4 H), δ 1.95 (m, 12 H), δ 1.58 (m, 4 H), δ 1.29 (m, 40 H), δ 0.92 (m, 6 H). We could not obtain a spectrum that displayed sharp enough peaks to use splitting as a diagnostic tool. Instead, we rely on chemical shift and integration to assign peaks. We believe the δ 4.00 peak includes exchanged CD_3OH protons. The CH_2Cl_2 peak is probably too weak to see compared to the final product protons; if it is present, it would be included in the δ 5.36 peak.

To assist in the assignment of the final product, we will first list the proton peaks for the starting materials. The ^{1}H-NMR peaks for C343 were previously listed in the model synthesis section above (see Figure 3.4). Figure 3.7 displays the ^{1}H-NMR spectrum of PE in $CDCl_3$ at 25°C. The spectrum was referenced to the chemical shift of TMS (δ 0.00). The 78 protons of PE are accounted for as follows: δ 8.52 (m, 3 H), δ 5.39 (m, 4 H), δ 5.24 (m, 1 H), δ 4.40 (m, 1 H), δ 4.02 (m, 5 H), δ 3.18 (m, 2 H), δ 2.32 (m, 4 H), δ 2.02 (m, 8 H), δ 1.64 (m, 4 H), δ 1.21 (m, 40 H), δ 0.91 (m, 6 H). The small peak at 7.27ppm is $CHCl_3$.

Table 3.1 lists all 15 protons of C343 and 78 protons of PE as they are assigned to the 84 protons of the final product. Some peaks correspond to protons that do not have the same chemical shift in both starting material and product. Those peaks are marked with a question mark and discussed sequentially below.

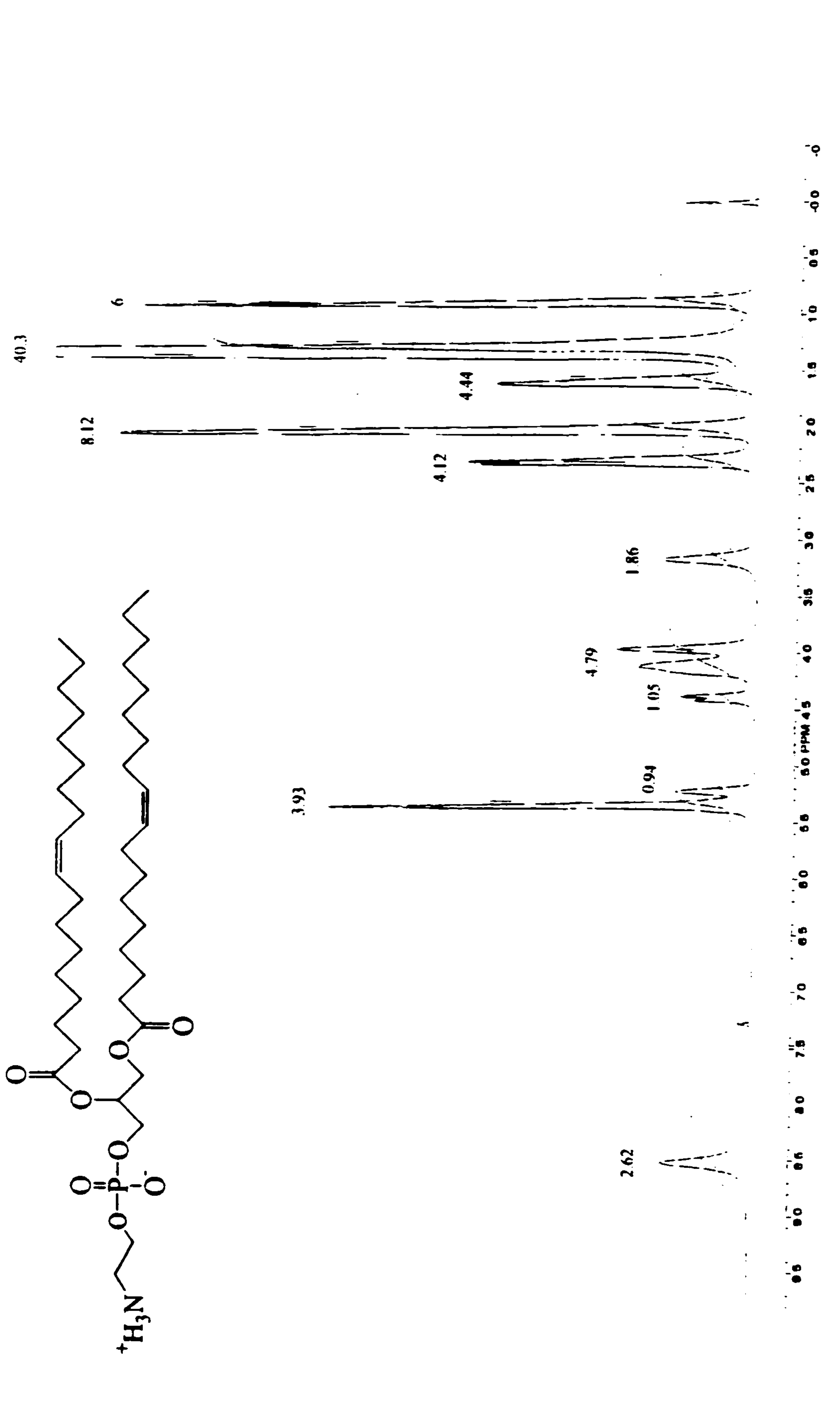

Figure 3.7. ^{1}H-NMR of PE dissolved $CDCl_3$.

Table 3.1. Comparison of 1H-NMR peaks of CLPE and the corresponding PE and C343 peaks.

Peak	PE	C343	Final Product
1		δ 10.95 (1 H)	?
2	?	?	δ 9.19 (1 H)
3	δ 8.52 (3 H)		?
4		δ 8.46 (1 H)	δ 8.49 (1 H)
5		δ 7.06 (1 H)	δ 7.02 (1 H)
6	δ 5.34 (4 H)		δ 5.32 (4 H)
7	δ 5.21 (1 H)		δ 5.17 (1 H)
8	δ 4.39 (1 H)		δ 4.31 (1 H)
9	δ 4.02 (5 H)		δ 4.00 (5 H)
10	?	?	δ 3.66 (2 H)
11		δ 3.40 (4 H)	δ 3.32 (4 H)
12	δ 3.15 (2 H)		?
13		δ 2.85 (4 H)	δ 2.74 (4 H)
14	δ 2.29 (4 H)		δ 2.23 (4 H)
15	δ 2.01 (8 H)	δ 2.01 (4 H)	δ 1.97 (12 H)
16	δ 1.59 (4 H)		δ 1.52 (4 H)
17	δ 1.28 (40 H)		δ 1.25 (40 H)
18	δ 0.88 (6 H)		δ 0.86 (6 H)

Peak 1 corresponds to a C343 proton that has no corresponding peak in the final product's spectrum. As we did in the model synthesis ^{1}H-NMR analysis, we assign this proton to the carboxylic acid proton. Therefore, this proton should not appear in the CLPE spectrum. Indeed, the proton does not appear in final product's spectrum. However, this can not be considered proof of the final product's identification because the proton is unlikely to appear when the analyte is dissolved in deuterated-methanol because proton exchange is expected to occur.

Peak 3 corresponds to three protons that are found as a broad peak in PE's spectrum. We assign these to the three ammonium protons. Again, these protons would not appear in the CLPE spectrum and do not appear in the final product's spectrum. Instead, CLPE should display a new proton corresponding to a single proton attached to

the peptide bond amine. We believe this proton is peak 2. We find that peak 2 does not integrate to 1 proton. This is to be expected because a secondary amine proton would exchange with the deuterated-methanol solvent. In fact, unless ^{1}H-NMR spectra are taken within minutes of dissolving the final product, we do not observe this peak supporting its identification as the amide proton. Again, that the three protons associated with peak 3 do not appear in the final product's spectrum is not proof of identification because proton exchange may occur.

Peak 12 corresponds to two protons present in PE's spectrum that do not appear in the final product. We assign these two protons to the alkyl protons one carbon removed from the ammonium group. In the spectrum of CLPE we should observe these two protons further down field because they would experience less shielding due to the peptide bond formed one position removed from their position. We find that peak 10 corresponds well to these two shifted protons.

Therefore, we find that the final product's ^{1}H-NMR spectrum is in good agreement with the spectrum that we would expect for CLPE. Also, the final product spectrum suggests that contamination by C343 is not significant. If C343 were a significant contaminant, we would expect the peaks associated with this chemical moiety to integrate to larger intensities relative to the PE peaks. Instead, these peaks integrate slightly smaller than expected. As a general rule, ^{1}H-NMR spectra have 10% error and therefore we can only conclude C343 contamination is not significant.

Figure 3.6 displays CLPE's spectrum synthesized by TPP/DPDS activation. We also obtained the ^{1}H-NMR spectrum of CLPE synthesized by CDI activation. Figure 3.8 displays this spectrum taken at 25°C in CD_2Cl_2:CD_3OD 9:1 solvent. Notice the spectrum

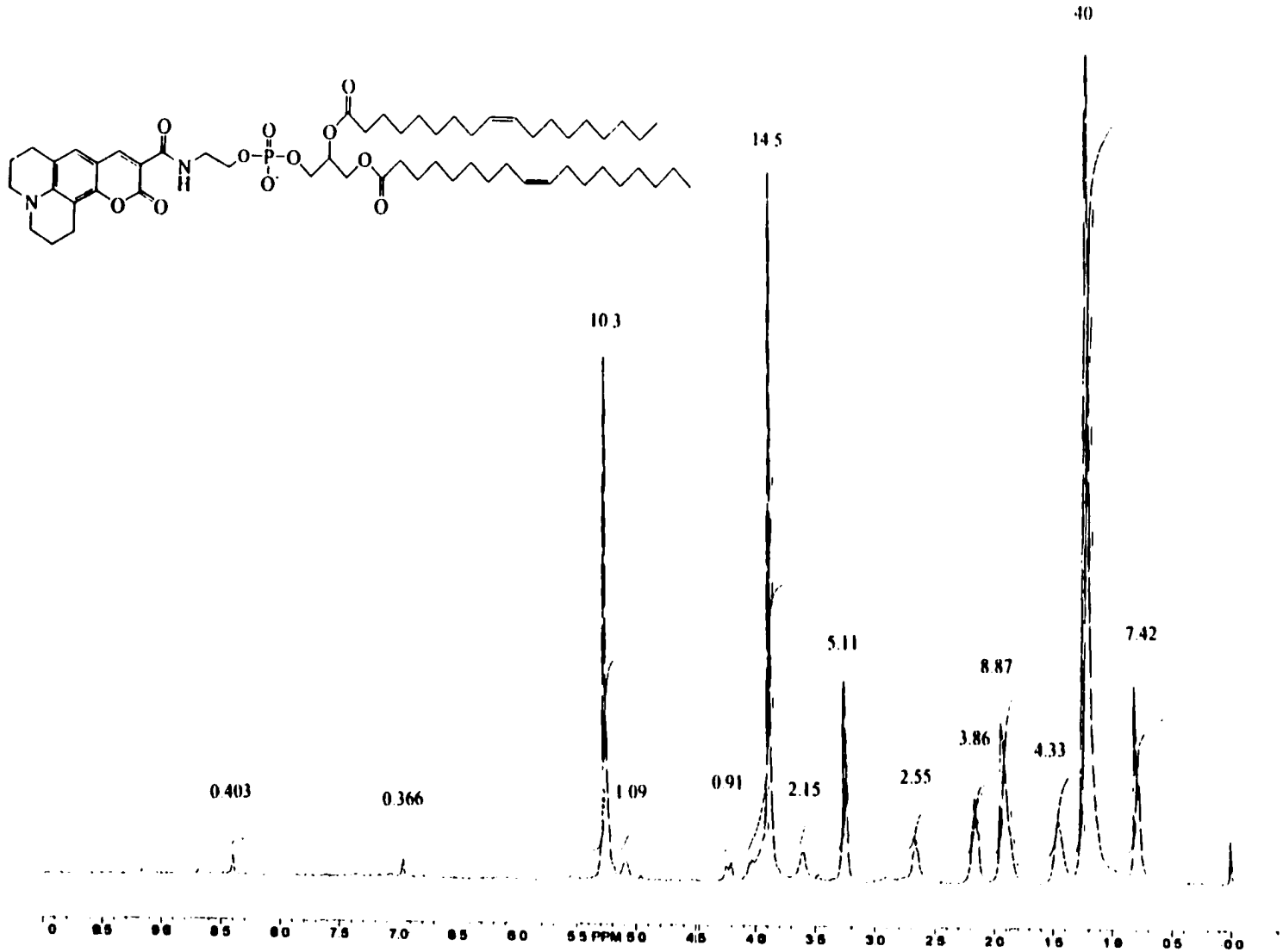

Figure 3.8. ^{1}H-NMR of CLPE prepared with CDI. Product dissolved in 9:1 CD_2Cl_2:CD_3OD.

shows the characteristic peaks similar to what we see in Figure 3.6, even though the integrated peaks are not diagnostic. Unfortunately, we did not isolate enough product to obtain a diagnostic spectrum. The TPP/DPDS synthesized CLPE displays a spectrum similar to the spectrum in Figure 3.8 when analyzed at lower concentrations. Based on this NMR spectrum along with the final product's behavior by TLC analysis we find that both TPP/DPDS and CDI synthesized CLPE. We did not feel a need to conclusively identify the CDI final product because we were satisfied with the alternative TPP/DPDS synthesis.

Obtaining a mass spectrometry (MS) spectrum of the final product positively identifying it as CLPE was challenging. Several attempts were initially made with positive and negative electrospray and FAB+, which revealed mass fragments no larger than 300 a.m.u. Phospholipids in general are difficult to obtain mass spectra of because they fragment easily. According to Avanti technical support, they will often scrape the phospholipid analyte from a TLC plate, dissolve the scrapings in an electrospray solvent, and then analyze with negative electrospray MS. They rarely perform MS on dye-labeled phospholipids because solvation problems can clog their instrument. CLPE was not only readily fragmented but also did not readily solvate in electrospray solvents. After much perserverance we finally achieved success with FAB+ with a CLPE sample synthesized with TPP/DPDS: m/z calc. 1011.6439, obs. 1011.6437 ($CLPE^{-}\bullet 2H^{+}$, 100%); calc. 1033.626, obs. 1033.629 ($CLPE^{-}\bullet H^{+}\bullet Na^{+}$, 6.8%).

In addition to NMR and MS, we have attempted other methods to identify CLPE as the final product with less than conclusive results. We attempted to measure the time-resolved anisotropy of the final product in a solution of 9:1 methylene chloride:methanol.

We found C343 to show a single rotational relaxation of 50 ps in this solvent solution. As expected, we found the rotational relaxation to be much slower for CLPE because of the larger molecular weight. Unfortunately, the anisotropy data is too noisy to allow us to determine if the data is best fit with a single long time component or a short and long component. If there is a short 50 ps component, the data could suggest C343 is a significant impurity. We find the data to be inconclusive.

We also attempted to use ^{13}C-NMR to identify CLPE. Appendix 3-II display the ^{13}C-NMR spectra of CLPE, C343, and PE solvated in 9:1 CD_2Cl_2:CD_3OD or $CDCl_3$ at 25°C. As can be seen by comparison of the spectra, the finger print bands of both C343 and PE appear in the CLPE spectrum. Unfortunately, a couple of the peaks in the CLPE spectrum do not have corresponding peaks in the C343 or PE spectra, i.e. 20.59 ppm, 33.22ppm, and 107.8ppm. In addition, we have trouble accounting for all 57 carbon nuclei. We count 54 clearly distinguishable nuclei. To complicate interpretation, Silverstein indicates there will be only a small chemical shift for the carbons near the peptide bond of CLPE. Since the coupling of C343 to PE involves net change of carbons, we find that it may not be possible to use ^{13}C-NMR to distinguish between a CLPE sample and a sample of PE and C343. Therefore, we find the data support CLPE being the final product but the evidence is too weak to draw conclusions.

Finally, we have obtained FT-IR spectra of the final product. Appendix 3.III displays the spectra for CLPE, C343, and PE (Nicolet-5PC-FTIR). Analytes were dissolved in methylene chloride and spotted onto sodium chloride cells. Two vibrational bands indicate CLPE is the final product. First, the 3330cm^{-1} vibration present in the CLPE spectrum is assigned to a secondary amide bond[11]. The vibration is not present

in either the C343 or PE spectra. Second, the 2133cm^{-1} peak present in the PE spectrum is assigned to the ammonium ion overtone that should disappear if the amine becomes substituted[11]. Indeed the peak does not appear in the CLPE spectrum. We find further assignments difficult. Many characteristic carboxylic and amine vibrations appear in the 500-1800cm^{-1} region. However, CLPE's spectrum contains too many bands in this region to be diagnostic.

Thus, while several of the diagnostic tools used to analyze and identify the CLPE final product provide only qualitative information, all these data at least point to the successful synthesis and purification of CLPE. More importantly, we find that ^{1}H-NMR and MS conclusively prove the identity of CLPE.

3.III.C. CLPE as a Probe of Lecithin Headgroup/Water Interfaces.

After we were confident we had synthesized CLPE, we checked the viability of CLPE as a lecithin interface probe. First, we wished to prove CLPE aligned correctly with other phospholipids with the coumarin labeled headgroup packed within the headgroup interface. Second, we needed to prove the spectroscopy of CLPE is similar to C343. Specifically, CLPE needs to absorb at a similar wavelength and fluoresce with significant intensity. In addition, we needed to find that CLPE shows polarity dependent spectroscopy. Finally, we needed to confirm that CLPE would detect the same solvation dynamics observed with C343.

We would like to compare the absorption and emission of CLPE with C343 to find if the derivatisation of C343 affects the spectroscopy. Unfortunately, the tendency of CLPE to aggregate seems to limit this possibility. Unlike C343 and C343-chloroaniline, CLPE contains a lipid group biologically designed to aggregate. Figure

3.9 displays the absorption spectrum of CLPE in 9:1 methylene chloride:methanol. We believe the double peaked spectrum arises from aggregation. Therefore, we found the best way to compare CLPE with C343 is to compare their absorption and emission within cyclohexane/lecithin/water reverse micelles. As we discussed in Chapter 2, we believe C343 is solvated in-between lipid headgroups within the reverse micelles. We expect the C343 substituent of CLPE to be solvated in a similar position. We might observe slight differences arising from their slightly different locations. However, assuming CLPE orients correctly with the C343 substituent within the headgroup region, we expect C343 and CLPE to have similar absorption and emission.

Figure 3.10 displays steady-state absorption and emission of C343 and CLPE in cyclohexane/lecithin/water reverse micelles. Clearly, the spectra are very similar. Because the absorption spectrum of CLPE is very similar to C343, which we have previously determined resides inside the reverse micelles (see Chapter 2), we believe that the CLPE fluorophore resides in the same environment. Second, the CLPE absorption spectrum displays a single peak that is only slightly narrower than C343 in the same environment. We would expect significant broadening or additional peaks identifying the differing environments if a percentage of the CLPE molecules were aligned counter to the pervading lecithin orientation. The parent fluorophore, C343, shows strong spectral dependence on solvent allowing its location in a heterogeneous sample to be determined[12-14]. The similarities in both the emission and absorption spectra indicate that the CLPE fluorophore is inside the micelles.

Figure 3.11 shows the absorption and emission of CLPE in cyclohexane/lecithin/water reverse micelles as a function of hydration. In Chapter 2, we

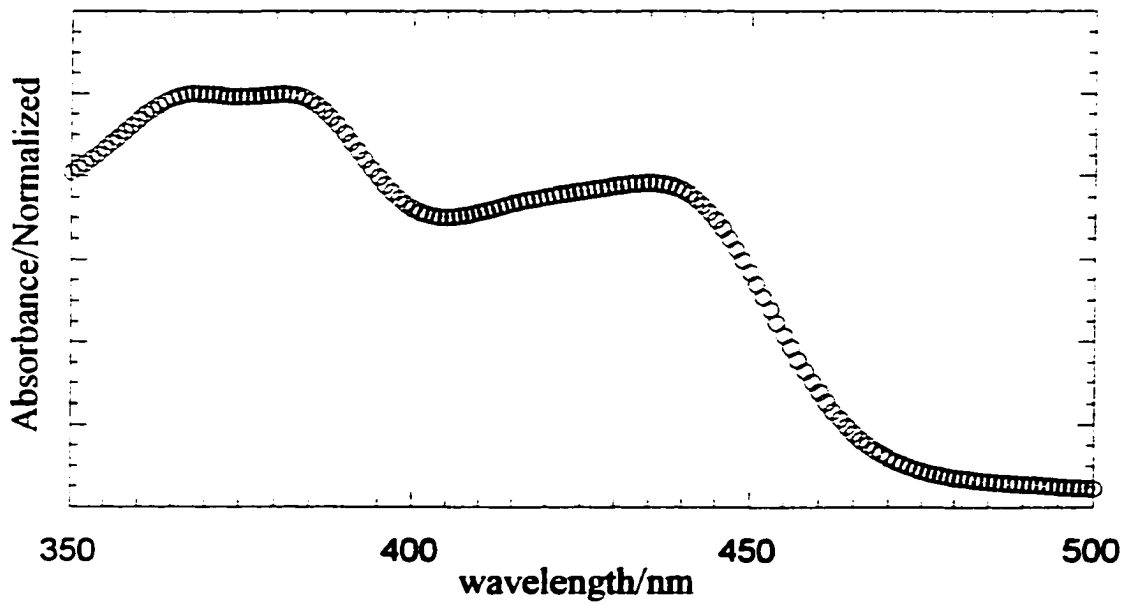

Figure 3.9. Absorption spectrum of CLPE in methylene chloride.

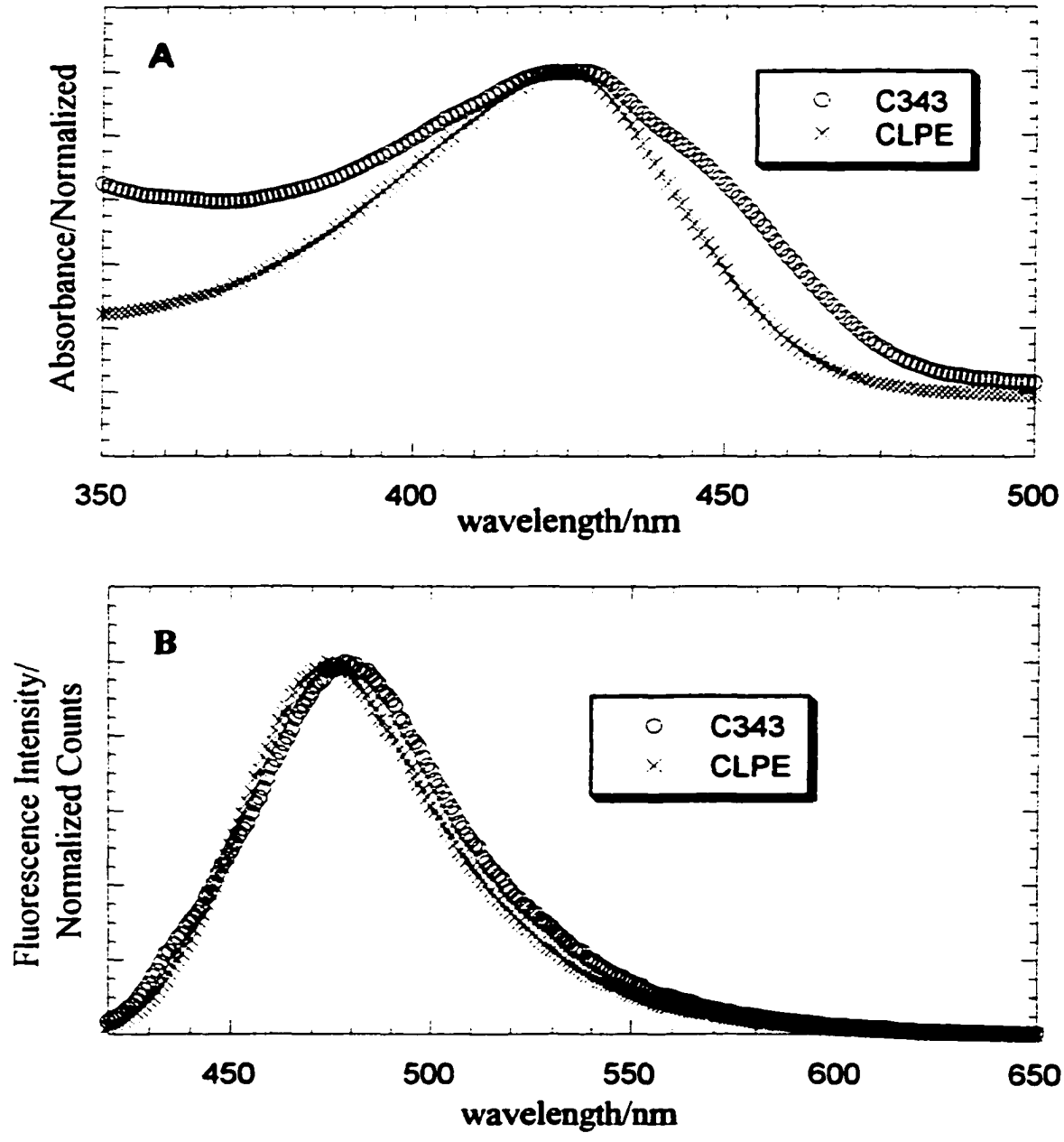

Figure 3.10. Absorption (A) and emission (B) of C343 and CLPE in cyclohexane/lecithin/water w = 6.4 reverse micelles.

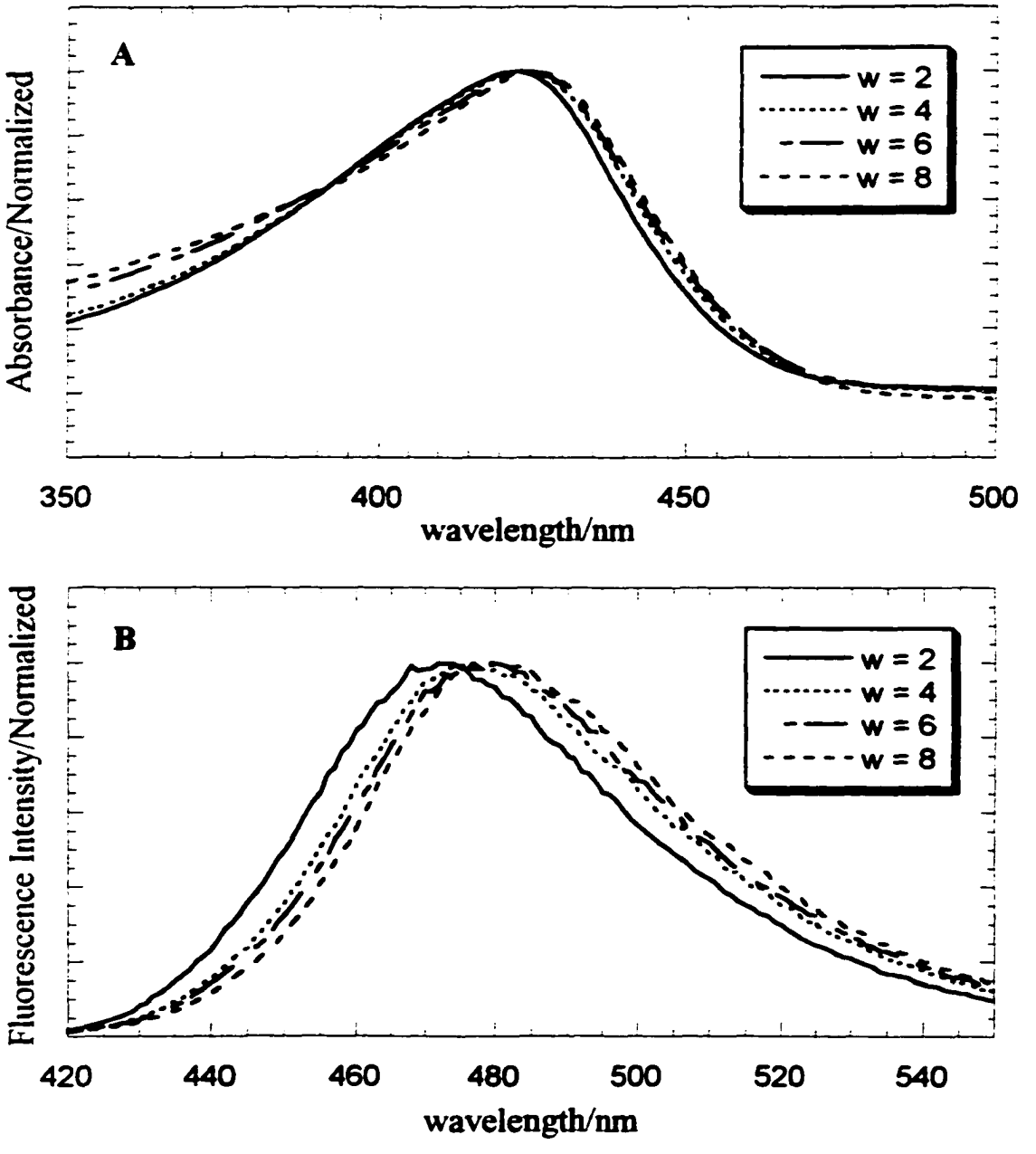

Figure 3.11. Absorption (A) and emission (B) of CLPE within cyclohexane/lecithin/water reverse micelles as a function of hydration.

observed red-shifting with increasing hydration for the C343 absorption and emission spectra in the same reverse micelles. The CLPE emission spectra show similar hydration dependent spectral shifting. In fact, the overall shift observed for CLPE from $w = 2.4$ to $w = 6.4$ is very similar to what we observed for C343. Again, this result is strong evidence CLPE is correctly aligned within the lecithin interface. If a percentage of CLPE molecules were incorrectly aligned, we would expect a corresponding proportion of the emission spectra to be insensitive to the hydration level. It also indicates that the CLPE resides in a similar environment as the C343. Figure 3.11 also shows that unlike the emission spectrum, the absorption spectrum of CLPE shows little hydration dependence. We are unsure as to why this is occurring. As we will refer to in subsequent chapters, this seems to be a general property of CLPE.

The most crucial test for CLPE's viability as a solvation dynamics probe was whether its spectral response accurately reflects solvent motion. In standard solvation dynamics probes, the intramolecular reorganization is small relative to the solvent reorganization and occurs on a time scale faster than we detect. However, it is possible that covalent attachment of the nonrigid PE to the fluorophore could introduce longer intramolecular vibrational relaxation pathways. To assess this issue and its effectiveness as a probe of solvation dynamics, we reproduced solvation dynamics measurements of cyclohexane/lecithin/water reverse micelles obtained with C343 (see Chapter 2) with CLPE as the probe. Table 3.2 lists results from these experiments. If the CLPE resided in a slightly different position or location within the micelles, we would expect some discrepancy between the dynamics observed with CLPE vs. C343. However, as shown in

Table 3.2, the results are remarkably similar. These results prove CLPE aligns correctly within the reverse micelle and detects the same dynamics as C343.

Table 3.2. Measured solvation dynamics components in cyclohexane/lecithin/water reverse micelles as a function of probe and hydration. $C(t) = \sum_i a_i * \exp(-t/\tau_i)$.

Environment	a_1	τ_1/fs	a_2	τ_2/ps	a_3	τ_3/ps
C343 in w = 5.8 reverse micelles	0.100 ± 0.003	420 ± 30	0.17 ± 0.03	17 ± 7	0.74 ± 0.07	340 ± 100
CLPE in w = 6.4 reverse micelles	0.11±0.01	620±10	0.22±0.01	11±1	0.68±0.01	210±10
C343 in w = 6.8 reverse micelles	0.13 ± 0.01	570 ± 70	0.25 ± 0.01	14 ± 1	0.62 ± 0.02	320 ± 40

In addition to time-resolved fluorescence Stokes shift measurements to assess the solvation dynamics, we also compared results from time-resolved fluorescence anisotropy of CLPE within cyclohexane/lecithin/water w = 6.4 reverse micelles with related measurements for C343. Like C343 (see Chapter 2), CLPE has only one ~2 ns rotational relaxation component. From these results, we conclude that C343 and CLPE reside in very similar rotationally restricted environments.

In summary, we have synthesized C343-chloroaniline and CLPE via peptide bond formation. We have shown either of these products can be synthesized by activating the C343 with either TPP/DPDS or CDI, although TPP/DPDS is preferred. N-acylation of the C343 carboxylic acid shows little if any change in the spectral characteristics of the C343 chromophore. Most importantly, we determined CLPE is a viable solvation dynamics probe of lecithin interfaces. Not only does CLPE correctly align within lipid

aggregates so that the C343 substituent is solvated at the lipid/water interface, but also detects the same dynamics observed with the underivatised C343 probe.

3.IV. Acknowledgements

The author would like to say a special thanks to all the monumental minds who have made the synthesis possible: Thomas A. Wynn, Dr. Jeffrey D. Kahl, Dr. Dustin McMinn, Joseph P. Bullock, Paul Gansle, Erik Kuester, Dr. Steve W. Burgess at Avanti Technical Support, and Prof. David Grainger. We also wish to thank Prof. S. H. Strauss, Prof. L. Hegedus, and Prof. E. Fisher for the use of their equipment.

References for Chapter 3

1. Luisi, P.L., *et al.*, *Reverse micelles as hosts for proteins and small molecules.* Biochim. Biophys. Acta, 1988. **947**: p. 209-46.

2. Petrossian, A., A.B. Kantor, and J.C. Owicki, *Synthesis and characterization of a highly fluorescent peptidyl-phosphatidylethanolamine.* J. Lipid Res., 1985. **26**: p. 767-73.

3. Hermanson, G.T., *Bioconjugate Techniques*. 1996, San Diego: Academic Press, Inc.

4. Haugland, R.P., ed. *Handbook of Fluorescent Probes and Research Chemicals*. Sixth ed. . 1998, Molecular Probes, Inc.: Eugene, OR.

5. Hof, M. and R. Hutterer, *Solvent relaxation of fluorescent labels as a new tool for the detection of polarity and rigidity changes in membranes.* Czech. J. Phys., 1998. **48**(4): p. 435-41.

6. Carey, F.A. and R.J. Sundberg, *Advanced Organic Chemistry Part B: Reactions and Synthesis*. Third ed. 1990, New York: Plenum Press.

7. Ellingson, J.S. and W.E.M. Lands, *Phospholipid reactivation of plasmalogen metabolism.* Lipids, 1968: p. 111-20.

8. Skipski, V.P., R.F. Peterson, and M. Barclay, J. Lipid Res., 1962. **3**: p. 467.

9. Pouchert, C.J., ed. *The Aldrich Library of NMR Spectra*. II ed. . Vol. 1. 1983, Aldrich Chemical Company, Inc.: Milwaukee, WI.

10. Honda, T., *et al.*, *Coumarin 343, $C_{16}H_{15}NO_4$.* Acta Crystallogr., Sect. C, 1996. **C52**(3): p. 679-81.

11. Silverstein, R.M., G.C. Bassler, and T.C. Morrill, *Spectrometric Identification of Organic Compounds*. 3rd. ed. 1974, New York: John Wiley & Sons, Inc.

12. Drexhage, K.H., *et al.*, *Water-soluble Coumarin Dyes for Flashlamp-pumped Dye Lasers.* Opt. Comm., 1975. **15**(3): p. 399-403.

13. Reynolds, G.A. and K.H. Drexhage, *New Coumarin Dyes with Rigidized Structure for Flashlamp-Pumped Dye Lasers.* Opt. Comm., 1975. **13**(3): p. 222-225.

14. Tominaga, K. and G.C. Walker, *Femtosecond experiments on solvation dynamics of an anionic probe molecule in methanol.* J. Photochem. Photobiol., A, 1995. **87**(2): p. 192-196.

Appendix 3-I

A. ^{1}H-NMR of CLPE prepared with TPP/DPDS. Product was dissolved in 9:1 CD_2Cl_2:CD_3OD. Spectrum was referenced to tetramethylsilane (TMS) at 0.00ppm. The 7.02ppm proton from this spectrum was used to normalize Figure 3.6.

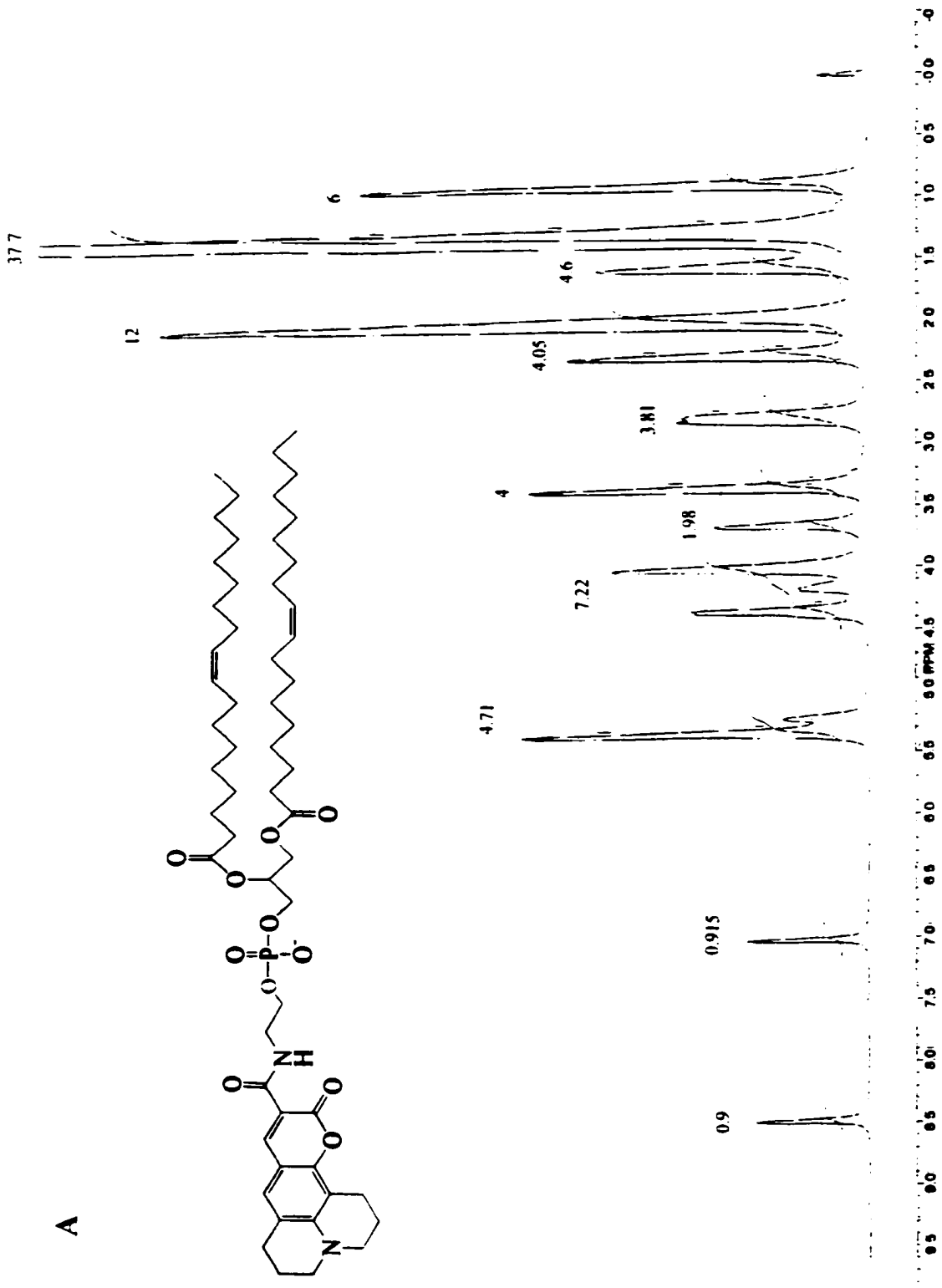

Appendix 3-II

A. ^{13}C-NMR of CLPE dissolved in 9:1 CD_2Cl_2:CD_3OD.

B. ^{13}C-NMR of PE dissolved in $CDCl_3$.

C. ^{13}C-NMR of C343 dissolved in 9:1 CD_2Cl_2:CD_3OD.

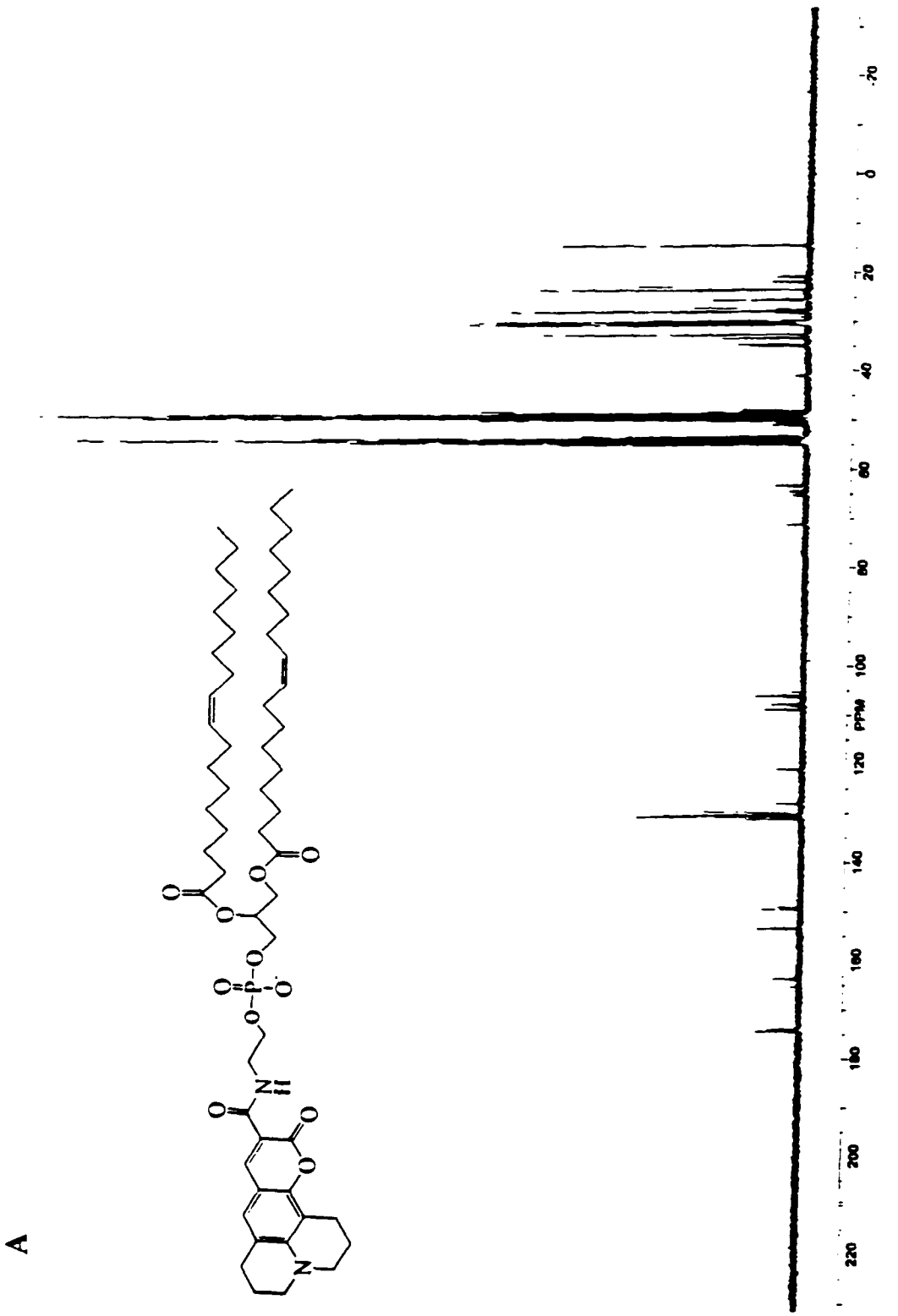

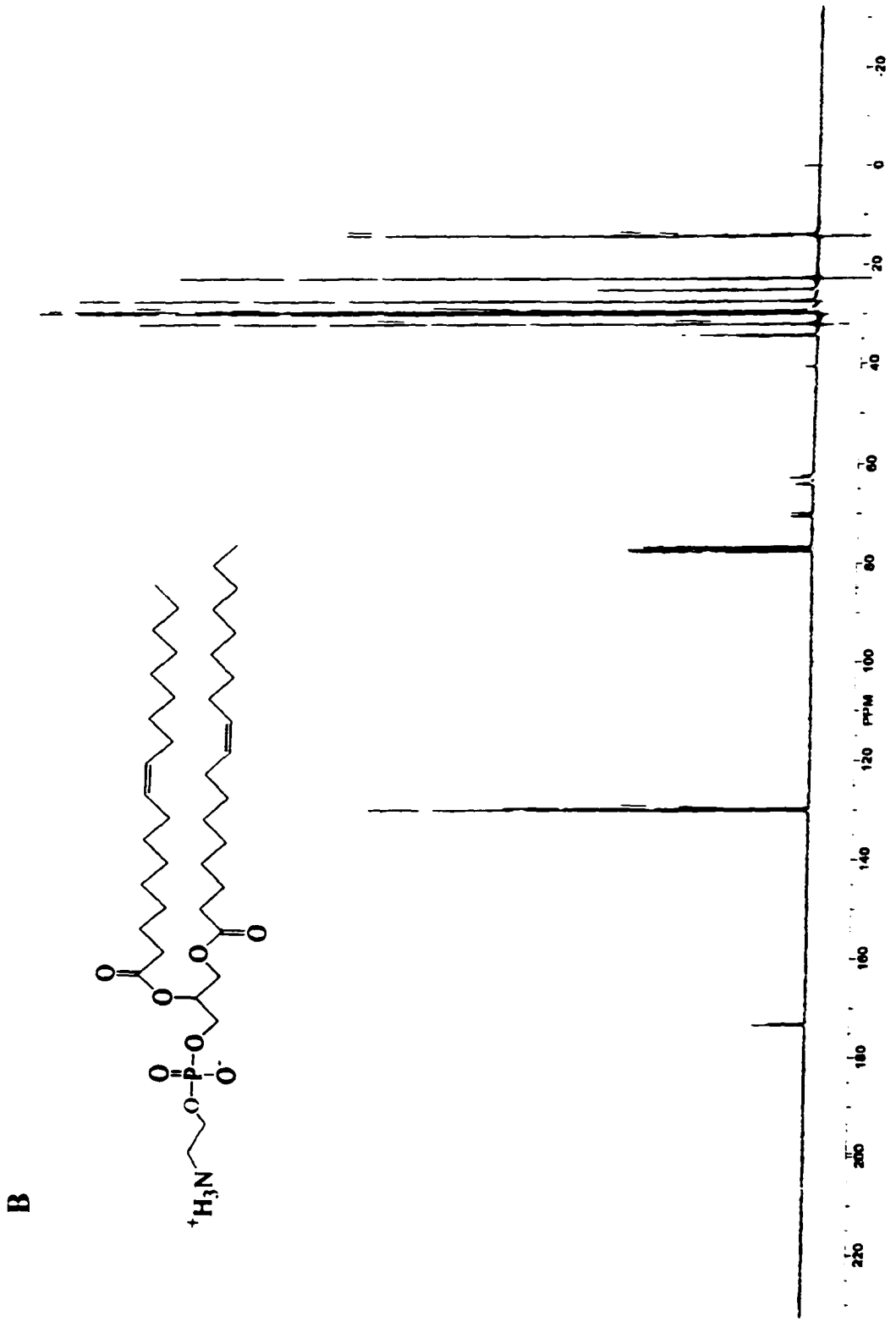

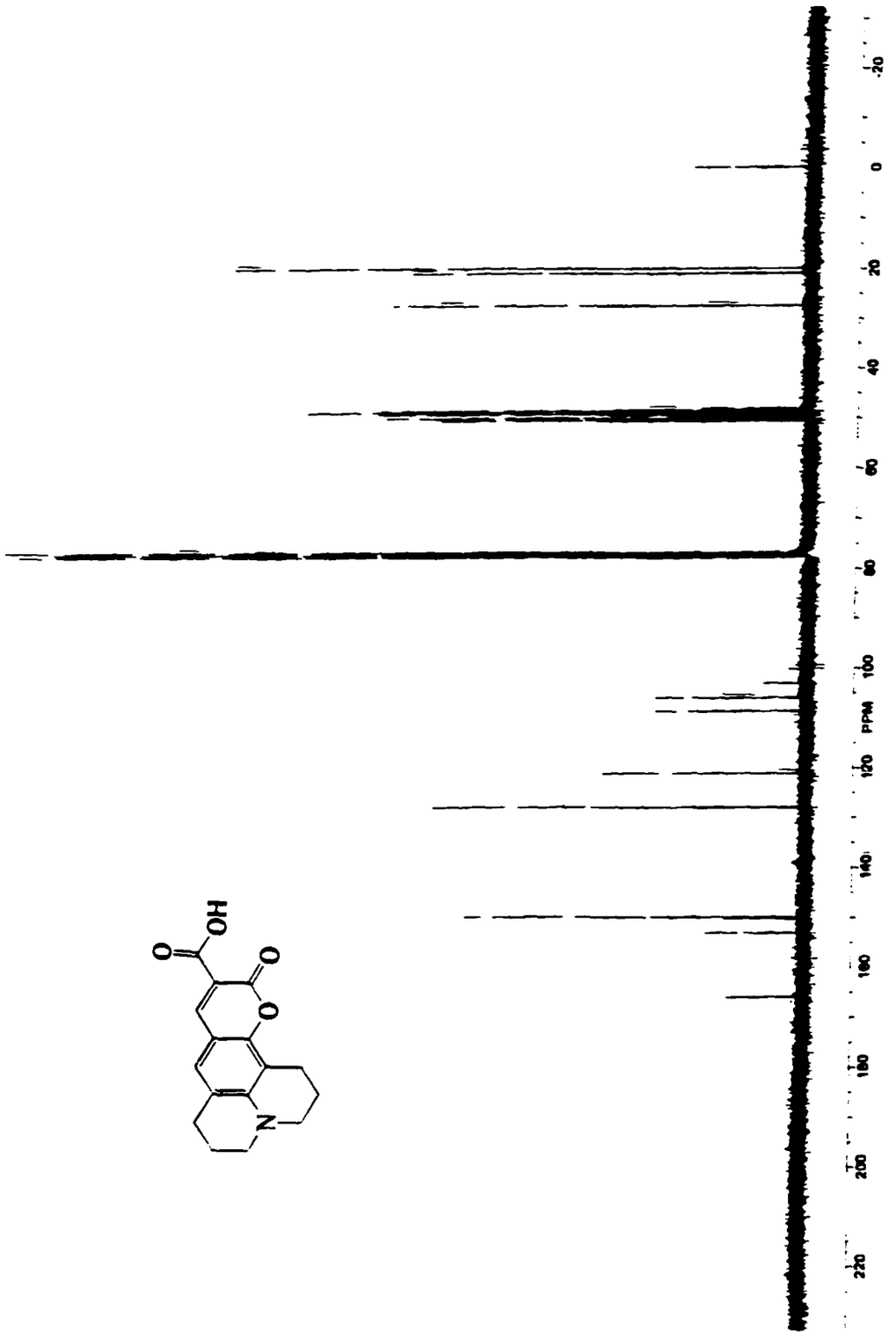

C

Appendix 3-III

A. FT-IR spectrum of CLPE (Nicolet-5PC-FTIR).

B. FT-IR spectra of C343 (Nicolet-5PC-FTIR).

C. FT-IR spectra of PE (Nicolet-5PC-FTIR).

D. FT-IR spectra of C343-chloroaniline (Nicolet Magna-IR 760).

E. FT-IR spectra of C343 (Nicolet Magna-IR 760).

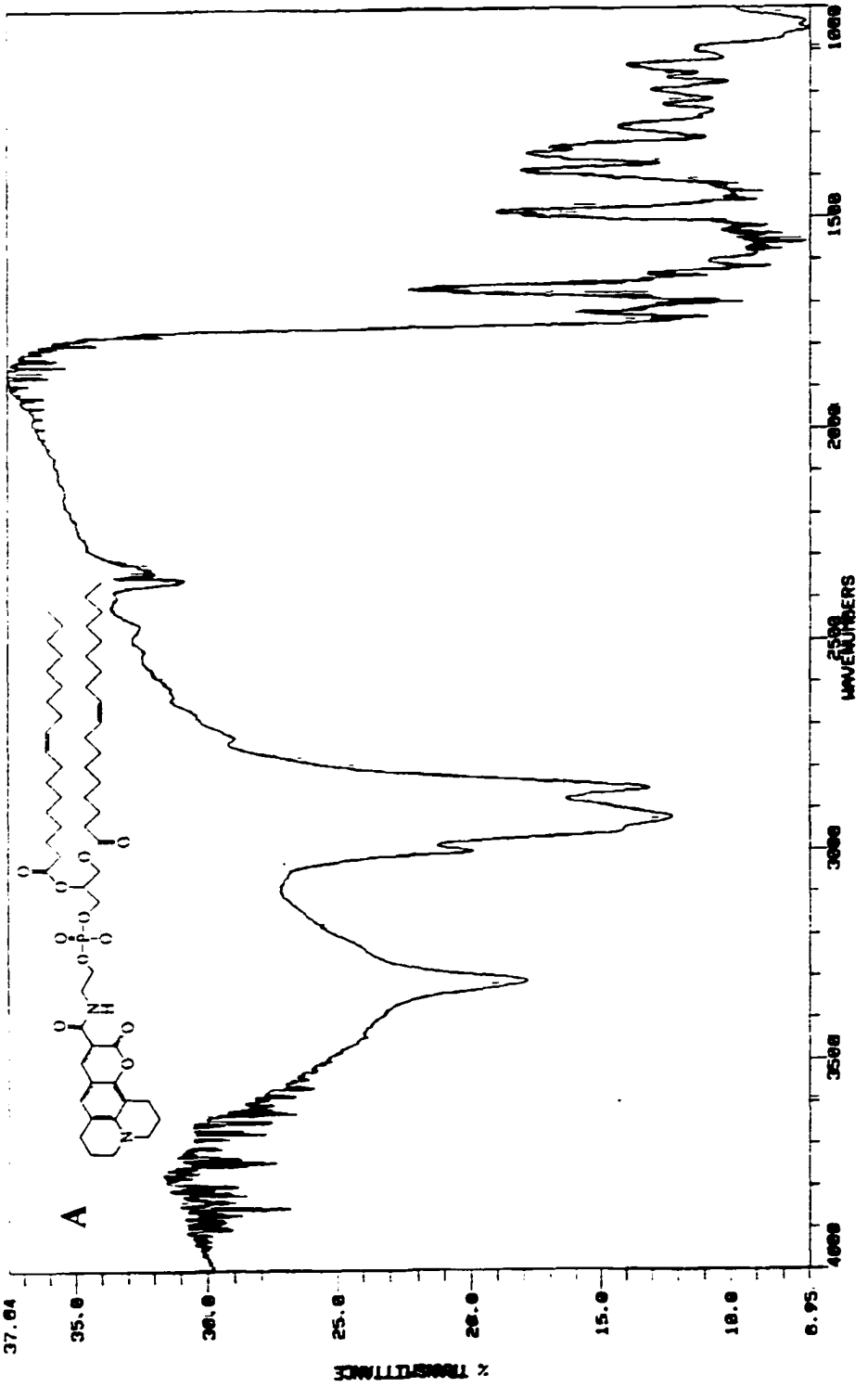

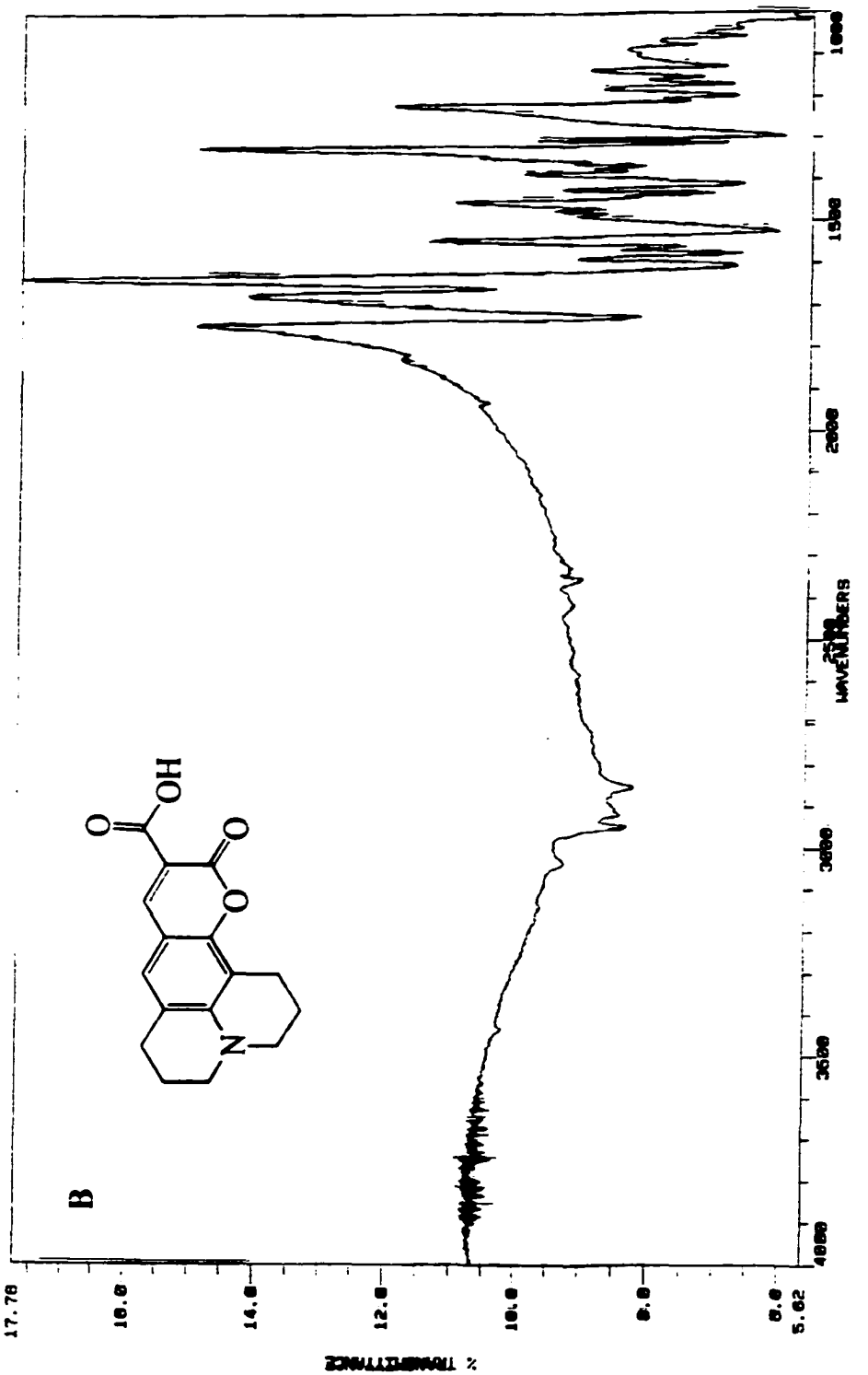

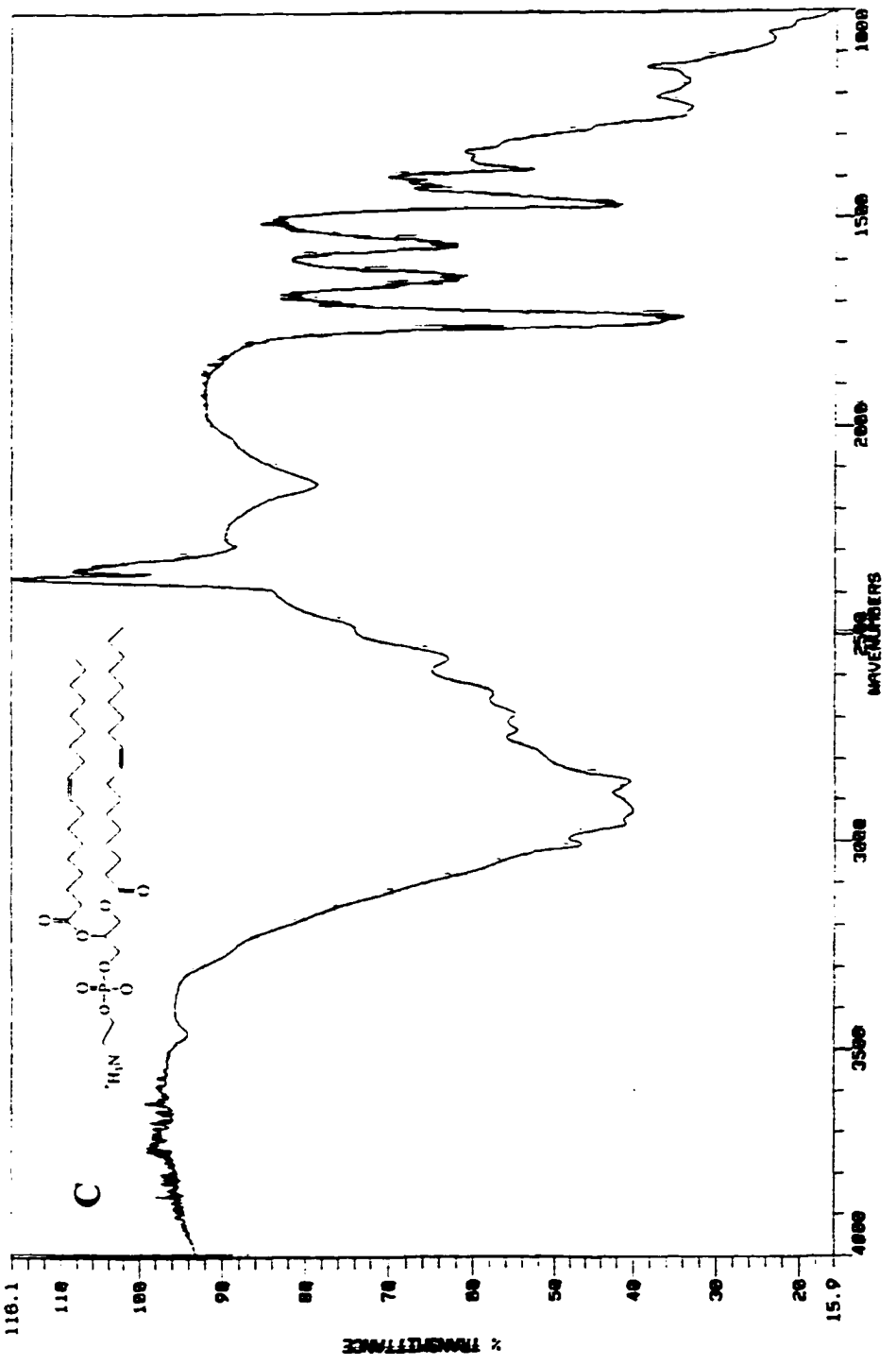

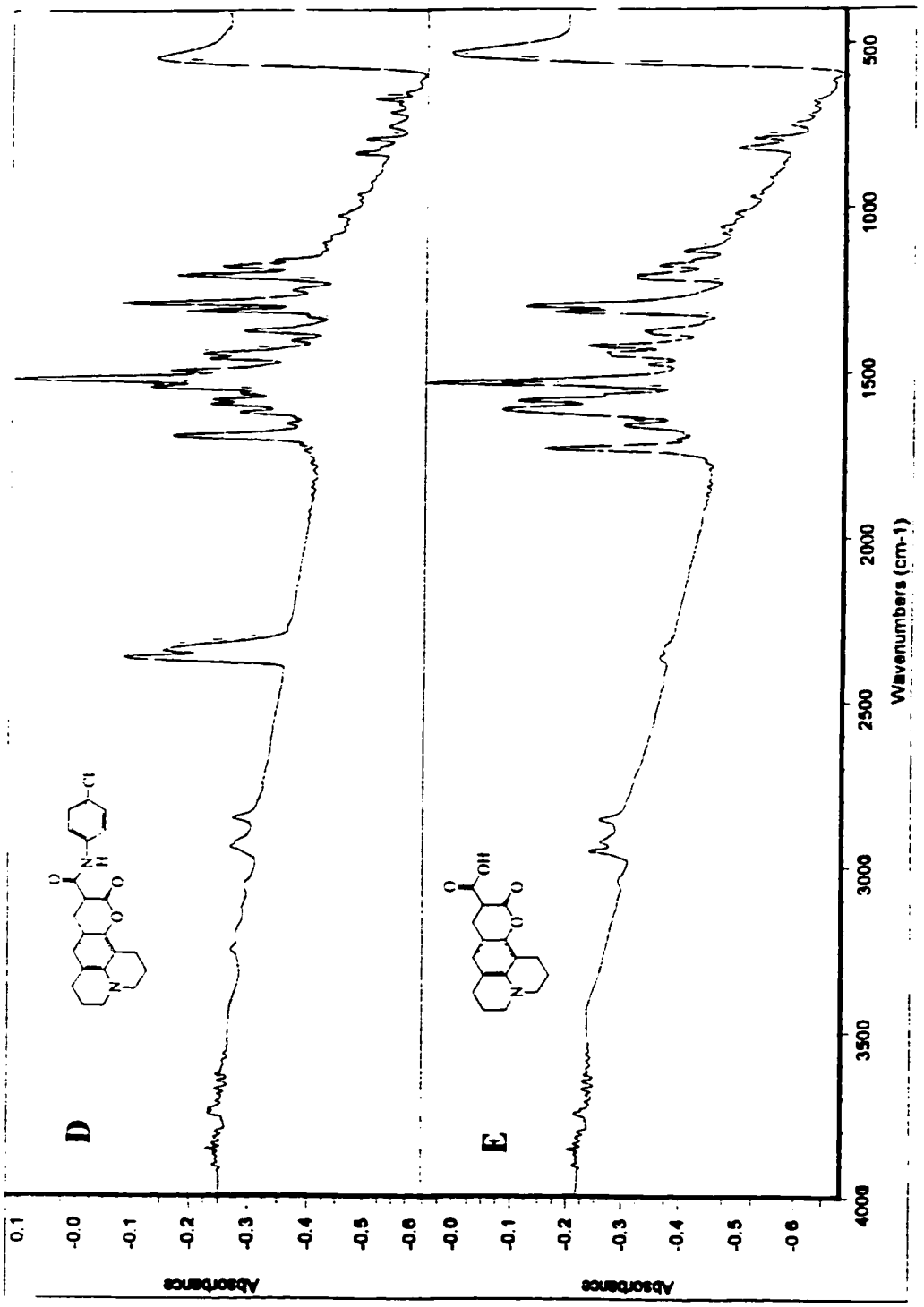

Chapter 4

Morphology as a Determinant of Solvation Dynamics Within Aqueous Reverse Micelles

4.I. Introduction

As was introduced in Chapter 2, reverse micelles are important systems for membrane interface research and can solubilize inorganic and organic solutes to increase solute stabilization or catalytic activity. Lecithin reverse micelles were initially prepared in simple solvents such as benzene and carbon tetrachloride[1-6]. Only serendipitously did researchers find that lecithin organogels are produced in various saturated alkyl solvents[7, 8]. Since their discovery, organogels have been the subject many studies and have proved at least as important as the earlier studies of isolated reverse micelles (see Chapter 2).

In contrast to lecithin reverse micelles prepared in cyclohexane that form extended tubular structures with increasing hydration (see Chapter 2), researchers have found lecithin reverse micelles prepared in benzene form spherical aggregates that retain their spherical form with increasing hydration[4, 9]. Unlike cyclohexane reverse micelles, the viscosity of the lecithin in benzene solution increases only minimally with

increasing hydration[4]. Benzene reverse micelles form aggregates of about 80 monomers of lecithin[4, 9, 10]. The number of monomers per micelle remains relatively constant as hydration is increased[9]. In contrast, the aggregation number for lecithin reverse micelles prepared in cyclohexane increases dramatically with increasing hydration up to the percolation threshold (see Chapter 2). The ternary phase diagrams for both cyclohexane and benzene reverse micelles have been obtained by Shervani et al.[11]. Reverse micelles can be observed at much higher water concentrations when prepared in benzene as compared to cyclohexane.

In both reverse micelle systems, distinct water types are predicted to exist as the hydration of the aqueous interior is increased[3, 12, 13]. As in Chapter 2, we define hydration levels with w values. As we will discuss, vibrational and NMR spectroscopy have shown that water interacts with the lipid headgroup in a similar fashion for both systems[2, 3, 6, 12, 14-17]. All dynamical studies have shown water mobility is significantly slower in reverse micelles and increases with increasing hydration[18-23].

Although most of the recent research concerning lecithin reverse micelles has centered on understanding the properties and structure of the organogel, both spherical and wormlike reverse micelles are used to model membranes and solubilize macromolecules as a means for partial immobilization of enzymes[9]. We have found that few examples exist that contrast the properties of the two different reverse micellar systems[12, 24]. Most studies assume both spherical and wormlike reverse micelles are equivalent mimics of lipid/water interfaces[8].

In this chapter, we propose that the reverse micelle morphology can produce a dramatic effect on the structures and dynamics of the aqueous interior. In Chapter 2, we

observed large differences between the dynamics observed within isooctane/AOT/water reverse micelles and cyclohexane/lecithin/water reverse micelles[25, 26]. We argued that because lecithin has a propensity to form more linear geometries, water is sequestered to a larger degree, changing the expected water structure and dynamics. We believe the same argument applies to benzene and cyclohexane reverse micelles because benzene micelles remain spherical at all hydration levels. Therefore, we expect morphology to play a role in the structure and dynamics within the reverse micelle interior. Wachtel et al.[9] have shown that differences between the behavior of lecithin in benzene and cyclohexane exist. They found ß–D-glucopyranoside precipitated upon addition of water in cyclohexane reverse micelles but not benzene. Differences in the structures and dynamics between the two reverse micelles could explain differences in reverse micelle solubilization properties and catalytic activity. In addition, because lipid morphology plays a role in lipid function[27], we may be able to help explain how lipid structure and dynamics relate to lipid function.

In this chapter, we determine the solvation dynamics of benzene/lecithin/water reverse micelles as a function of hydration and compare the results with the previously obtained dynamics of cyclohexane/lecithin/water reverse micelles from Chapter 2. We expect morphology to play a similar role as we presented in Chapter 2 for the difference between AOT and lecithin reverse micelles. Unfortunately, the benzene reverse micelle system proved to be a difficult system to analyze. As we will discuss, we have concerns that defined reverse micelle aggregates do not form in benzene at low hydrations. Therefore our comparison between benzene and cyclohexane reverse micelles will be limited to reverse micelles at elevated hydrations.

4.II. Experimental

4.II.A. Raw Materials

Lyophilized egg phosphatidylcholine (lecithin) was purchased from Avanti Polar Lipids, Inc. Samples were stored at −10°C and were used without further purification. Lecithin samples were always prepared from newly opened bottles. CLPE was used as the fluorescent probe (see Chapter 3 for preparation). CLPE was stored in a desiccator under vacuum. For comparison, we also prepared reverse micelles with C343 (Exciton, Inc., used without further purification). Benzene was used without further purification (Fisher, ACS certified). Added water was of high purity (Milli-Q filtered, 18.2 $M\Omega/cm^2$ resistivity).

4.II.B. Reverse Micelle Preparation

Approximately 2 mg of CLPE was dispersed in 500 mg of lecithin. This corresponds to 340:1 molar ratio of lecithin:CLPE. In order to homogeneously disperse the CLPE amongst the lecithin, the two components were co-solvated in 1:1 methylene chloride:methanol followed by repeated evaporation and dispersion into benzene. This procedure is described in detail in Chapter 3 for CLPE/lecithin/cyclohexane reverse micelles. For comparison, reverse micelles were prepared with C343 instead of CLPE. These samples were prepared with the exact same procedure as CLPE even though C343 does not need to be dispersed within the lecithin. The repeated evaporation decreases the amount of inherent water included in lecithin. ^{1}H-NMR analysis of the CLPE/lecithin after the evaporation and dispersion cycles revealed 0.4 ± 0.1 mol water per mol lecithin. All reverse micelles were prepared by dissolving the lipids in 10 ml of benzene, adding

the required amount of water, shaking overnight, and filtering through 0.1 μm syringe filters (PTFE, Whatman). We found that placing circulated samples under nitrogen reduced CLPE oxidation. Therefore, all samples used in upconversion experiments were placed in a vacuum tight sample holder. Samples were subjected to three freeze-pump-thaw cycles before being placed under nitrogen.

4.II.C. Particle Size Analysis

We performed particle size analysis of the reverse micelles using the dynamic light scattering instrument. We found the error in the measured radii was larger than the size difference among the different hydrated reverse micelles that were analyzed. Table 4.1 displays the results. We find that our reverse micelles have a radius of approximately 2.8 nm. Wachtel et al. found the their $w = 1$ reverse micelles to have a radius of 1.5 nm[9]. Assuming the water molecular volume is about 30 $Å^3$ and the reverse micelle aggregation number is 80, Wachtel would measure $w = 6$ reverse micelles to have a radius of 2.9 nm. Therefore, we find that our reverse micelles agree with previous characterizations.

Table 4.1. Dynamic light scattering measurements of benzene/lecithin/water reverse micelles.

Reverse Micelle Sample	Particle Size/nm
$w = 2.4$	2.5 ± 0.5
$w = 4.4$	2.8 ± 0.8
$w = 8$	2.8 ± 0.4

4.II.D. Fluorescence Upconversion Analysis

Analysis procedures were described in Chapter 1. Briefly, three different time length transients were taken at each wavelength, namely, 2 ps, 33 ps, and 500 ps. Using TCSPC, we found the lifetime of CLPE within the reverse micelles to be 2.5 ns at 480 nm while we found C343 in pure benzene to be 4.4 ns at 480 nm. Fluorescence transients were fit taking these lifetimes into account (see Chapter 1).

4.III. Results and Discussion

4.III.A. C343 as a Probe of the Reverse Micelle Interior

Before synthesizing CLPE, we first prepared $w = 5$ benzene/lecithin/water reverse micelles with C343 to determine the extent to which it would reside within the aqueous interior. C343 proved to be an effective probe of the reverse micelle interior of cyclohexane/lecithin/water reverse micelles (see Chapter 2). Unlike cyclohexane, however, C343 has a significant solubility in benzene. In general, coumarins are very soluble in benzene because of their characteristic conjugated ring system.

Anisotropy revealed that C343, to a large extent, is not incorporated into the reverse micelles. Time-resolved anisotropy revealed C343 in this micelle sample rotationally relaxes with two components, a long 2.5 ns component and a shorter 35 ps component. Table 4.2 lists anisotropy results obtained for benzene samples. Because the faster time component of C343 dissolved in the reverse micelles is almost exactly the same as C343 in pure benzene, we conclude the faster component arises from C343 dissolved in benzene unassociated with the reverse micelles. Based on the corresponding amplitudes, we find that approximately 75% of the C343 molecules are freely dissolved

in the benzene continuous phase. (We assume that C343 has the same lifetime whether dissolved in benzene or incorporated into the reverse micelles.)

Table 4.2. Anisotropy of C343 and CLPE in different environments.

Sample[†]	a_1	τ_1	a_2	τ_2	θ_c
C343 in Pure Benzene	100%	38.5 ± 0.6 ps	-	-	-
C343 in $w = 5$ Benzene/Lecithin/Water Reverse Micelles	72.0 ± 0.5%	35.3 ± 0.5 ps	28.0 ± 0.3%	2.5 ns[‡]	-
CLPE in $w = 2.4$ Benzene/Lecithin/Water Reverse Micelles	17.5 ± 0.5%	62 ± 7 ps	82.5 ± 0.5%	2.5 ns[‡]	14°
CLPE in $w = 4.4$ Benzene/Lecithin/Water Reverse Micelles	19.6 ± 0.8%	59 ± 6 ps	80.4 ± 0.8%	2.5 ns[‡]	15°
CLPE in $w = 6.4$ Benzene/Lecithin/Water Reverse Micelles	18 ± 2%	90 ± 20 ps	82 ± 2%	2.5 ns[‡]	15°

[†]Amplitudes have been normalized for easy comparison. Actual amplitudes ranged from 0.36 to 0.4 when added together.
[‡]Long time components were beyond the measured timescale of the experiment. Fits to data held this component constant.

Static spectroscopy also indicates that very few of the C343 molecules are incorporated inside the reverse micelles. Figure 4.1 shows the absorption and emission spectra of C343 dissolved in benzene/lecithin/water reverse micelles as a function of micelle hydration. Because only about 25% of the C343 molecules are incorporated into the reverse micelles, micelle hydration to has little influence on the absorption and emission of C343. These results confirm our expectation that C343 would not be a viable probe for benzene reverse micelles. In addition, they verify our ability to recognize the environmental position of the solvated probe.

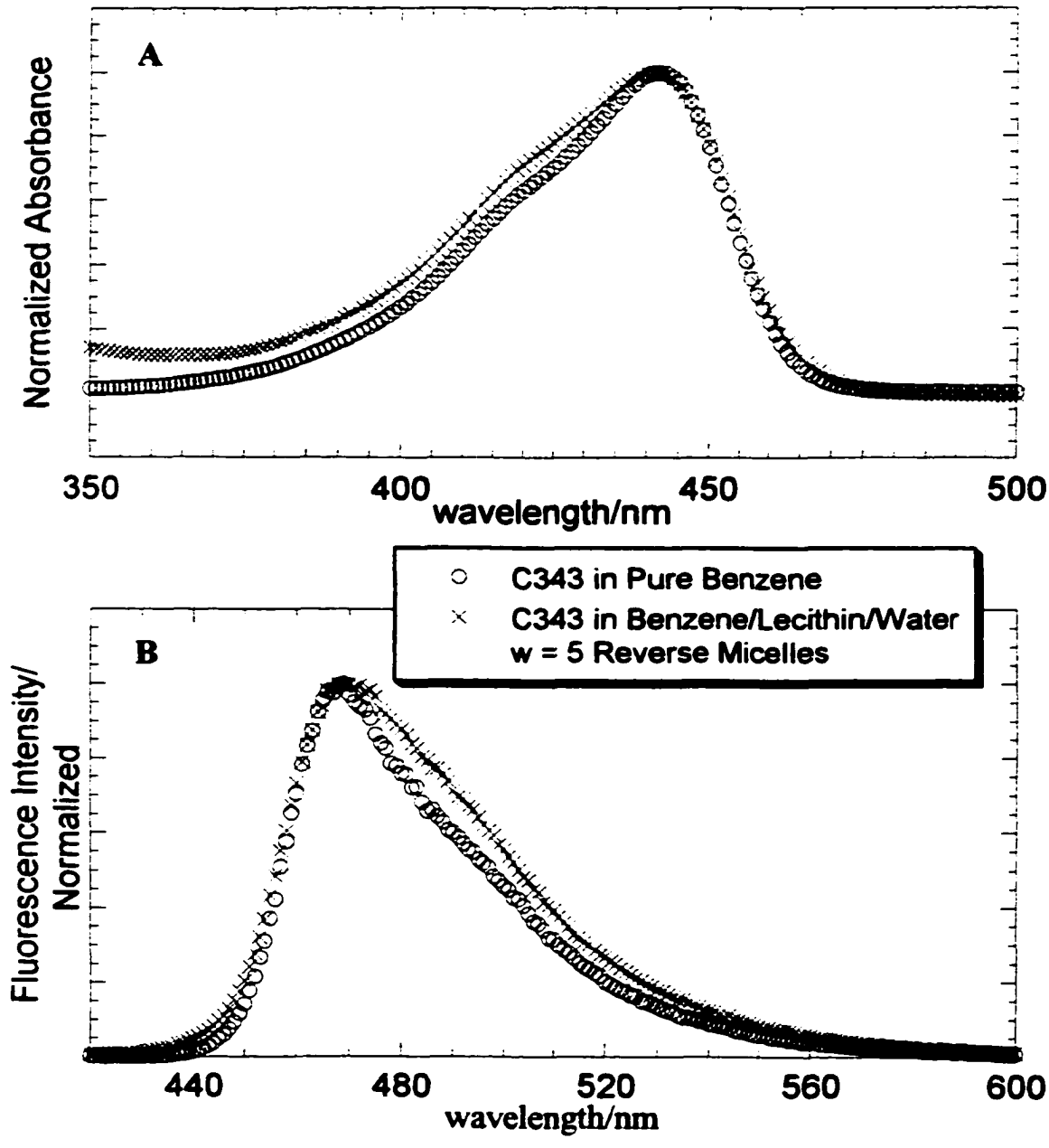

Figure 4.1. Absorption (A) and emission (B) of C343 in w = 5 benzene/lecithin/water reverse micelles and in pure benzene.

4.III.B. CLPE as a Probe of the Reverse Micelle Interior

We probed benzene/lecithin/water reverse micelles as a function of hydration, similar to the analysis of cyclohexane/lecithin/water reverse micelles in Chapter 2. Table 4.3 summarizes the solvation dynamics we observe for benzene reverse micelles as a function of hydration. The most striking trend displayed in Table 4.3 is the fast 100 - 200 fs component as a function of hydration. At the $w = 2.4$ hydration, this component accounts for 40% of the solvent relaxation. We contrast this with Chapter 2 results that found at the $w = 4.8$ hydration level, cyclohexane reverse micelles show no relaxation faster than 200 ps. At the same time, the fast component for benzene reverse micelles does not grow in amplitude with hydration as we observed with cyclohexane reverse micelles. Instead the amplitude dips in value at the $w = 4.4$ hydration level before increasing again at $w = 6.4$ hydration level.

Table 4.3. Measured solvation dynamics components in benzene/lecithin/water reverse micelles as a function of hydration. $C(t) = \sum_i a_i * \exp(-t/\tau_i)$.

Sample	a_1	τ_1/fs	a_2	τ_2/ps	a_3	τ_3/ps
Coumarin 153 in Pure Benzene†	0.37	234	0.60	1.89	0.03	25
$w = 2.4$	0.38 ± 0.01	145 ± 5	0.21 ± 0.01	8 ± 1	0.41 ± 0.01	240 ± 20
$w = 4.4$	0.29 ± 0.02	100 ± 10	0.18 ± 0.02	10 ± 2	0.53 ± 0.02	190 ± 10
$w = 6.4$	0.60 ± 0.01	85 ± 3	0.16 ± 0.01	5 ± 1	0.24 ± 0.01	160 ± 20

†Obtained from ref. [28].

The results are not easily interpreted and may indicate that CLPE does not probe the reverse micelle interior at low hydration. The work of Maitra et al.[12] showed benzene/lecithin/water reverse micelles at low hydration have a considerable number of lecithin monomers present. They have found that only at hydration levels above $w = 8$ do

the nonaggregated monomers disappear. Therefore, it is possible a significant fraction of CLPE molecules are dissolved in the reverse micelle system as free-floating monomers or submicellar aggregates. We expect CLPE to have a greater propensity to be solvated as submicellar aggregates than do lecithin monomers because the charged ammonium headgroup moiety has been replaced with a benzene soluble dye molecule. Therefore, submicellar aggregates may need to be even a greater consideration for us than for Maitra et al.

The existence of solvated submicellar aggregates at low hydration does not present a significant problem in cyclohexane reverse micelles. Capitani et al.[24] used ^{1}H-NMR analysis of lecithin in cyclohexane with little water present and found significant aggregation. The same analysis was performed on a comparable lecithin in benzene system and they found little aggregation. In addition, work by Hayashi et al.[29] found the critical micelle concentration (CMC) of dipalmitoylphosphatidylcholine (DPPC, a lipid very similar to lecithin) to be two orders of magnitude greater in benzene than in cyclohexane. Clearly, the monomer effect is more significant for benzene reverse micelles. However, we stress that studies find that solvated monomers are less of a concern as the hydration of lecithin increases or the lecithin concentration increases above the CMC[4, 12].

For comparison in Table 4.3, we have included the solvation response of benzene determined by Maroncelli et al.[28] using Coumarin 153 as the solvated probe. (We have also measured the benzene response in our laboratory with similar results.) The benzene response is characterized by a significant fast component that occurs over a 230 fs timescale. It is possible that the fast component we observe in benzene reverse micelles

arises from benzene and not fast aqueous dynamics inside the reverse micelles. At the same time, it is difficult to rationalize a 40% fast relaxation component arising from the interior of a $w = 2.4$ reverse micelle. However, if CLPE is solvated as submicellar aggregates, there is certainly an equilibrium between submicellar and micellar incorporated states because the solvation dynamics change with increasing hydration of the reverse micelle sample.

If CLPE exists as submicellar aggregates at low hydrations, this could explain the amplitude of the fast relaxation component as a function of hydration. Specifically, at the low hydration level, $w = 2.4$, a significant fraction of CLPE molecules would exist as submicellar aggregates and the fast component would correspond to the fast response of benzene. At a higher hydration level, $w = 4.4$, CLPE becomes significantly incorporated within the reverse micelles and the benzene response drops off. However, at this hydration level, it may be possible that the reverse micelle interior begins to show fast relaxation on this timescale. If the hydration level is increased further, $w = 6.4$, CLPE is fully incorporated into the reverse micelles but the fast relaxation becomes more significant within the micelle interior.

We also report static spectroscopy, fluorescence quenching, and time-resolved anisotropy measurements of CLPE in benzene reverse micelles. They all lend little support or refute of the theory that CLPE dissolves as submicellar aggregates at low hydration. Static spectroscopy results suggest that CLPE is incorporated into the reverse micelles with no indication CLPE resides in more than one environmental location. Figure 4.2 displays the absorption and emission spectra of CLPE in benzene/lecithin/water reverse micelles as a function of hydration. For comparison,

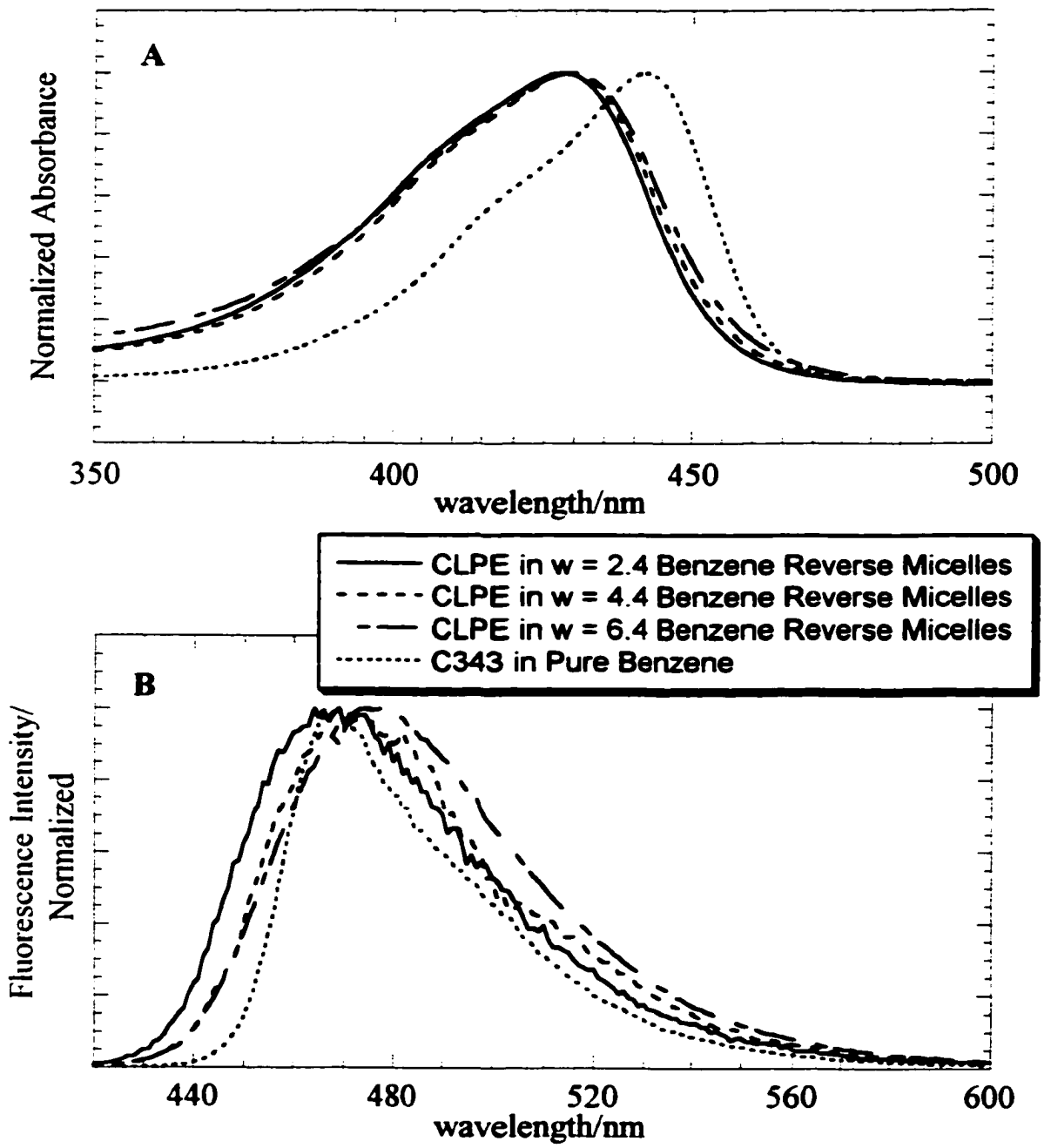

Figure 4.2. Absorption (A) and emission (B) of CLPE in benzene/lecithin/water reverse micelles as a function of hydration and C343 in pure benzene.

Figure 4.2 also displays the absorption and emission of C343 dissolved in pure benzene. First, we find that the absorption and emission bandwidths associated with CLPE are broader than C343 in pure benzene indicating CLPE resides in a more heterogeneous environment. We also find that the CLPE spectra are shifted relative to C343 in pure benzene. This suggests CLPE is incorporated into an environment different from pure benzene. It is possible the attachment of PE to C343 has changed the electronic structure of C343 and therefore a direct comparison between the spectroscopy of C343 and CLPE is unwarranted. However, we have shown in Chapter 3 that the spectroscopy of C343 remains largely intact after covalent attachment of PE (see Figure 3.10).

If we compare the absorption and emission spectra of CLPE as a function of hydration, we find little evidence for CLPE residing in more than one environmental location. In Figure 4.2b we find that the emission spectra shifts continuously to red wavelengths as hydration increases. First, this indicates CLPE is sensitive to the micelle water loading and is therefore incorporated within the aqueous interior. However, CLPE may still be only partially incorporated into the reverse micelle interior and still display this trend. Following this possibility, if a fraction of CLPE were not incorporated within the micelle, we would expect to see a portion of the emission spectrum that was insensitive to hydration. Clearly, the emission spectrum shifts continuously with hydration and does not reveal the presence of a hydration independent CLPE population. In Figure 4.2a we find that the absorption spectra display little hydration dependence. We have already presented in Chapter 3 that the absorption spectrum of CLPE in cyclohexane reverse micelles has little response to hydration (see Figure 3.11a).

We also measured the absorption of CLPE in benzene. Figure 4.3 displays the absorption of CLPE in pure benzene along with C343 in pure benzene, CLPE in $w = 2.4$ benzene reverse micelles, and CLPE in $w = 6.4$ cyclohexane reverse micelles. The most obvious characteristic of CLPE in pure benzene is the large bandwidth associated with the absorption. This suggests CLPE is self-aggregating which we would expect. We have already presented evidence for this in Chapter 3 (see Figure 3.9). Most important is that the peak is shifted relative to CLPE in $w = 2.4$ benzene reverse micelles. If CLPE existed in this aggregate state at the $w = 2.4$ hydration level, we would expect a small hump or broad background in the spectrum corresponding to the dissolved submicellar aggregates. We do not observe such a hump. However, because the spectrum is so broad, the fraction of CLPE molecules in the submicellar aggregate state may be to low to be detected in the absorption spectrum. Also, Figure 4.3 shows that the absorption of CLPE in benzene reverse micelles is shifted significantly relative to CLPE in cyclohexane reverse micelles. We have found that the CLPE absorption maximum is about 425 nm for cyclohexane reverse micelles (Chapter 3) and vesicle interfaces (Chapter 5), as well as C343 in cyclohexane reverse micelles (Chapter 2). Therefore, CLPE's absorption maximum in benzene reverse micelles being 432 nm is an exception to the rule.

Another method we used to determine the location of CLPE in the benzene reverse micelles was fluorescence quenching. The goal was to extinguish CLPE's emission with a quencher only soluble in either the aqueous interior of the reverse micelles or the organic continuous phase. The degree of quenching would indicate the fraction of CLPE molecules located inside and outside the reverse micelles. Prior to

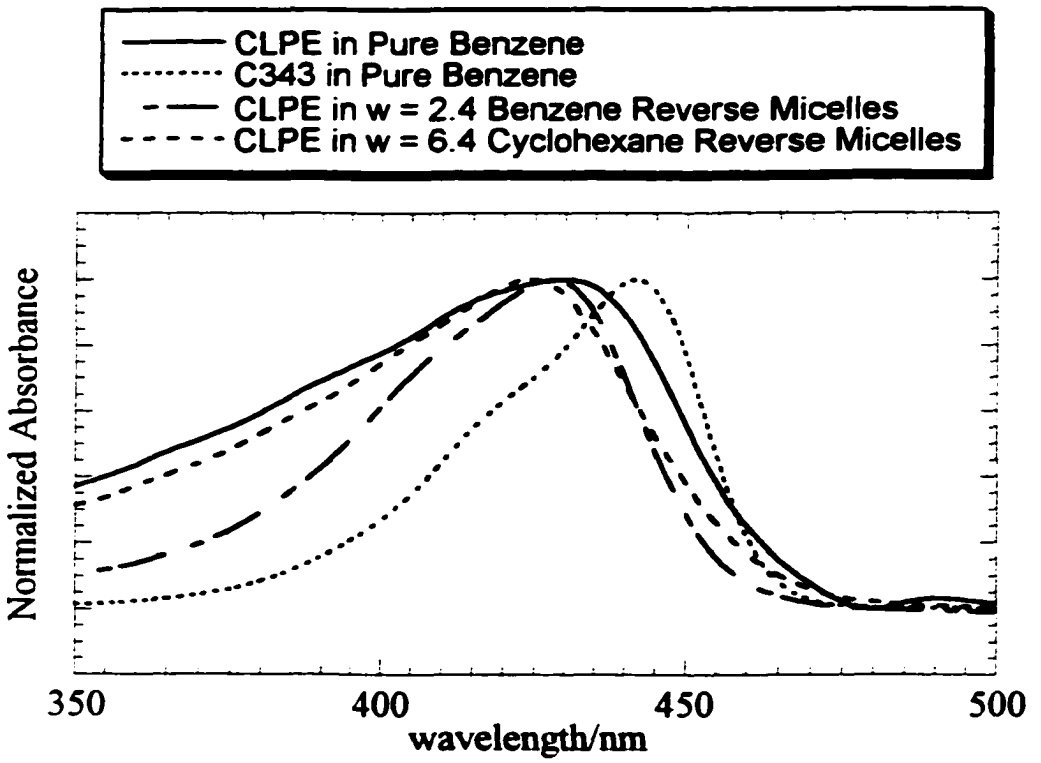

Figure 4.3. Absorbance of CLPE in pure benzene in comparison with CLPE in benzene and cyclohexane reverse micelles and C343 in pure benzene.

quenching CLPE, we measured quenching of C343. If quenching was observed, we then attempted to quench CLPE in reverse micelles. Quenchers used were: 1-bromobenzene, 1-chlorobenzene, potassium iodide (KI), fluorescein, and manganese dichloride ($MnCl_2$). Only KI and $MnCl_2$ quenched C343 in bulk water. However, absorption and emission spectra indicated some interaction of C343 with all the quenchers. Despite their effectiveness in bulk water, KI and $MnCl_2$ did not quench fluorescence within lecithin reverse micelles regardless of the probe. We did observe quenching of C343 by 0.5M KI in AOT reverse micelles. Thus, results from these experiments were inconclusive.

As a final test in locating the position of CLPE in benzene micelles, we performed time-resolved anisotropy measurements as a function of hydration. The results are displayed in Table 4.2. At all hydration levels, we observe a fast rotational relaxation of about 60 ps and a slow relaxation that we have held constant at 2.5 ns. (2.5 ns proved to be a convenient time component to approximate the collective rotational diffusion time of benzene reverse micelles.) As discussed in Chapter 1, the appearance of two time components may be the result of one of two situations: 1) the emission may arise from two different sources, or 2) a single source residing in an inhomogeneous environment may display two modes of rotational relaxation, that is, fast wobbling motion and rotational diffusion of the collective micelle aggregate. One could argue that C343 is an impurity in the synthesized CLPE. In fact, as we discussed in Chapter 3, C343 is indeed an impurity. However, we believe no more than 5-10% mol/mol of the CLPE sample is C343. Thus free C343 can not account for an anisotropy component that accounts for 20% of the relaxation. More importantly, the rotational relaxation is too slow to correspond to C343 in benzene (see Table 4.2). Also, it is possible that a fraction of the

CLPE submicellar aggregates are dissolved in the organic continuous phase and therefore are the source of the 60 ps component. We find this highly unlikely by comparing the time components. CLPE is more than three times the molecular weight of C343 and probably greater than this if it exists as submicellar aggregates. Therefore, we would expect the rotational relaxation to be greater than 100 ps.

We conclude the fast anisotropy component refers to a wobble motion of CLPE in an aggregated state. Because there is a possibility submicellar aggregates of CLPE have rotational relaxation longer than the resolution of our measurements (>1 ns) we find the data to neither support nor refute the presence of submicellar aggregates. As presented in Chapter 1, we can convert the amplitude of the wobbling motion into a corresponding cone angle of motion. We have used equation 1.4 to determine the cone angles presented in Table 4.2. We compare cone angles to suggest the structure of the interface; greater cone angles indicate a less restricted interface. According to Table 4.2, hydration has little effect on the structure of the lipid/water interface within benzene reverse micelles. This finding contradicts previous studies by others. Using ^{31}P-NMR, the phosphorous moiety within the lecithin headgroup shows increased mobility with increasing hydration of benzene/lecithin/water reverse micelles[2, 3].

In light of the inconclusive nature of the benzene reverse micelles as a function of hydration we hesitate to interpret solvation dynamics results in terms of an increasing spherical cavity. While static spectroscopy, quenching measurements, or anisotropy measurements can not confirm or refute it, we find it possible that at low hydration levels CLPE may not be incorporated into organized spherical micelles. Therefore we choose to not compare the dynamics we observe within the micelles as a function of hydration.

Instead, we compare benzene reverse micelles with cyclohexane reverse micelles at the w = 6.4 hydration level. At this hydration level, benzene reverse micelles should be well formed organized aggregates[12]. In addition, the reverse micelles are prepared at concentrations fifty times above the CMC[30, 31]. We are confident the dynamics we measure within these reverse micelles represent motion within fully organized reverse micellar aggregates.

4.III.C. Comparison of Benzene and Cyclohexane w = 6.4 Reverse Micelles

In Chapter 2, we showed that cyclohexane reverse micelles bind a greater amount of water than was predicted by IR and NMR techniques. We contended that at least 4.8 water molecules per headgroup became incorporated into the headgroup region. These results were contrasted with AOT spherical reverse micelles that indicate that much less water becomes incorporated into the headgroup region. While the different surfactant headgroups of AOT and lecithin certainly play a role in determining the amount of water that binds to the headgroup, we contend that the differing morphology, of the spherical vs. wormlike reverse micelles, also plays a role. More specifically, we argue that lecithin must sequester water into the headgroup region to form wormlike tubular micelles. We expected to find the amount of bound water to reflect IR and NMR predictions in benzene reverse micelles like we found for AOT in Chapter 2. These reverse micelles are spherical, therefore, they sequester water into the headgroup region only because of specific headgroup water interactions which IR and NMR are most sensitive to (see Chapter 2). As opposed to AOT, this experiment directly tests our hypothesis because the surfactants were identical, only the organic continuous phase and morphology varied.

In addition to morphology effecting water pool structure, we also believe the morphology is related to the micelle structure as a whole. We theorize that the formation of wormlike tublular micelles in cyclohexane are driven by the propensity of the lecithin alkyl chains to exclude organic solvent and form more linear geometries. The opposite is thought to be true for benzene reverse micelles with benzene acting as a cosurfactant, thus facilitating the spherical structure[12]. If benzene acts as a cosurfactant, then one would expect the benzene intercalation between lecithin molecules to lead to reduced order of the alkyl tails. This interpretation is supported by IR spectral studies. Cavallaro et al. have probed cyclohexane reverse micelles using IR spectroscopy[32]. They assessed the lateral packing order of the alkyl chains by comparing the C-H stretching modes at 2855 and 2930 cm^{-1}, corresponding to methylene symmetric and asymmetric stretching modes. They argue that a decrease in the ratio A_{2930}/A_{2855} indicates increased packing order. This is borne out in their studies comparing reverse micelles with varying hydration where they show that packing order increases at higher hydration levels. In contrast, the same kind of analysis for IR data of benzene reverse micelles[16] shows a higher ratio for the same hydration level. This indicates that the alkyl tails in the benzene/lecithin/water reverse micelles are less organized than in cyclohexane. This would undoubtedly impact the organization of the headgroups as well and could lead to less strongly bound water at the benzene interface because the interfacial order is reduced.

We observe a significant difference in the time-resolved anisotropy of CLPE in benzene and cyclohexane reverse micelles. Anisotropy measurements in cyclohexane were discussed in Chapter 3. There, we found no subnanosecond rotational relaxation,

indicating CLPE is rotationally restricted within the wormlike micelles. In contrast, Table 4.2 reveals that CLPE in benzene micelles shows a wobbling component and samples a conical angle of about 15°. Therefore, supporting our theory that benzene reverse micelles are more disordered aggregates than cyclohexane reverse micelles, we find that the lipid/water interface within benzene reverse micelles is significantly less ordered than the cyclohexane reverse micelles. We expect the reduced interfacial order to influence the solvation dynamics as well.

Table 4.4 displays the solvation dynamics measured in $w = 6.4$ benzene and cyclohexane reverse micelles. Both amplitudes and time constants show that solvent motion in benzene reverse micelles is substantially faster than in cyclohexane. Figure 4.4 shows the time correlation function for benzene and cyclohexane reverse micelles demonstrating this difference. In addition to the dynamics, Table 4.4 also lists the overall shift in fluorescence peak maximum, indicated by $\Delta\nu_{max}$. We find that benzene reverse micelles have a greater $\Delta\nu_{max}$. All these measurements show that CLPE detects a more disorganized lipid/water interface within benzene reverse micelles.

Table 4.4. Measured solvation dynamics components in $w = 6.4$ benzene/lecithin/water and cyclohexane/lecithin/water reverse micelles. $C(t) = \sum_i a_i * \exp(-t/\tau_i)$.

Sample	a_1	τ_1/fs	a_2	τ_2/ps	a_3	τ_3/ps	$\Delta\nu_{max}$/cm^{-1}
CLPE in Benzene $w = 6.4$ Reverse Micelles	0.60 ± 0.01	85 ± 3	0.16 ± 0.01	5 ± 1	0.24 ± 0.01	160 ± 20	858
CLPE in Cyclohexane $w = 6.4$ Reverse Micelles	0.11 ± 0.01	620 ± 10	0.22 ± 0.01	11 ± 1	0.68 ± 0.01	210 ± 10	625

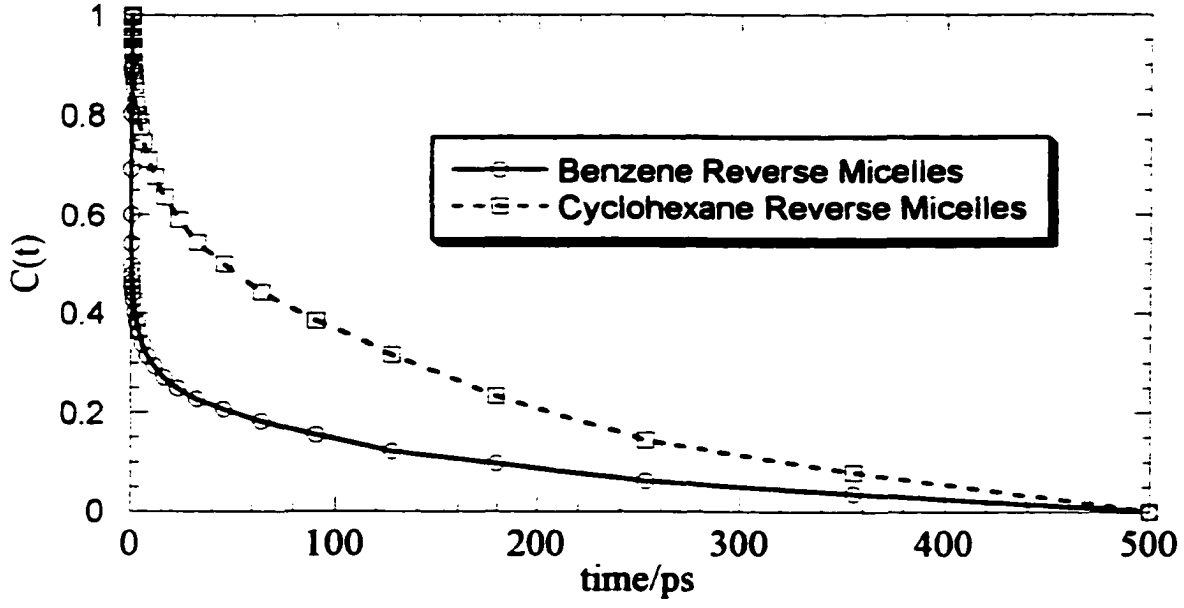

Figure 4.4. Time correlation function determined for w = 6.4 benzene and cyclohexane reverse micelles.

The differences we observe between benzene and cyclohexane reverse micelles are surprising based on previous studies by other workers using primarily NMR and IR spectroscopies. These studies measured properties of a particular group within the reverse micelle interior and observed how the given property changed with hydration. In general, these studies find that whether the reverse micelle is prepared in benzene or cyclohexane, the groups behave similarly. For example, ^{31}P-NMR studies in both benzene[2, 3] and cyclohexane[14, 15] find that phosphorous mobility steadily increases with hydration. Likewise, IR spectra of headgroup P=O and C=O stretching frequencies show increased water interaction with increasing hydration for both benzene and cyclohexane reverse micelles[6, 14, 16, 17]. Also, OH stretching of water behaves similarly with increasing hydration for both systems[12, 16]. We note that some of the papers cited above do show differences once the hydration of the cyclohexane reverse micelles reaches the percolation threshold (see Chapter 2). However, at the $w = 6.4$ hydration level the reverse micelles are below the percolation threshold and therefore these studies predict similar behavior for the different reverse micelles.

As we discussed in Chapter 2, some workers have used NMR and IR studies to denote and quantify different water types within the reverse micelle interior, namely, strongly bound, bound, and free. If we estimate the proportion of free water within $w = 6.4$ benzene and cyclohexane reverse micelles based on our dynamical results, we find IR and NMR predictions to match what we find in benzene reverse micelles more closely than cyclohexane reverse micelles. Based on results presented in Chapter 2, we estimate that only about 1 water molecule per headgroup in cyclohexane reverse micelles can be labeled free water at the $w = 6.4$ hydration level. Conversely, solvation dynamics results

for benzene reverse micelles indicate 60% of the solvent relaxation is subpicosecond or "free" in response. As only an estimate, these results suggest that about 3 - 4 water molecules per headgroup are free water. We can most easily compare our estimates with the findings by Maitra et al.[12] They estimated the fraction of bound and free waters for benzene and cyclohexane reverse micelles in the same paper and found there are approximately equal numbers of the two water types in both reverse micelles at the w = 6.4 hydration level. Boicelli et al. found the same result but only for benzene reverse micelles[13]. We should also mention that various older studies concluded free water does not appear to be present in benzene reverse micelles until hydration levels exceed w = 8 - 10[2, 5, 6]. Our results suggest that this is not the case.

As part of our theory presented in Chapter 2, we concluded that the formation of a core water pool within the reverse micelle is a prerequisite for the appearance of free water type relaxation. We propose that the spherical nature of the benzene reverse micelles facilitates core water pool formation where cyclohexane reverse micelles do not. This hypothesis is strongly supported by recent calculations by Faeder and Ladanyi who have simulated the water in a model AOT reverse micelle[33]. They observe a bulklike water pool forming for w = 5. In reverse micelles formed with the nonionic surfactants Triton X-100 and Brij-30, the solvation dynamics are significantly faster in the system that forms spherical droplets[34]. This may indicate the formation of a spherical water pool in the micellar interior with bulklike ultrafast water relaxation.

4.IV. Conclusions

We have synthesized a lipophilic probe molecule that has allowed us the investigate the solvation dynamics of water in benzene/lecithin/water reverse micelles. Unfortunately, the possible presence of unincorporated CLPE submicellar aggregates at low hydration levels keeps us from analyzing benzene reverse micelle dynamics as a function of hydration. However, by comparing the reverse micelles with elevated hydration levels, we find that in the benzene based reverse micelles, the solvation dynamics are significantly faster than in the cyclohexane gel at the same hydration level. We attribute these results to a combination of morphology in the benzene reverse micelles that supports water pool formation and to a reduced amount of order in the micellar interface that arises from the spherical nature of the micelles.

References for Chapter 4

1. Fung, B.M. and J.L. McAdams, *The interaction between water and the polar head in inverted pphosphatidylcholine micelles.* Biochim. Biophys. Acta, 1976. **451**: p. 313-20.

2. Klose, G. and F. Stelzner, *NMR investigations of the interactions of water with lecithin in benzene solutions.* Biochim. Biophys. Acta, 1974. **363**: p. 1-8.

3. Boicelli, C.A., *et al.*, *Interactions of small molecules with phospholipids in inverted micelles.* Chem. Phys. Lett., 1982. **89**(6): p. 490-5.

4. Elworthy, P.H. and D.S. McIntosh, *The interaction of water with lecithin micelles in benzene.* J. Phys. Chem., 1964. **68**(12): p. 3448-52.

5. Walter, W.V. and R.G. Hayes, *Nuclear magnetic resonance studies of the interaction of water with the polar region of phosphatidylcholine micelles in benzene.* Biochim. Biophys. Acta, 1971. **249**: p. 528-38.

6. Davenport, J.B. and L.R. Fisher, *Interaction of water with egg lecithin in benzene solution.* Chem. Phys. Lipids, 1975. **14**: p. 275-90.

7. Kumar, V.V., C. Kumar, and P. Raghunathan, *Studies on licithin reverse micelles: optical birefringence, viscosity, light scattering, electrical conductivity, and electron microscopy.* J. Colloid Inter. Sci., 1984. **99**(2): p. 315-23.

8. Walde, P., *et al.*, *Phospholipid-based reverse micelles.* Chem. Phys. Lipids, 1990. **53**: p. 265-88.

9. Wachtel, E., S. Federman, and N. Greenspoon, *Interaction of carbohydrates with phosphatidylcholine inverse micelles.* Israel J. Chem., 1992. **32**: p. 113-9.

10. Barclay, L.R.C., *et al.*, J. Am. Chem. Soc., 1984. **106**: p. 6740.

11. Shervani, Z., *et al.*, *Water solubilization investigations of phosphatidylcholine reveres micelles.* Colloid. Surf., 1991. **60**: p. 161-73.

12. Maitra, A., T.K. Jain, and Z. Shervani, *Interfacial water structure in lecithin-oil-water reverse micelles.* Colloid Surf., 1990. **47**: p. 255-67.

13. Boicelli, C.A., M. Giomini, and A.M. Giuliani, *Infrared characterization of different water types inside reverse micelles.* Appl. Spec., 1984. **38**(4): p. 537-9.

14. Shervani, Z., T.K. Jain, and A. Maitra, *Nonconventional lecithin gels in hydrocarbon oils.* Colloid Polym. Sci., 1991. **269**: p. 720-6.

15. Capitani, D., E. Rossi, and A.L. Segre, *Lecithin microemulsion gels: an NMR study.* Langmuir, 1993. **9**: p. 685-9.

16. Tsai, Y.-S., *et al.*, *Fourier transform infrared studies on phospholipid hydration: phosphate-oriented hydrogen bonding and its attenuation by volatile anesthetics.* Mol. Pharm., 1987. **31**: p. 623-30.

17. Arcoleo, V., *et al.*, *Study of lecithin reverse micelles by FT-IR spectroscopy.* Prog. Colloid Polym. Sci., 1997. **105**: p. 220-3.

18. Enders, A. and G. Nimtz, *Dielectric relaxation study of dynamic properties of hydrated phospholipid bilayers.* Ber. Bunsenges. Phys. Chem., 1984. **88**: p. 512-517.

19. Klosgen, B., *et al.*, *Dielectric spectroscopy as a sensor of membrane headgroup mobility and hydration.* Biophys. J., 1996. **71**(6): p. 3251-3260.

20. Takahashi, A., T. Takizawa, and Y. Nakata, *A deuteron NMR study of the dynamics of water molecules bound tightly to the phosphate group in dipalmitoyl-phosphatidylcholine-D2O system.* J. Phys. Soc. Jpn., 1996. **65**(2): p. 635-642.

21. Volke, F., *et al.*, *Dynamic properties of water at phosphatidylcholine lipid-bilayer surfaces as seen by deuterium and pulsed field gradient proton NMR.* Chem. Phys. Lipids, 1994. **70**(2): p. 121-131.

22. Whaley Hodges, M., *et al.*, *Water translational motion at the bilayer interface: An NMR relaxation dispersion measurement.* Biophys. J., 1997. **73**(5): p. 2575-2579.

23. Lakowicz, J.R. and D. Hogen, *Dynamic properties of the lipid-water interface of model membranes as revealed by lifetime-resolved fluorescence emission spectra.* Biochemistry, 1981. **20**: p. 1366-1373.

24. Capitani, D., A.L. Segre, and R. Sparapani, *Lecithin microemulsion gels: a NMR study of molecular mobility based on line widths.* Langmuir, 1991. **7**: p. 250-3.

25. Willard, D.M., R.E. Riter, and N.E. Levinger, *Dynamics of polar solvation in lecithin/water/cyclohexane reverse micelles.* J. Am. Chem. Soc., 1998. **120**(17): p. 4151-60.

26. Riter, R.E., D.M. Willard, and N.E. Levinger, *Water immobilization at surfactant interfaces in reverse micelles.* J. Chem. Phys. B, 1998. **102**(5): p. 2705-14.

27. Cullis, P.R. and B. De Kruijff, *Lipid polymorphism and the functional roles of lipids in biological membranes.* Biochim. Biophys. Acta, 1979. **559**: p. 399-20.

28. Horng, M.L., *et al.*, *Subpicosecond measurements of polar solvation dynamics: Coumarin 153 revisited.* J. Phys. Chem., 1995. **99**(48): p. 17311-17337.

29. Hayashi, M., K. Fukushima, and A. Kitamura, *Micelle formation of diacylglycerophosphocholines in organic solvents. I. Effects of the solvents on Krafft points.* Chem. Phys. Lipids, 1983. **33**(3): p. 233-9.

30. Sadaghiani, A.S., A. Noori, and A. Khan, *Lecithin reverse micelles: NMR study of solution structure of lecithin in toluene, benzene, and decanol.* J. Surf. Sci. Tech., 1991. 7(2): p. 163-75.

31. Giomini, M., *et al.*, *The use of NMR parameters for the evaluation of the critical micelle concentration of lecithin in reverse micellar systems.* Chem. Phys. Lett., 1989. **158**(3,4): p. 334-40.

32. Cavallaro, G., *et al.*, *Structural investigation of water/lecithin/cyclohexane microemulsions by FT-IR spectroscopy.* J. Colloid Inter. Sci., 1995. **176**: p. 281-5.

33. Faeder, J. and B.M. Ladanyi, *Structure and dynamics inside model reverse micelles of varying size.* J. Chem. Phys., 1999. **in preparation**.

34. Pant, D. and N.E. Levinger, *Polar Solvation Dynamics in Brij-30 and Triton X-100 Nonionic Microemulsions and Model Polymer Solutions.* J. Phys. Chem. B, 1999. **in preparation**.

Chapter 5

Solvent Motion at Lecithin Vesicle Interfaces

5.I. Introduction

Most of the fundamental biochemical functions in cells involve membranes at some point[1]. Cellular tasks performed by membranes include providing the barrier that encloses cellular compartments, actively passing ions or molecules inside and out of compartments, transmitting information through conformational changes induced in membrane components, housing enzymes that catalyze transmembrane reactions, and providing a substrate for membrane-bound reactions. Essentially, membranes consist of lipid bilayers composed of two oppositely aligned phospholipid layers with polar headgroups facing towards the polar exterior/interior and nonpolar lipid chains facing inward towards the opposite layer. Living membranes can be very complex, composed of various phospholipid types and lipid solvated sterols and proteins. To understand cellular functions, we need to understand membrane properties such as motion, structure, and organization.

In particular, the chemical composition and physical properties of the headgroup domain are important to membrane function. Water/headgroup interactions have been shown to be influential in such cellular activities as vesicle fusion[2]. The lipid interface

is also believed to be an important barrier in the passive transport of small molecules and ions across the membrane[3]. In addition, phospholipid surfaces have been shown to catalyze protein activation[4]. To understand these cellular activities, we need to understand how the headgroup region is organized, both in physical composition and time evolution. We need to know what dynamics occur at the interface and how those dynamics are a function of the various water and headgroup interactions that are present.

In order to understand the cellular function of living membranes, researchers typically find that simplified model membranes are more easily interrogated than real biological samples. Model membranes consisting of simple one-component or few-component phospholipid bilayers have played a seminal role in the study of membranes. Such a simplistic approach is deemed absolutely necessary in order to take full advantage of modern physical experimental techniques including, magnetic resonance spectroscopy (NMR and ESR), differential-scanning calorimetry, micromechanics, and scattering and diffraction techniques[5]. One of the reasons we previously interrogated reverse micelles composed of phospholipids was to determine dynamics that would be theoretically similar to dynamics present at membrane interfaces (see chapters 2 & 4). In theory, reverse micelles represent a simple membrane composed of a single water/lipid interface. However, reverse micelles restrict a small water pool instead of bordering into bulk water. Also, because lipid chains align in bilayers for vesicles while they align into an organic phase in reverse micelles, lipid-chain interactions might influence water/headgroup properties in different ways for the two systems. Therefore, a more realistic representation of a living membrane would be a liposome. Liposomes are spherically shaped vesicles composed of lipid bilayers with an aqueous buffer inside and

out. We will be using the terms liposomes and vesicles interchangeably. Unilamellar liposomes can be prepared, representing the simplest yet structurally similar cellular membrane mimic[6].

Various studies using model membranes have shown that the lipid interface represents a structurally restricted environment relative to the properties observed in bulk water. There is considerable evidence that water forms strong associations with various polar moieties of lipid headgroups. Polar headgroups of phospholipids interact through an extensive network of hydrogen, ionic, and covalent bonds. Inter- or intra-molecular hydrogen bonds can occur between the hydroxyl, phosphate, amino, ester C=O, and carboxylic acid groups[7]. The molecular dynamics simulation performed by Pasenkiewicz-Gierula et al. revealed that 70% of a lipid membrane composed of dimyristoylphoshatidylcholine (DMPC) molecules are linked by water bridges via hydrogen bonds[8].

As the work by Pasenkiewicz-Gierula et al. seems to suggest, water participates in the structure and organization of lipid bilayers. Studies have shown the ordering of model membranes is strongly dependent on water concentration. It has been observed for PC bilayers that the orientational order of lipid solvated probes is significantly reduced by an increase of water content[9, 10]. Molecular dynamics simulations have also shown that significant artifacts in orientational polarization and potential profiles associated with the headgroup domain result when simulations include varying amounts of water[11].

Much of our understanding of the lipid/water interface comes from research surrounding the hydration forces of lipids[12]. These are forces that dominate the interaction of all phospholipid membranes as they approach within 1-2 nm of each other.

Bilayers are covered with a layer of polar groups that must hold onto the solvent into which they would otherwise dissolve. The tenacity of holding this water is part of a natural tension in amphiphilic aggregates, a balance between the high energy of a hydrocarbon/water interface and the energy lowering adsorption of solvent. Essentially, it costs energy to remove the water, and therefore, two approaching lipid surfaces tend to repel each other. This force is usually referred to as the 'hydration force' because it was initially ascribed to the ordering of water molecules[11]. However, another possible source of the repulsion is direct interaction of the surfaces by protrusion of flexible groups. Some simulations suggest that the force is a result of both solvent and steric interactions but separating the contributions is extremely difficult[11, 13]. This is because lipid composition tends to alter both the degree of water polarization and the dynamic protrusion of the lipid interface.

Studies surrounding the hydration force of lipids reveal that water forms a variety of lipid associations and the polarization of water, induced by the bilayer, extends several nanometers into the bulk water solution. As hypothesized for DMPC bilayers[14], water can occupy three different situations while interacting with membranes: it can be i) tightly bound to the polar headgroups at the interface, ii) trapped in the intermembrane space where it swells the system, and iii) free from the membrane phase, when it is present in excess and macroscopically separated from the hydrated membrane system[15]. ^{2}H-NMR studies have shown as few as 5 and as many as 16 waters per lipid can be strongly bound and indicate as many as 23 waters per lipid can be 'associated' with the bilayer[16, 17]. Simulations performed by Perera et al. found the perturbed water interface to have a width of 1.22 nm, indicating two layers of perturbed water

molecules line the membrane surface[18]. However, whether water can be broken down into *more* than two types, strongly bound and free, as we have postulated in chapter 2, remains controversial[19].

On top of determining the organization and dynamics at bilayer interfaces, we would also like to understand under what conditions the interface changes and to what degree. Cholesterol is the main sterol of animal organisms and plays a central role in modulating chemical and physical properties of membrane bilayers in eukaryotic cells[20]. The structure of cholesterol along with other pertinent structures is shown in Figure 5.1. A large number of studies of cholesterol/phospholipid bilayer model membranes have been carried out, using a wide range of physicochemical techniques[21-24].

These studies have found cholesterol to have a dramatic effect on the ordering of lipid phases. Briefly, cholesterol incorporation into bilayers has four effects: first, it broadens and eventually eliminates the cooperative gel to liquid-crystalline phase transition of phospholipid bilayers; second, it decreases the area per molecule of the liquid-crystalline state; third, it increases the orientational order of the hydrocarbon chains of liquid-crystalline bilayers; and fourth, it decreases the passive permeability of phospholipid bilayers above their gel to liquid-crystalline phase transition temperatures[25]. Because cholesterol tends to order lipid bilayers, it appears that an important role of cholesterol is to make the membrane insensitive to changes in the external environment, such as high hydrostatic pressure[26]. Essentially, cholesterol seals and orders bilayers in the liquid-crystalline phase.

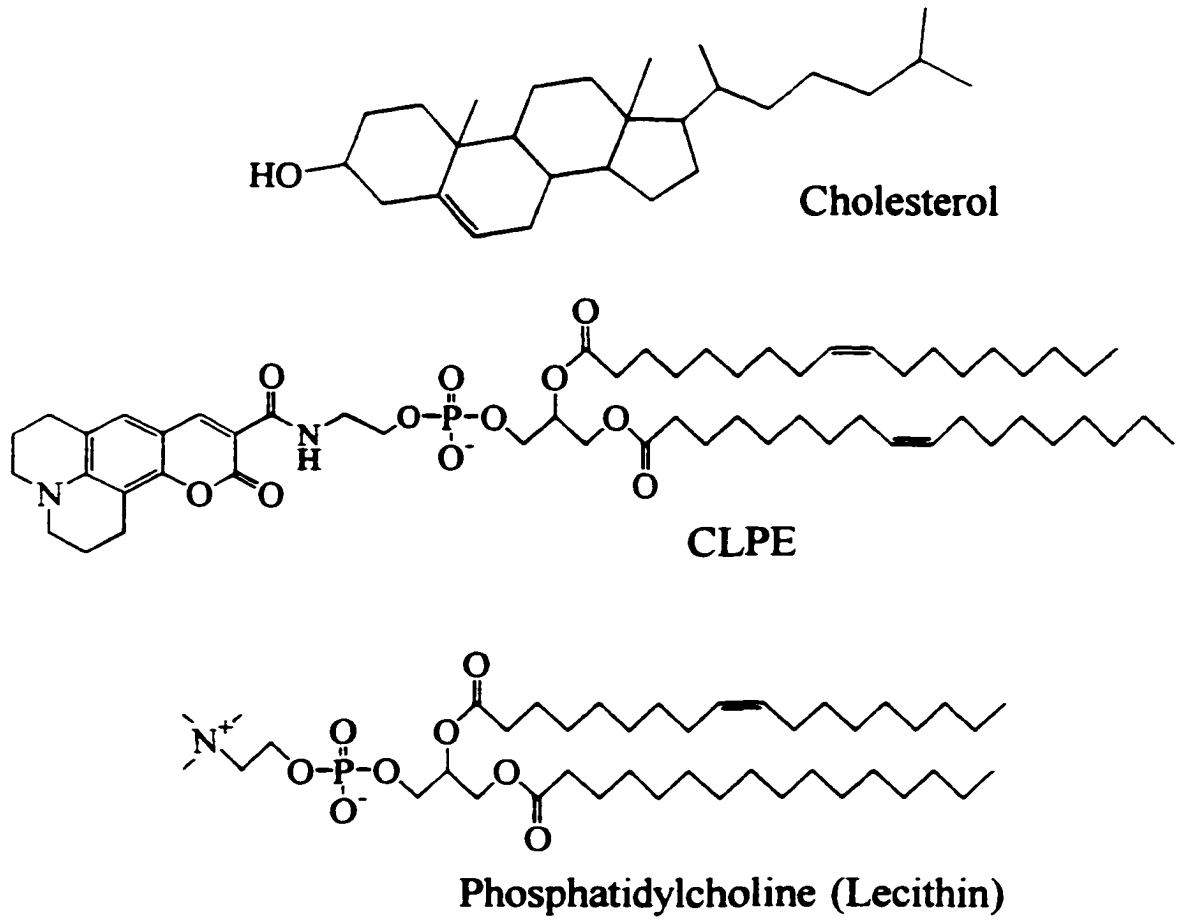

Figure 5.1. Chemical structures of cholesterol, our probe molecule (CLPE), and the phospholipid used to prepare vesicle bilayers (lecithin).

Although we currently know a considerable amount about the overall effect of cholesterol on phospholipid bilayer phase transitions, our understanding of phospholipid-cholesterol interactions at the molecular level, especially at the polar headgroup interfacial region, is incomplete[25]. We do know that the presence of cholesterol results in a red shift in the fluorescence of 1-(4-trimethyammonium-phenyl)-6-phenyl-1,3,5-hexatriene (TMA-DPH) and 2-dimethylamino-6-lauroylnaphthalene (Laurdan)[27, 28]. The red shift is interpreted as an indication that cholesterol dehydrates the probe environment. Both probes are thought to sit alongside lipid chains but in a region between the headgroups and lipid chains. In addition to spectroscopic experiments, several simulations have predicted the behavior of cholesterol. Robinson et al. reported that cholesterol has two preferred locations: the cholesterol hydroxyl group either interacts with the DMPC carbonyls deep within the bilayer or it interacts with the headgroups and water closer to the interface[29]. Other simulations have also found that cholesterol tends to position itself deep within the bilayer so that only the hydroxyl group is in contact with the headgroup domain. Because of this cholesterol acts as a spacer between headgroups[30, 31]. Whether the spacing results in greater headgroup mobility remains controversial. To what extent the headgroup/water structure is changed by the presence of cholesterol remains unclear.

In this chapter, we report on lipid interface solvation dynamics for two different vesicle systems. First, we measure the ultrafast motion at a lecithin vesicle interface. This represents the first time ultrafast motion has been measured at a lipid bilayer interface. We should note that two other papers by Datta et al.[19] and Hof et al.[32] also measured solvation dynamics associated with lipid vesicles. However, neither group was

able to detect motion on a timescale below 50 ps. In addition, neither group specifically interrogated the headgroup domain as our work does. We compare the dynamics we observe with bulk water dynamics to understand to what degree the lipid interface is a restricted environment. In addition, we compare the lipid vesicle motion to the motion we measured previously in reverse micelles (see chapter 2). The comparison indicates how well a reverse micelle interface serves as a bilayer interface mimic. Second, we measure the motion of lecithin vesicle interfaces with 33 mol percent cholesterol incorporated within the bilayer. We compare the observed motion to dynamics at the vesicle interface in the absence of cholesterol to determine the effect cholesterol has on headgroup domain dynamics. By comparing these results to NMR and molecular dynamic studies, we postulate on the organization of the headgroup region.

5.II. Experimental

5.II.A. Sample Preparation

Lyophilized egg phosphatidylcholine (lecithin) was purchased from Avanti Polar Lipids, Inc. Samples were stored at –70 °C prior to use and were used without further purification. CLPE was synthesized according to methods outlined in Chapter 3. CLPE was stored in a vacuum desicator. Cholesterol (5-cholester-3β-ol, 99+%, Sigma) was stored at –10 °C prior to use and used without further purification. Phosphate buffered saline (PBS) solution[33] was prepared by adding 2.56g sodium dihydrogen phosphate and 22.48g disodium hydrogen phosphate heptahydrate into approximately 500ml of water (Milli-Q filtered, 18.2MΩ/cm^2 resistivity) and the pH was adjusted to 7.2-7.4 with a pH poteniometer. Then, 87.66g sodium chloride was added before finally bringing the

total volume to 1.0L with additional water. Final solutions were diluted 10:1 in water before use.

Liposomes were prepared according to the procedures outlined by New[6]. Lecithin vesicles were prepared by weighing 166 mg egg PC into a cuvette, while 111 mg egg PC and 28 mg cholesterol were weighed for cholesterol vesicles. The cholesterol vesicles were prepared with a 2:1 lipid:cholesterol mole ratio that proved to be near the saturation limit for these vesicles. 2 mg of CLPE was added to each of the samples. Amounts correspond to a 75:1 molar ratio of lipid:labeled lipid. To allow complete dispersion of the CLPE with the egg PC, cuvette contents were dissolved in 1:1 chloroform:methanol solvent mixture. Organic solvent was then removed by blowing nitrogen gas over the sample. Further drying was accomplished by placing the cuvettes in a vacuum desicator overnight. Dry lipids were dispersed in 10 ml of PBS solution. The PBS solution was first purged of oxygen gas by lightly bubbling nitrogen gas through the solution immediately before addition.

If phospholipids are dispersed into aqueous solution with minor shaking, multilamellar vesicles are formed. However, our research required unilamellar vesicles to ensure we were probing water/headgroup dynamics. One way this is accomplished is by forming vesicles with diameters smaller than several hundred nanometers. New[6] outlines various procedures for preparing small unilamellar vesicles (SUV).

We initially attempted to prepare SUV's utilizing a lipid extruder (Prof. Graham, CSU, Physiology Department; The Extruder, Lipex Biomembranes, Inc.). Aqueous lipid dispersions were squeezed through polycarbonate 100nm filters with pressurized nitrogen gas. Filtered dispersions produced vesicles of about 90nm in diameter with little loss of

lipid material on the polycarbonate membrane. Unfortunately, at the lipid concentrations we wished to work at (approx. 25 mg/ml), the vesicle solution appeared milky white even with repeated filtration of up to 30 times. Only at lipid concentrations of 1 mg/ml did the filtered vesicles show only minor cloudiness. At this lipid concentration, the lipid:CLPE molar ratio would be about 7:1 assuming 0.2 mg/ml of CLPE is the required concentration to produce a measurable upconversion signal. New[6] recommends that fluorescently labeled lipids should remain at molar ratio above 50:1 to prevent fluorescence exciton perturbations.

In order to keep lipid concentrations high enough to stay above the 50:1 molar ratio but still produce a clear solution, we decided to form smaller vesicles. Even smaller SUV's can be formed by probe sonication (Prof. Tamkun, CSU, Physiology Department; Branson Sonifier 450). In this method, a titanium metal tip is positioned within an extra thick glass cuvette holding a few milliliters of aqueous dispersed lipids. Vesicles were sonicated at approximately 2.5 kHz for 1 hour until solutions became transparent. Cuvettes were placed in ice baths during the sonication. To collect titanium metal particles that dislodge from the probe tip during sonication, samples were centrifuged at 15 kHz for 15 min. (Prof. Ishii, CSU, Physiology Department; Sorvall RC-5 Superspeed Refrigerated Centrifuge). Samples appeared very transparent. Dynamic light scattering measured the lecithin vesicles to have a radius of 30(±15)nm while the cholesterol vesicles measured 30(±14)nm.

5.II.B. Experimental Apparatus, Data Analysis, and Methods

Static absorbance, static fluorescence, time-resolved anisotropy, dynamic light scattering, fluorescence lifetime, and fluorescence upconversion apparatus have been

described in Chapter 1. For time-resolved anisotropy and fluorescence upconversion experiments, samples were circulated with a peristaltic pump fitted with PTFE tubing. In addition, the sample reservoir was submerged in a water bath kept at 22 ± 1 °C. At room temperature, lecithin remains in the liquid-crystalline phase. Before being placed in front of the laser, samples were placed in an airtight reservoir under nitrogen gas.

Data analysis has been described in Chapter 1. Briefly, single wavelength fluorescence transients from a wavelength range of 435 nm to 525 nm were obtained in 10 nm increments. Transients were obtained over several time periods, in particular 2, 30, and 500 ps.

Problems resulted from exposing vesicles to laser excitation for long periods of time. Normally all the transients from a single sample are taken in one 24 hour period. Unfortunately, after a few hours of laser exposure, the fluorescence spectrum displayed permanent blue shifting. Blue shifting occurred with both lecithin and cholesterol vesicle samples. Control samples left unexposed to laser light showed no shifting over a 24 hour period. The amount of shifting appeared to be proportional to laser exposure time. Absorbance spectra indicated little, if any, shifting with exposure.

Avanti technical support pointed out that lipids tend to degrade in one of two possible spots. Either by hydrolysis of the ester bonds or breakdown of double bonds in unsaturated lipid chains. To test if the laser was breaking down double bonds, we prepared vesicles composed of DMPC which is a phospholipid consisting of completely saturated lipid chains. DMPC vesicles were left circulating in front of the laser beam overnight. Static fluorescence before and after exposure revealed the spectra of CLPE did indeed shift several nanometers in this time period. We concluded the blue shifting

was a result of ester hydrolysis. Unfortunately, the problem is not easily corrected because water cannot be removed from our system.

We found taking transients from a series of vesicle samples could mitigate sample degradation. We measured a 30 ps transient at 528 nm fluorescence at the beginning and end of laser exposure. We compared both beginning and ending transients of a given sample and transients of different samples to ensure that data was reproducible. Most samples were exposed to laser light for no more than three hours. We never observed a significant change in the compared transients. In addition, steady-state fluorescence spectra were taken before and after exposure and compared in a similar fashion as the transients. Blue shifting always occurred over the three-hour exposure but never more than two nanometers. The variability of the fluorescence spectra from sample to sample was also on the order of 1-2 nm.

5.III. Results

Figure 5.2 shows the absorption spectra of CLPE in both vesicle samples. CLPE's frequency peak maximum is only slightly blue shifted by the presence of cholesterol, that is 425 vs. 425.5 nm. The blue edge shoulder that is more prevalent in the choleserol vesicles is apparently associated with lecithin molecules. This shoulder appears in both vesicle and reverse micelle lecithin samples with or without chromophores present. Over a twenty-four hour period, vesicle samples become cloudier and the blue edge shoulder will show roughly a 50% increase in intensity. However, because spectral characteristics of the probe molecule remain unchanged and data was always taken within a few hours of preparation, the effect has not been a concern. The

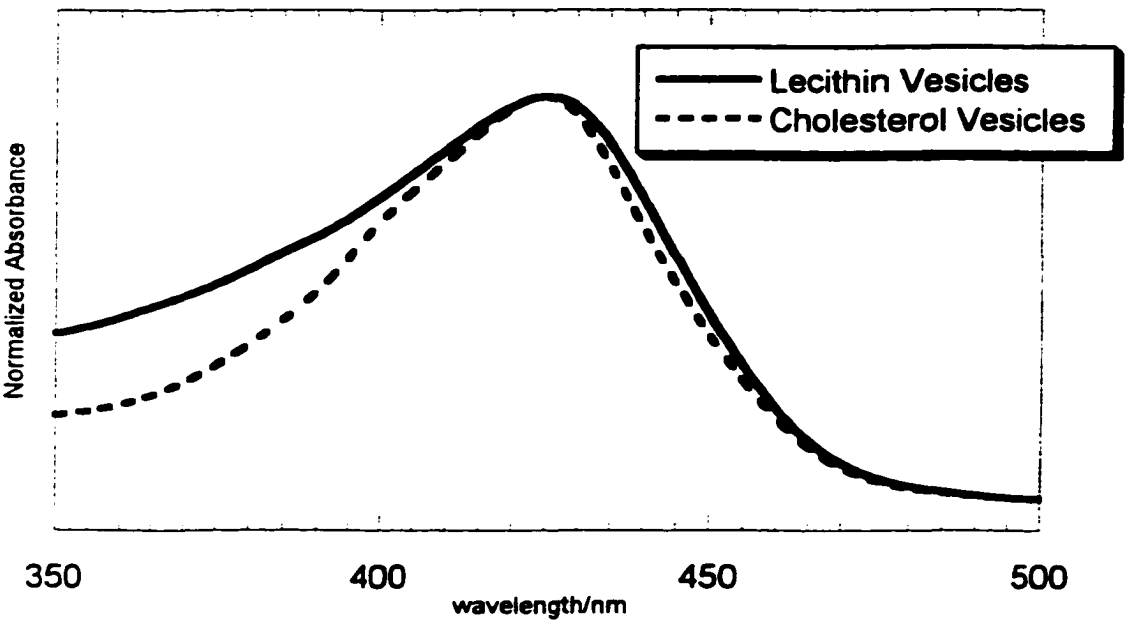

Figure 5.2. Absorption of CLPE incorporated into lecithin vesicles with and without 33 mol% cholesterol.

shoulder is more prevalent in the cholesterol spectrum only because the spectra have been normalized.

Figure 5.3 displays the emission spectra for CLPE in both vesicle systems. We also display the CLPE emission spectrum inside cyclohexane/lecithin/water $w = 6.4$ reverse micelles (see Chapter 3) and C343 in pH 9 bulk water (see Chapter 2). The corresponding emission peak maximum for each sample is as follows: 493nm, C343/water; 484nm, CLPE/cholesterol vesicles; 481nm, CLPE/lecithin vesicles; and 474nm CLPE/reverse micelles. CLPE's emission spectrum when incorporated into reverse micelles is blue shifted significantly from its spectrum in vesicles. Concentrating on the emission from the two vesicle samples, we also observe that the presence of cholesterol red shifts CLPE's spectrum. Notice, however, the red shift is mostly the result of a smaller frequency bandwidth of the cholesterol sample. For comparison, we display the emission spectrum of C343 in bulk water which is significantly red shifted from any of the heterogeneous environments. Unfortunately, the emission spectrum of CLPE in bulk water can not be acquired because of its extremely low solubility. The emission spectrum of C343 should be similar to CLPE because, as we showed in Chapter 3, they give rise to similar emission spectra when placed in cyclohexane/lecithin/water $w = 6.4$ reverse micelles.

To determine the motional freedom of the probe molecules, we also measured time-dependent anisotropy. Table 5.1 lists the rotational relaxation components for CLPE in both vesicle samples. In addition, Table 5.1 displays the rotational relaxation for C343 in bulk water and also in lecithin vesicles. In order to determine the degree to which C343 would become incorporated into the vesicles, we measured the anisotropy of

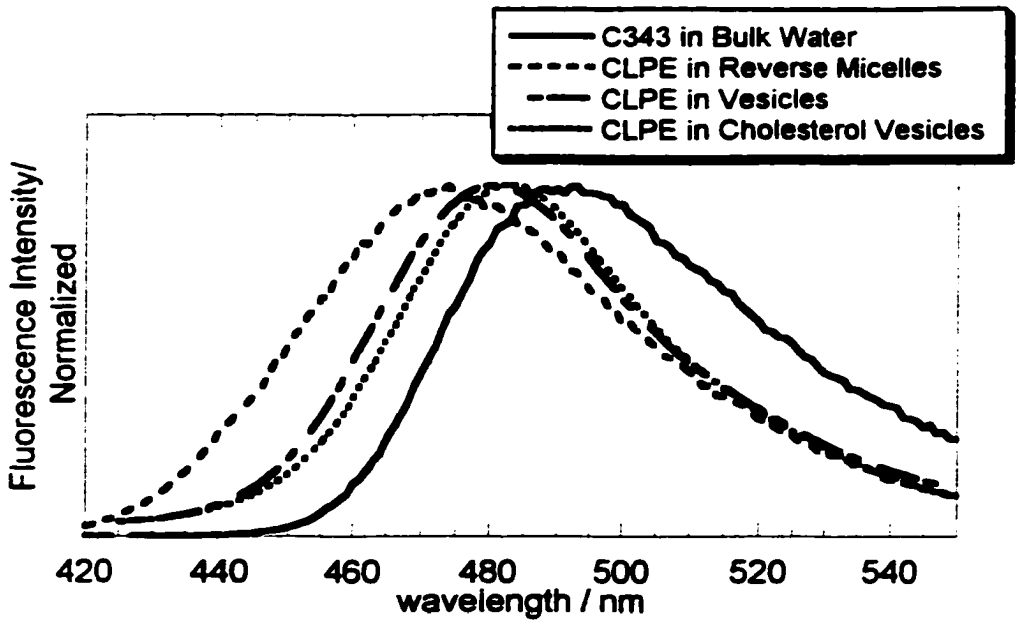

Figure 5.3. Emission spectra of C343 in bulk water, CLPE in w = 6.4 cyclohexane/lecithin/water reverse micelles, CLPE incorporated into lecithin vesicles, and CLPE incorporated into lecithin vesicles containing 33 mol percent cholesterol.

C343 in lecithin vesicles. If C343 was significantly incorporated, the results could possibly provide a comparison with the CLPE solvation dynamics results. The C343 vesicles were prepared in the same manner as the CLPE vesicles. From Table 5.1, we find that C343 shows a single rotational relaxation component. All the other samples listed in Table 5.1, show two components. We will discuss the origin of these components below.

Table 5.1. Time-dependent fluorescence anisotropy of C343 and CLPE in various environments. Anisotropy measurements were fit with single- or bi-exponential decays: $r(t) = a_1*\exp(-t/\tau_1) + a_2*\exp(t/\tau_2)$.

Environment	a_1	τ_1 / ps	a_2	τ_2 / ns
C343 in Bulk Water†	0.37 ± 0.04	83 ± 8	-	-
C343 in Lecithin Vesicles	0.29 ± 0.04	70 ± 8	0.10 ± 0.04	2 ± 6
CLPE in Lecithin Vesicles	0.04 ± 0.01	37 ± 9	0.32 ± 0.01	1.9 ± 0.5
CLPE in Cholesterol Vesicles	0.04 ± 0.01	40 ± 16	0.34 ± 0.01	2.7 ± 1.6

†Taken from ref. [34]

Figure 5.4 displays the separate wavelength transients used to construct TRES for each vesicle sample. The transients were normalized at 500 ps to the emission spectra displayed in Figure 5.3. Solvation dynamics were measured through the time-correlation function (eqn 1.1). The time-correlation function was fit with a multi-exponential function. The fit parameters are displayed for both vesicle systems in Table 5.2. For comparison we also display the solvation dynamics observed with CLPE incorporated into cyclohexane/lecithin/water $w = 6.4$ reverse micelles (Chapter 3) and C343 in pH = 9 bulk water. In addition to the solvation dynamics, Table 5.2 also displays the overall change in fluorescence peak maximum ($\Delta\nu_{max}$).

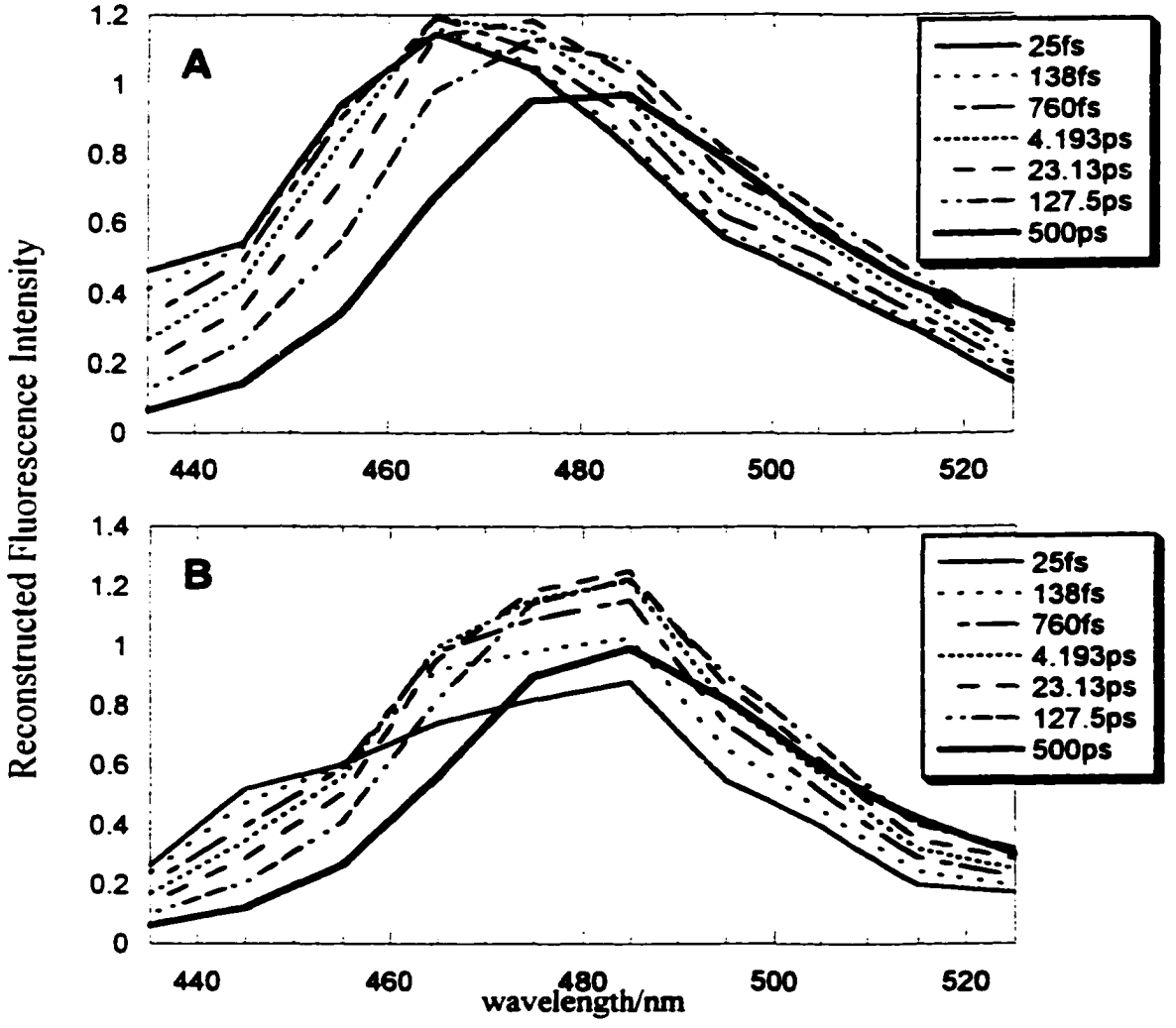

Figure 5.4. Time-resolved emission spectra (TRES) for lecithin vesicles (A) and lecithin vesicles with 33 mol percent cholesterol (B).

Table 5.2. Multi-exponential fits of the time correlation functions, C(t), for C343 and CLPE solubilized in various aqueous environments. $C(t) = \sum_i a_i \exp(-t/\tau_i)$

Environments	a_1	τ_1 / ps	a_2	τ_2 / ps	a_3	τ_3 / ps	$\Delta\nu_{max}$ / cm^{-1}
C343 in Bulk Water[†]	0.3 ± 0.3	0.2 ± 0.1	0.7 ± 0.3	0.6 ± 0.1	-	-	965
CLPE in Reverse Micelles	0.11 ± 0.01	0.62 ± 0.01	0.22 ± 0.01	11 ± 1	0.68 ± 0.01	210 ± 10	625
CLPE in Lecithin Vesicles	0.16 ± 0.01	0.65 ± 0.08	0.23 ± 0.01	11 ± 1	0.61 ± 0.01	210 ± 20	623
CLPE in Cholesterol Vesicles	0.22 ± 0.01	0.24 ± 0.02	0.18 ± 0.02	9 ± 1	0.60 ± 0.04	330 ± 50	374

[†]Obtained from ref. [35].

The results presented in Table 5.2 show a number of interesting features. First, we find significant relaxation occurring on the subpicosecond timescale at vesicle interfaces with and without cholesterol. We will draw comparisons to bulk water relaxation that also occurs on the subpicosecond timescale, as displayed in Table 5.2 for C343 in bulk water. Second, the dynamics and overall shift observed for lecithin vesicles and reverse micelles are essentially the same. Third, cholesterol does influence the dynamics observed at a lecithin vesicle interface. Table 5.2 shows that the first time component becomes faster while the last time component becomes slower. More dramatically, the overall frequency shift is decreased for cholesterol vesicles.

5.IV. Discussion

5.IV.A. Probe Environment

Assuming the steady-state spectroscopy of CLPE is polarity sensitive, we expected to observe several trends in the absorption and emission of CLPE in the different lipid/water environments. In reverse micelle systems, we could increase the hydration of the reverse micelle and follow the steady-state spectroscopy of CLPE to

indicate its position. For vesicle systems, hydration is not a variable. Instead, we compare the vesicle interface spectroscopy to other lecithin interfaces we have probed. We expected the steady-state spectroscopy of CLPE to indicate the vesicle interface was more polar than reverse micelle interfaces but less polar than bulk water. To surmise these expectations we have presumed the amount of water in a particular environment is proportional to the polarity. Various reverse micelle and lipid bilayer studies have found lipids are not fully hydrated until levels reach at least $w > 9$[16, 36, 37]. Therefore, because the reverse micelles we have probed have not reached this hydration level and by definition vesicle interfaces are fully hydrated, we expected vesicle interfaces to be more polar. Of course by the same reasoning, we expected neither the reverse micelles nor the vesicle interfaces to be as polar as bulk water. We also expected to find the polarity of the vesicle interface to decrease in the presence of cholesterol. Previous studies have found that cholesterol tends to dehydrate the lipid interface, thus decreasing the polarity and producing a blue shift in a probe's spectra relative to an interface with no cholesterol[28, 38].

Contrary to our expectation, we found the absorption spectra of CLPE in different environments to remain, to a large extent, unchanged with changing polarity. We have observed this in Chapters 3 & 4. In Chapter 4, increasing the hydration of benzene reverse micelles had little effect on the absorption spectra. In Chapter 3, although slightly more sensitive, the same trend was seen in cyclohexane reverse micelles. Figure 5.2 shows the absorption spectra for CLPE in lecithin and cholesterol vesicles. If we were to also display the absorption spectrum of C343 in bulk water and CLPE in $w = 6.4$ cyclohexane reverse micelles as was done in Figure 5.3, there would be little difference

between the four spectra. As illustrated in Figure 5.2, CLPE's spectrum shifts only 0.5 nm with the presence of cholesterol, but more importantly, the bandwidth narrows. Because the shift is too small to be considered significant and CLPE's absorption spectrum has proved insensitive to polarity changes in previous experiments, we draw no conclusions from the differences in the absorption peak maximum. Instead, we focus on the difference in bandwidth of the two spectra that we will discuss below.

Unlike its absorption peak, CLPE's emission peak maximum has proved to be very sensitive to solvent polarity. In Chapters 3 & 4, CLPE displayed a hydration dependent emission peak maximum for both cyclohexane and benzene reverse micelles. Figure 5.3 shows that the CLPE emission peak maximum in the vesicle samples blue shifts from C343 in bulk water. Therefore, as expected, the vesicle interfaces represent a less polar environment than bulk water. Figure 5.3 also shows that the CLPE emission peak maximum in vesicle systems red shifts from that observed in $w = 6.4$ cyclohexane reverse micelles. Again, we expect this shift. Because the emission peak maximum for the vesicle systems lies between the peaks observed in bulk water and reverse micelles, we feel confident CLPE is positioned where it was designed to reside, at the lipid/water interface.

Comparing lecithin vesicles with and without cholesterol, Figure 5.3 reveals that the emission peak maximum for cholesterol vesicles red shifts relative to lecithin vesicles. This shift indicates that the cholesterol vesicle surface is more polar than the lecithin vesicle surface. As stated above, this is neither what we expect nor what others have measured. Instead of comparing emission peak maximum for the two vesicle systems, we pay more attention to the bandwidth. Because the bandwidth represents the

variety of polar environments the population of probe molecules sample as a whole, the decreased bandwidth indicates there are fewer accessible environments for CLPE in cholesterol vesicles. Notice from Figure 5.3 that most of the red shift that occurs for CLPE in cholesterol vesicles results from a decreased bandwidth on the blue edge. We conclude cholesterol does not increase the headgroup region polarity, but rather, reduces the range of polar configurations CLPE may occupy at the cholesterol vesicle interface. Also notice that cholesterol reduces the bandwidth in the absorption spectrum displayed in Figure 5.2. As we will discuss below, cholesterol seems to tighten a lipid interface that would likely reduce possible probe configurations and possibly eliminate some configurations, i.e. more polar configurations, preferentially. In this way, cholesterol can have little effect on the interface polarity, while at the same time, inducing a red shift in the absorption spectrum.

In addition to steady-state absorption and emission of CLPE in vesicles, we also measured the time-dependent anisotropy. The primary goal was to confirm that the CLPE is localized within the vesicles. We have designed our probes to reside within the headgroup interface region. We are confident CLPE does not misalign within the lipid bilayer and probe the hydrophobic interior because the charged phosphate group of CLPE should keep the headgroup aligned toward the aqueous exterior. Moreover, emission spectra suggest we are probing a relatively polar environment, as discussed above. Therefore, we anticipate two possible situations: 1) CLPE is correctly aligned at the interface, or 2) CLPE is free floating as an aqueous-solvated monomer.

Lecithin vesicles prepared with C343 as the probe molecule nicely illustrate how time-dependent anisotropy may be used to determine probe location. We initially

attempted to determine the degree to which C343 is incorporated into vesicle interfaces with the hope that CLPE would not be essential to determine vesicle interface dynamics. We found C343 is resides in both the continuous aqueous solution and within the vesicle bilayer structure. For C343 residing in the aqueous solution, we expect to see a rotational relaxation component of about 83 ps (Table 5.1). For C343 residing in the vesicle structure, we expect to see rotational relaxation that occurs on a much longer timescale, similar to the rotation time of a vesicle. Indeed Table 5.1 shows that C343 shows two rotation relaxation components corresponding to free and lipid solvated C343. Comparing amplitudes and assuming C343 has similar emission intensity in both environments, we find approximately 26% of the C343 probes are incorporated into the vesicle structure.

From Table 5.1, we see that the anisotropy of CLPE in lecithin vesicles with and without cholesterol reveals two relaxation components. In both vesicle samples, the amplitudes indicate 11% of the rotational relaxation is accounted by a fast 40ps component. As discussed in Chapter 1, the fast component could arise, either from a fraction of CLPE molecules that are unincorporated into the vesicles or from heterogeneous rotational relaxation even thought the entire population of CLPE molecules is incorporated into the vesicles.

It is highly unlikely that CLPE is not incorporated. The 40 picosecond component is faster than the rotation of the bare C343 aqueous solvated probe; Table 5.1 shows C343 rotates at less than half the rate with a 83 ps component in bulk water. Unincorporated CLPE should rotate more slowly than C343 not two times faster. It is also unlikely that CLPE is either impure or degrading during preparation or analysis. If the sample

included free C343 from either contamination or breakdown of CLPE, 40ps is still too fast to correspond to rotational motion of C343. In addition, the breakdown of CLPE into fluorescent components smaller than C343 while still maintaining similar spectral properties is inconceivable. Also, laser exposure seems to have no effect on anisotropy measurements. While CLPE in lecithin vesicle samples that were exposed to laser light showed fluorescence shifting in the steady-state spectrum, there was no change in time-dependent anisotropy at the beginning to the end of the 20 hour period. Therefore, these data indicate CLPE aligns correctly and incorporates into vesicle bilayers and the fast anisotropy relaxation component corresponds to a wobbling motion. We use the wobbling motion to indicate lipid/water interface structure. Using equation 1.4 and the results from Table 5.1, we find that CLPE wobbles in a cone angle of 11° in lecithin vesicles both with and without cholesterol.

Based on the measured wobble of CLPE, we conclude that cholesterol has no ordering effect on the probe. As will be discussed further, this finding seems to be in conflict with steady-state fluorescence (discussed above) and solvation dynamics results (discussed below) that suggest cholesterol constricts the interface. In addition, others have found using fluorescently labeled lipids like CLPE that cholesterol disorders the interface, producing a broader cone angle for probe wobbling[38].

We state a final few notes concerning time resolved anisotropy of CLPE. We have measured the time resolved anisotropy of CLPE in $w = 6.4$ cyclohexane reverse micelles and observed no fast rotational relaxation that may be attributed to a wobbling motion (see Chapter 3). Similarly, C343 in the same micelles shows no rotational relaxation faster than several nanoseconds. In contrast, CLPE in $w = 6.4$ benzene reverse

micelles shows significant wobbling motion corresponding to motion restricted to a cone angle of about 15° (see Chapter 4). Therefore, the anisotropy data indicates that the structure of lecithin vesicle interfaces is less ordered than within $w = 6.4$ cyclohexane reverse micelles but more ordered than $w = 6.4$ benzene reverse micelles. As will be discussed, vesicle interfaces and the cyclohexane reverse micelle interiors display very similar solvation dynamics. Finally, we measured the time-resolved anisotropy of CLPE incorporated into vesicles prepared with DMPC. As mentioned above, we prepared vesicles with DMPC in order to determine lipid hydrolysis. As expected, the results indicated a 40 ps wobble component that accounted for 12% of the relaxation similar to lecithin vesicles. Therfore, lipid chain saturation has no measurable effect on the anisotropy of CLPE.

5.IV.B. Solvation Dynamics at a Lecithin Vesicle Interface

We expect a lecithin vesicle interface to show restricted motion relative to what is observed in bulk water. As a general rule, dynamics should slow with increasing molecular weight and increasing solvent association. While it is clear that dynamics are slower at lipid interfaces, we aim to learn what specific motions that can occur at the interface and to what degree they proceed. These experiments present a unique perspective to these unknowns because they represent the first ultafast detection of solvation dynamics specifically within the headgroup domain of a lipid bilayer.

First, we compare the overall solvent and solvent motion of bulk water vs. the vesicle interface. Table 5.2 lists $\Delta\nu_{max}$ for C343 in bulk water and CLPE in lecithin vesicles. We find that in response to CLPE's excitation, the lecithin vesicle interface has a smaller $\Delta\nu_{max}$ value than bulk water. This indicates the headgroup region does not

reorient to the same extent as bulk water. Therefore, as we would expect, the vesicle interface represents a restricted environment relative to bulk water.

Focusing on the measured solvation dynamics, we expect to see the restricting influence of the lipid interface. We know, for example, that the properties of water molecules in the vicinity of a biomolecule differ appreciably from those of bulk water[39, 40]. In a molecular dynamics study, Shinoda et al. found that rotational diffusion of water slows down an order of magnitude when it surrounds either the phosphate or choline headgroup moieties[41]. We find three time components for solvent relaxation at a vesicle interface (Table 5.2). Knowing that water relaxes on a subpicosecond timescale, we can assign the fastest component to free water. Therefore, because we measure 84% of the solvent relaxation to be slower than free water, the solvent motion at a vesicle interface is much more restricted than bulk water motion.

Finding the headgroup domain largely depleted of free water is not very surprising based on experimental and molecular dynamics studies. For example, ^{2}H-NMR experiments reveal a minimum of 11-16 water molecules/lipid is needed to form a primary hydration shell around a phosphatidylcholine headgroup[16]. In a simulation, Perera et al.[13] similarly found 15.5 waters/lipid in the first headgroup solvation shell, showing strong headgroup interactions. If we assume that the solvent response to CLPE's excitation is limited to only a few water layers distance for the excited probe, then it is not surprising we observe little free water type relaxation.

While relaxation components quoted in Table 5.2 refer to ultrapure bulk water, the vesicle samples were prepared in PBS solution. The ionic strength of the buffered solution should show a negligible effect on solvation dynamics. Even at elevated ion

concentrations, ~1M, relaxation is only slightly longer than pure water[35]. PBS solution is about 0.1M in the sodium chloride concentration. Thus, our assumption that the PBS solvation dynamics response is the same as pure water is warranted.

There are several possibilities as to where the free water detected by CLPE resides. Essmann and Berkowitz[42] have proposed the hydration force of lipid bilayers could orient water as far as a couple of water layers into solution, corresponding to about 12 Å. If this perturbed water layer shows reduced motion, the free water component must reside beyond it, outside the headgroup domain. Another possibility is that trapped water exists within the headgroup domain with no strong interactions. For example, a simulation by Perera et al. found DPPC sequesters about 4 waters/lipid between headgroups that are not directly associated with headgroup moieties[13]. A third possibility is that lipid membrane undulations force a percentage of the probe molecules to protrude momentarily out into a less structured aqueous environment. This would expose probe to bulk-like water. For example, in a 10 ns simulation, Essmann and Berkowitz found the nitrogen atoms of the headgroup move, on average, up to 5 Å into the water phase[42]. The actual scenario is probably a combination of these possibilities.

While it seems certain that water near or incorporated into the lipid interface are strongly perturbed, direct assignment of the relaxation components to water types is unfeasible. At the lecithin vesicle interface, we observe two time components of 11 and 240 ps that are too slow to be related to free water (Table 5.2). Bound water most certainly comprises part of these components, but distinguishing water dynamics from concerted water/headgroup dynamics is impossible. Unlike reverse micelles discussed in Chapter 2, we can not observe vesicle interface dynamics as a function of hydration. We

believe that the longer 240 ps component corresponds to headgroup motion. Simulations have shown that diffusive headgroup motion occurs on the picosecond to nanosecond timescale[41, 43]. In addition, Pasenkiewicz-Gierula et al. found that headgroup-headgroup associations formed via charged pairs and water bridges have lifetimes in the picosecond to nanosecond timescale[44]. These studies suggest that headgroups could react to a probe perturbation on a 240 ps timescale. Whether strongly bound water associated with headgroups is a component of this motion, still remains unclear. We have seen a similar time component within cyclohexane reverse micelles in Chapter 2 and attributed it to strongly bound water/lipid headgroup motion. If motion within reverse micelles is similar to motion at vesicle interfaces, then the 240 ps component is likely due to strongly bound water relaxation.

The 11 ps component at the lecithin vesicle interface is most likely due to water type relaxation because it is to be too fast to correspond to headgroup motion. We present three possible models for the origin for the component. First, this component could correspond to strongly bound water and longer components, as previously discussed, are headgroup motions. In this model, we assume two types of water exist, strongly bound and free. In a simulation by Shinoda et al., water hydrated at the headgroup shows rotational relaxation in the $10 - 20$ ps range[41]. If solvent relaxation operates at vesicle interfaces the same way as we observed with cyclohexane reverse micelles, then this scenario is unlikely. In Chapter 2, we found that for cyclohexane reverse micelles at the $w = 4.8$ hydration level, all water is strongly bound and relaxes with a greater than 200 ps component. Therefore, a second model follows the findings of Chapter 2 and assumes three types of water exist, that is strongly bound, bound, and free.

The 11ps component would correspond to bound water. We offer no definitive evidence, but find the components are strikingly similar to the components we observed within cyclohexane reverse micelles. We will expand on the comparison between dynamics at the vesicle interface with those measured within cyclohexane reverse micelles below. The final model has been proposed by Nandi and Bagchi[45]. They proposed that a two-state water model might be sufficient for describing dielectric relaxation with multiple relaxation components. They argue that strongly bound water exchanging with free water could allow for separate relaxation components. In this model, we assume the longest time component is strongly bound water and the 11 ps component arises from the exchange of strongly bound water with free water. There is ample evidence to suggest that water within the headgroup domain exchanges on a timescale that would account for the 11 ps component we observe. In a simulation by Shinoda et al., water within the headgroup solvent shell had a residence time of several picoseconds[41]. Similarly, Alper et al. found the residence time to be 10 - 20ps[46].

While the longest time component we observed at the lecithin vesicle interface was 240 ps, there is evidence to suggest that longer time components exist. Our experiments sampled fluorescence to 500 ps, making relaxation components longer than this beyond our observation. Solvation dynamics studies by others indicate 600 ps to 10 ns relaxation components exist in vesicle systems[19, 32]. Even if we extended our measurements to observe longer solvent responses, we could not directly compare our observations because these studies did not directly probe the headgroup domain. Datta et al. imply the nanosecond time components they observe might correspond to the relaxation of strongly bound water. If this is the case, the 240 ps component we observe

would be the result of either water exchange dynamics or a type of headgroup relaxation motion unrelated to bound water. Obviously, further solvation dynamic experiments and simulations are needed to resolve the origins of the observed dynamics.

5.IV.C. Comparison of Solvent Motion at a Vesicle Interface with Motion within Cyclohexane Reverse Micelles

In Chapter 2, we suggested that the dynamics we observed within lecithin reverse micelles indicate the dynamics that would be observed at a lipid bilayer. Others have determined that water/headgroup interactions are similar for both reverse micelles and bilayers[47, 48]. Thus comparison of the two systems is warranted.

While water/headgroup interactions are similar for both lecithin reverse micelles and vesicles, the lecithin aggregates have significant structural differences that could impact dynamics. Vesicles are comprised of lipid bilayers with bulk water both inside and out. We expect the lipid chains in reverse micelles would be much more disorganized compared to bilayers. While lipid chains in reverse micelles interact with organic solvent molecules, lipid chains in vesicles participate in lipid/lipid interactions. Thus, there should be differences in lipid chain interaction that result in differences at the water/headgroup interface, as we observed in Chapter 4.

More importantly, we expect differences in dynamics because lecithin headgroups are hydrated to a greater extent in vesicles than in reverse micelles. To reiterate the argument made earlier, various reverse micelle and lipid bilayer studies have found lipids are not fully hydrated until levels reach at least $w > 9$[16, 36, 37]. Because the reverse micelles we have probed have not reached this hydration level and by definition vesicle interfaces are fully hydrated, we expect a thicker lipid/water interface for vesicles. As

presented above, we find this to be the reason CLPE's fluorescence spectrum shifts further to the red in vesicles than in reverse micelles. Therefore, because vesicle interfaces are hydrated to a greater extent, we would expect greater water relaxation.

Surprisingly, the dynamics we observe at a vesicle interface were almost exactly the same as the dynamics we observed within cyclohexane/lecithin/water $w = 6.4$ reverse micelles (Table 5.2). Not only are the dynamics very similar, but $\Delta\nu_{max}$ is also almost exactly the same. Clearly, lecithin reverse micelles at elevated hydrations represent very good dynamical mimics of lecithin vesicle interfaces.

As we have discussed above, it seems certain based on the results of others that a vesicle interface perturbs a greater amount of water than what is contained in a $w = 6.4$ reverse micelle[16-18, 46, 49]. Vesicles produce a hydration layer that extends at least a nanometer into the bordering bulk solution[13]. Obviously, reverse micelles do not possess the capacity to produce a similar layer. Yet, the dynamics and the $\Delta\nu_{max}$ associated with the dynamics are the same with or without this extended hydration layer. This suggests that the structure and motion of the nearest neighbor solvent shell primarily determines the observed dynamics. If the dynamical solvation sphere of CLPE is limited to chemical moieties within ~1nm in diameter, the environment will appear the same whether within a reverse micelle or at a vesicle interface. Additionally, the lecithin interface may shield the hydration layers from perturbing forces and effectively reduce the solvation sphere of molecules such as CLPE. In other words, the hydration force between the headgroups and bordering bulk water may be so great that the electronic reconfiguration induced by CLPE may be a small perturbation on the system in comparison. This would explain why we observe a shift in CLPE's fluorescence yet no

change in dynamics when we compare lecithin reverse micelles with vesicles. More specifically we find that the polarity is a function of long range interfacial order and potential, while the dynamics are a function of a confined sphere.

5.IV.D. Solvation Dynamics at a Lecithin Vesicle Interface with 33 mol% Cholesterol

As discussed in the introduction, addition of cholesterol to lipids in the liquid-crystalline phase results in reduced permeability, an increase in molecular order, condensation of the lipid molecules, and a small increase in membrane thickness[29]. These effects are believed to arise from the rigidity of the cholesterol ring system causing gauche to trans isomerizations in surrounding lipid chains to become less probable. Many studies have found that the increased order of the lipid chains results in dehydration of the lipid bilayer[15, 20, 28]. However, these studies have probed the bilayer with the boundary defined as the hydrocarbon/water interface (see Figure 5.5).

Our interest lies in the effect of cholesterol on the headgroup domain that is much less clear than the effect cholesterol has on the membrane structure as a whole. Cholesterol as a predominately hydrophobic molecule that lies buried within the lipid bilayer (see Figure 5.5). It is interesting to note that cholesterol by itself has a low aqueous solubility, but it can be incorporated into phospholipid membranes in very high concentrations, that is 1:1 ratios in many model membranes[6]. Despite its nonpolar character, the hydroxyl group of cholesterol is able to form a hydrogen bond that keeps the molecule anchored to the headgroup region. A simulation by Robinson et al. found cholesterol to be relatively mobile in its headgroup associations with the hydroxyl

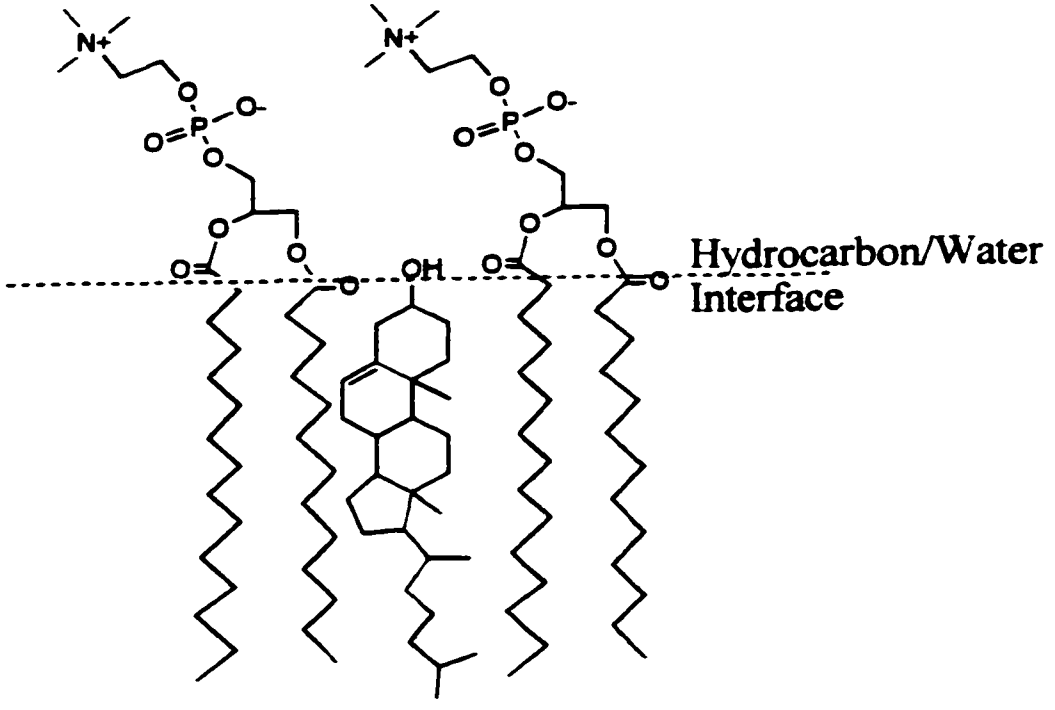

Figure 5.5. Structure and location of cholesterol in a phosphatidylcholine lipid bilayer.

residing in two primary positions: deep in the membrane adjacent to the lipid carbonyls or nearer to the surface and interacting with the headgroups or water molecules[29]. Vanderkooi revealed that the minimal energy structure involves a hydrogen bond between the cholesterol hydroxyl group and the PC carbonyl group[50]. These findings and others[11, 30, 31] suggest that cholesterol molecules prefer to have their hydoxyl oxygens near the hydrocarbon/water interface and therefore leave spatial gaps in the bilayer surface, as depicted in Figure 5.5.

The effect of the cholesterol positioning on the conformations and interactions of PC headgroups remains controversial. Two different simulations by Gabdoulline et al.[31] and Tu et al.[30] have presented very different pictures. Gabdoulline found the cholesterol spacing effect to cause greater headgroup freedom. Furthermore, they found an increased propensity for the headgroups to point down toward the bilayer, significantly reducing the electrostatic potential across the bilayer surface. They offered no experimental findings to support their results. The simulation by Tu et al. predicted very different headgroup behavior. They found the bilayer/water interface to be more abrupt in the presence of cholesterol with the phosphate-to-nitrogen section of the headgroup nearly lying flat along the interface. The flat orientation leads to a greater orientational polarization of the water molecules throughout the system. They find the addition of cholesterol increases the electrostatic potential across the bilayer surface. Tu et al. compare their results to X-ray diffraction measurements on egg PC/cholesterol monolayers that found the magnitude of the dipole potential increased from 415 mV in pure egg PC to 446 mV in 1:1 egg PC:cholesterol monolayers[51]. Tu et al. suggest the

differences between the two simulations might be an artifact of the excessively condensed bilayer produced by the simulation protocal employed by Gabdoulline et al.

Somewhat surprisingly, we find similar solvation dynamics with or without out cholesterol incorporation. As with lecithin vesicles, for vesicles with cholesterol we observe a fast 240 fs component attributed to free water, an intermediate 9 ps component attributed to bound and/or exchanging water, and a long 330 ps component attributed to a headgroup motion possibly coupled to strongly bound water. Observing the three components is not very surprising because cholesterol is not expected to alter headgroup interactions. In other words, because we expect cholesterol to be removed from the headgroup region, water will still be incorporated within the headgroup domain and the headgroups will still maintain similar interactions with the water and each other. Several studies have found that only the hydroxyl group of cholesterol has any significant interaction within the headgroup region and the hydrogen bonding interaction should be similar to the water/headgroup interactions already present[9, 14, 29]. However, because cholesterol is expected to alter the way headgroups conform within the region, we do expect time components and amplitudes to change to some degree.

While not very dramatic, we do observe a few noteworthy changes in the observed dynamics when cholesterol is incorporated (see Table 5.2). First, the long component corresponding to headgroup motion becomes longer suggesting a more constricted headgroup. Second, the free water component is somewhat larger in amplitude and faster relative to lecithin vesicles without cholesterol. The larger amplitude indicates a greater proportion of free water contributes to the solvation response. The larger free water response could be the result of the greater free space

provided by the presence of cholesterol, increased lipid undulations exposing CLPE to a greater extent than without cholesterol, or CLPE residing on average in a more exposed polar environment. We also find the free water relaxing with a faster time component indicating less structured water. However, we draw conclusions with caution. The fast dynamics we observe occur at the same time a large growth in intensity occurs (see Figure 5.2), which may be obscuring our certainty in this time component. Finally, we find the amplitude of the intermediate component decreases, but yet, the time component remains essentially unchanged. This most likely indicates the proportion of free water has increased, therefore, reducing the proportion of the bound or exchanging water component. More interestingly, because the time component remains constant, we find that either the properties of the bound water remain the same or, if this component represents an exchange process, the rate of exchange is not altered. Clearly, we need a simulation that specifically follows water motion and headgroup interactions to sort out the motions we are observing.

The most dramatic change we observe by adding cholesterol to lecithin vesicles is the large reduction in $\Delta\nu_{max}$ (see Table 5.2). This indicates the cholesterol interface is significantly more confined. However, at the same time, we observe very similar solvation dynamics. In other words, because cholesterol remains buried away from the headgroup domain and therefore does not alter dipole/dipole type interface interactions, we observe similar dynamics with or without cholesterol present. However, because the interface seems to constrict with the incorporation of cholesterol, the dynamics we observe do not proceed to the same degree as an interface without cholesterol.

Clearly, we find our measurements to correlate better with the simulation by Tu et al. A tightened, more abrupt, interface would certainly explain the reduced $\Delta\nu_{max}$. Moreover, it would also explain the decreased bandwidths within cholesterol vesicles we observe for CLPE's absorption and emission spectra. Also, observing the solvation dynamics long time component increasing upon cholesterol incorporation points to more order headgroups. We can also envision a tighter interface reducing the amount of strongly bound and bound water sites, thus increasing the relative proportion of free water relaxation. Tu et al. also found that the constricted interface leads to a greater headgroup potential. This increased potential could explain why the emission of CLPE red shifts slightly when cholesterol is incorporated into vesicles. It is possible the increased potential restricts CLPE to more polar configurations. As discussed in the previous section, the increased potential might lead to a reduced solvation response, thus contributing to the reduced $\Delta\nu_{max}$ but at the same time leaving the dynamics relatively unaltered.

If we take our results as experimental validation of the simulation by Tu et al., these results indicate that cholesterol facilitates decreased permeation of small ions and solutes across a lipid bilayer in two ways. First, as previous studies have shown, cholesterol constricts lipid chains, dehydrating the bilayer interior. In addition, our work and the simulation by Tu et al. suggest the constricted headgroup region also becomes a barrier because of the increased potential and also the decreased $\Delta\nu_{max}$ that indicates the headgroup region is less able to solvate a traversing solute.

5.V. Conclusions

In hindsight, we find several different procedures that could improve the present experiment. First, we have been concerned with the degradation of the vesicles with exposure to laser light. As mentioned in the experimental section, we observed a blue shifting of CLPE's emission spectrum and the growth of a short wavelength peak in the absorption spectrum with laser exposure. It is possible lecithin degradation could be occurring during the probe sonication procedure. New recommends that this procedure be carried out in a deoxygenated atmosphere[6]. Unfortunately, we did not have the facilities to accomplish this suggestion. At some point, we would like to duplicate these results and know that the vesicle sample was structurally intact throughout the measurements.

Future experiments could be done to help validate these findings. Unlike what we found with CLPE, other researchers have observed headgroup labeled probes to show reduced anisotropy and blue shifting in the emission spectrum when cholesterol is incorporated into the bilayer[38, 52]. Ideally, we would like to duplicate our solvation dynamics results using these molecules as our probes. Unfortunately, these probes absorb at wavelengths shorter than the doubled output of a Ti:sapphire laser. However, it might be possible to use a tripled output of a Ti:sapphire laser for excitation. The results could then be compared to the present results, possibly justifying the current conclusions.

We would also like to determine solvation dynamics at a vesicle interface as a function of vesicle diameter. Hof et al. has already performed these experiments and has observed faster dynamics in the less ordered smaller vesicles[32]. These experiments

used probes that reside deeper than the hydrocarbon/water interface. We would like to observe if vesicle curvature effects the headgroup dynamics. The vesicles prepared in the current experiment were relatively small vesicles measuring only about 58nm in diameter. At this diameter, the dynamics inside the vesicles are most likely different than outside. Therefore, measuring the dynamics for large vesicles, i.e. greater than 200nm in diameter, could provide interesting results. Unfortunately, larger vesicles increase laser scatter that can make measurement difficult. Preparation for the proposed experiments would entail developing methods for vesicle preparation that would balance scatter with lipid and probe concentration.

In summary, we have measured the solvation dynamics at lecithin vesicle interfaces. As expected, relative to bulk water, we find that the vesicle interface is less polar, has a smaller overall dynamic response, and shows longer multi-component relaxation. The dynamic response at the vesicle interface consists of three components: a fast subpicosecond component attributed to free water, an 11 ps component attributed to loosely bound water and/or water exchanging between free and bound states, and a 240 ps component attributed to headgroup motion possibly coupled to strongly bound water. Surprisingly, we find the solvation dynamics at a lecithin vesicle interface to be essentially the same as those seen within $w = 6.4$ cyclohexane reverse micelles. We conclude the solvation shell that responds to electronic excitation of our probe, CLPE, is relatively small. In addition, we propose that the solvation response around the probe is reduced because of the strong electrostatic potential that exists across the headgroup/water interface. Also, we have measured the dynamics at a lecithin vesicle interface with 33 mol% cholesterol incorporation. We find the dynamics to have similar

components as those seen for the lecithin interface. Differences between the two interfaces include a slower headgroup type motion and a faster and greater proportion of free water relaxation. Most dramatically, we find the overall dynamic response of the cholesterol interface to be greatly reduced. We conclude cholesterol incorporation results in a tighter interface as has been presented in a simulation by Tu et al.[30]

References for Chapter 5

1. Gennis, R.B., *Biomembranes: Molecular Structure and Function*. Springer Advanced Texts in Chemistry, ed. C.R. Cantor. 1989, New York: Springer-Verlag. 533.

2. Prestegard, J.H. and M.P. O'Brien, *Membrane and vesicle fusion*. Annu. Rev. Phys. Chem., 1987. **38**: p. 383-411.

3. Marrink, S.-J. and M. Berkowitz, *Water and Membranes*, in *Permeability and Stability of Lipid Bilayers*, E.A. Disalvo and S.A. Simon, Editors. 1995, CRC Press: Ann Arbor. p. 21-48.

4. Zwaal, R.F.A. and H.C. Hemker, Haemostasis, 1982. **11**: p. 12.

5. Jorgensen, K., J.H. Ipsen, and O.G. Mouritsen, *Lipid-Bilayer Heterogeneity*, in *Membranes and Cell Signaling*. 1997, JAI Press, Inc. p. 19-38.

6. New, R.R.C., ed. *Liposomes: A Practical Approach*. The Practical Approach Series, ed. D. Rickwood and B.D. Hames. 1990, IRL Press: New York. 301.

7. Watts, A. and L.C.M.v. Gorkom, *Surface Organization of Lipid Bilayers*, in *The Structure of Biological Membranes*, P.L. Yeagle, Editor. 1992, CRC Press: Ann Arbor. p. 307-36.

8. Pesenkiewicz-Gierula, M., *et al.*, *Hydrogen bonding of water to phospatidylcholine in the membrane as studied by a molecular dynamics simulation: location, geometry, and lipid-lipid bridging via hydrogen-bonded water*. J. Phys. Chem. A, 1997. **101**(20): p. 3677-91.

9. Shin, Y.-K., D.E. Budil, and J.H. Freed, *Thermodynamics and dynamics of phosphatidylcholine-cholesterol mixed model membranes in the liquid crystalline state: effects of water*. Biophys. J., 1993. **65**: p. 1283-94.

10. Tanaka, H. and J.H. Freed, *Electron spin resonance studies on ordering and rotational diffusion in oriented phosphatidylcholine multilayers: evidence for a new chain ordering transition*. J. Phys. Chem., 1984. **88**: p. 6633-44.

11. Tobias, D.J., K. Tu, and M.L. Klein, *Atomic-scale molecular dynamics simulations of lipid membranes*. Curr. Opin. Colloid Inter. Sci., 1997. **2**: p. 15-26.

12. Rand, R.P. and V.A. Parsegian, *The forces between interacting bilayer membranes and the hydration of phospholipid assemblies.*, in *The Structure of Biological Membranes*, P. Yeagle, Editor. 1992, CRC Press: Ann Arbor. p. 251-306.

13. Perera, L., U. Essmann, and M.L. Berkowitz, *Role of water in the hydration force acting between lipid bilayers.* Langmuir, 1996. **12**: p. 2625-9.

14. Faure, C., J.-F. Tranchant, and E.J. Dufourc, *Comparative effects of cholesterol and cholesterol sulfate on hydration and ordering of dimyristoylphosphatidylcholine membranes.* Biophys. J., 1996. **70**: p. 1380-90.

15. Marinov, R. and E.J. Dufourc, *Thermotropism and hydration properties of POPE and POPE-cholesterol systems as revealed by solid state 2-H and 31-P-NMR.* Eur. Biophys. J., 1996. **24**: p. 423-31.

16. Borle, F. and J. Seelig, *Deuterium T1 relaxation time studies of phosphatidylglycerol, phosphatidylethanolamine and phosphatidylcholine.* Biochim. Biophys. Acta, 1983. **735**: p. 131-6.

17. Arnold, K., L. Pratsch, and K. Gawrisch, *Effect of poly(ethylene glycol) on phospholipid hydration and plarity of the external phase.* Biochim. Biophys. Acta, 1983. **728**: p. 121-8.

18. Perera, L., U. Essmann, and M.L. Berkowitz, *The role of water in the hydration force-molecular dynamics simulations.* Progr. Colloid Polym. Sci., 1997. **103**: p. 107-15.

19. Datta, A., *et al.*, *Solvation dynamics of Coumarin 480 in vesicles.* J. Phys. Chem. B, 1998. **102**(31): p. 6114-7.

20. Bernsdorff, C., *et al.*, *Effect of hydrostatic pressure on water penetration and rotational dynamics in phospholipid-cholesterol bilayers.* Biophys. J., 1997. **72**: p. 1264-77.

21. Yeagle, P.L., ed. *The Biology of Cholesterol.* . 1988, CRC Press: Boca Raton.

22. Finegold, L., ed. *Cholesterol in Membrane Models.* . 1993, CRC Press: Ann Arbor.

23. Vist, M.R. and J.H. Davis, *Phase equilibria of cholesterol/dipalmitoyphosphidylcholine mixtures: 2H-NMR and differential scanning calorimetry.* Biochemistry, 1990. **29**: p. 451-64.

24. Finean, J.B., *Interaction between cholesterol and phospholipid in hydrated bilayers.* Chem. Phys. Lipids, 1990. **54**: p. 147-56.

25. McMullen, T.P.W. and R.N. McElhaney, *Physical studies of cholesterol-phospholipid interactions.* Curr. Opin. Colloid Inter. Sci., 1996. **1**: p. 83-90.

26. Reis, O., R. Winter, and T.W. Zerda, *The effect of high external pressure on DPPC-cholesterol multilamellar vesicles: a pressure-tuning Fourier transform infrared spectroscopy study.* Biochim. Biophys. Acta, 1996. **1279**: p. 5-16.

27. Bernsdorff, C., A. Wolf, and R. Winter, *The effect of temperature and pressure on structural and dynamic properties of phospholipid/sterol mixtures-a steady-state and time-resolved fluorescence anisotropy study.* Zeitschrift fur Physik. Chemie, Bd., 1996. **193**: p. S. 151-173.

28. Parasassi, T., *et al.*, *Cholesterol modifies water concentration and dynamics in phospholipid bilayers: a fluorescence study using laurdan probe.* Biophys. J., 1994. **66**: p. 763-8.

29. Robinson, A.J., *et al.*, *Behavior of cholesterol and its effect on head gropu and chain conformations in lipid bilayers: a molecular dynamics study.* Biophys. J., 1995. **68**: p. 164-70.

30. Tu, K., M.L. Klein, and D.J. Tobias, *Constant-pressure molecular dynamics investigation of cholesterol effects in a dipalmitoylphosphatidylcholine bilayer.* Biophys. J., 1998. **75**: p. 2147-56.

31. Gabdoulline, R.R., G. Vanderkooi, and C. Zheng, *Comparison of the structures of dimyristoylphosphatidylcholine in the presence and absence of cholesterol by molecular dynamics simulations.* J. Phys. Chem., 1996. **96**: p. 15942-6.

32. Hof, M. and R. Hutterer, *Solvent relaxation of fluorescent labels as a new tool for the detection of polarity and rigidity changes in membranes.* Czech. J. Phys., 1998. **48**(4): p. 435-41.

33. Mishell, B.B. and S.M. Shiigi, eds. *Selected Methods in Cellular Immunology*. . 1980, W. H. Freeman & Company: San Francisco.

34. Pant, D. and N.E. Levinger, *Polar solvation dynamics of H2O and D2O at the surface of zirconium nanoparticles.* J. Phys. Chem. B, 1999. **in press**.

35. Riter, R.E., D.M. Willard, and N.E. Levinger, *Water immobilization at surfactant interfaces in reverse micelles.* J. Chem. Phys. B, 1998. **102**(5): p. 2705-14.

36. Walter, W.V. and R.G. Hayes, *Nuclear magnetic resonance studies of the interaction of water with the polar region of phosphatidylcholine micelles in benzene.* Biochim. Biophys. Acta, 1971. **249**: p. 528-38.

37. Davenport, J.B. and L.R. Fisher, *Interaction of water with egg lecithin in benzene solution.* Chem. Phys. Lipids, 1975. **14**: p. 275-90.

38. Bernik, D.L. and R.M. Negri, *Local Polarity at the polar head level of lipid vesicles using dansyl fluorescent probes.* J. Colloid Inter. Sci., 1998. **203**: p. 97-105.

39. Rupley, J.A. and G. Careri, *Protein hydration and function.* Adv. Protein Chem., 1991. **41**: p. 37-172.

40. Pethig, R., *Protein-water interactions determined by dielectric methods.* Annu. Rev. Phys. Chem., 1992. **43**: p. 177-205.

41. Shinoda, W., M. Shimizu, and S. Okazaki, *Molecular dynamics study on electrostatic properties of a lipid bilayer: polarization, electrostatic potential, and the effects on structure and dynamics of water near the interface.* J. Phys. Chem. B, 1998. **102**: p. 6647-54.

42. Essmann, U. and M.L. Berkowitz, *Dynamical properties of phospholipid bilayers from computer simulation.* Biophys. J., 1999. **76**: p. 2081-9.

43. Shinoda, W., N. Namiki, and S. Okazaki, *Molecular dynamics study of a lipid bilayer: convergence, structure, and long-time dynamics.* J. Chem. Phys., 1997. **106**(13): p. 5731-43.

44. Pasenkiewicz-Gierula, M., *et al.*, *Charge pairing of headgroups in phosphatidylcholine membranes: a molecular dynamics simulation study.* Biophys. J., 1999. **76**: p. 1228-40.

45. Nandi, N. and B. Bagchi, *Dielectric relaxation of biological water.* J. Phys. Chem. B, 1997. **101**: p. 10954-61.

46. Alper, H.E., D. Bassolino-Klimas, and T.R. Stouch, *The limiting behavior of water hydrating a phospholipid monolayer: a computer simulation study.* J. Chem. Phys., 1993. **99**(7): p. 5547-59.

47. Grdadolnik, J., J. Kidric, and D. Hadzi, *Hydration of phosphatidylcholine reverse micelles and multilayers-an infrared spectroscopic study.* Chem. Phys. Lipids, 1991. **59**: p. 57-68.

48. Grdadolnik, J., J. Kidric, and D. Hadzi, *An FT-IR study of water hydrating dipalmitoylphosphatidylcholine multibilayers and reversed micelles.* J. Molec. Struc., 1994. **322**: p. 93-103.

49. Nagle, J.F. and M.C. Wiener, *Structure of fully hydrated bilayer dispersions.* Biochim. Biophys. Acta, 1988. **942**(1): p. 1-10.

50. Vanderkooi, G., *Computation of mixed phosphatidylcholine/cholesterol bilayer structures by energy minimization.* Biophys. J., 1994. **66**: p. 1457-68.

51. McIntosh, T.J., A.D. Magid, and S.A. Simon, *Cholesterol modifies the short-range repulsive interactions between phosphatidylcholine bilayers.* Biochemistry, 1989. **28**: p. 17-25.

52. Kimura, Y. and A. Ikegami, *Local dielectric properities around polar region of lipid bilayer membranes.* J. Membrane Biol., 1985. **85**: p. 225-31.

Chapter 6

Concluding Remarks

Our goal was to measure solvation dynamics near phospholipid interfaces. More specifically, we intended to determine to what degree dynamics are restricted relative to bulk water. In all samples examined, we found that motion was significantly reduced near a lipid interface relative to bulk water. Responses were reduced both from the presence of longer time components and from smaller overall solvent response indicated by smaller $\Delta\nu_{max}$ values. Biologists and biochemists tend to view lipid interfaces as barriers for migration of solutes. We find that the interface represents a unique environment with dynamical properties distinct from properties in bulk solution. Therefore, the interface is more than just a barrier, possibly facilitating chemistry in its unique dynamical environment that would otherwise be unable to proceed in bulk solution.

These experiments represent the first ultrafast detection of solvent motion near phospholipid interfaces and can therefore reveal the presence of free water type relaxation near a lipid interface for the first time. Our results indicate that, in general, free water type relaxation is not a major response at lipid interfaces. As we found in cyclohexane/lecithin/water reverse micelles, free water relaxation can be totally absent at low hydration levels. Only in spherical reverse micelles prepared in benzene and at

elevated hydration levels did we observe free water relaxation that was a source of over half of the overall solvent response. In general, we observed solvent responses that were dominated by relaxation greater than tens of picoseconds. While we expected a reduced presence of free water, these experiments were the first to determine the degree to which this occurred.

As expected, we found as the hydration of the interface increased, the faster relaxation components accounted for a greater proortion of the solvent response. In theory, the lipids act as a dynamical barrier that restricts motion. The headgroups contain highly polar moieties that tend to form strong associations with water molecules and surrounding headgroups. These associations should act to reduce motion of lipids and water together as a whole. However, water associations should become saturated after several water molecules per headgroup have associated. Therefore, additional water molecules residing near an interface should show reduced headgroup associations and faster relaxation.

Whether water molecules partition into distinct water types near an interface remains controversial. As we presented in Chapter 2, we found evidence that distinct water types do exist with each type displaying distinct relaxtional motion. These water types were labeled strongly bound, bound, and free water. We were able to observe the distinct water types because we were able to observe the dynamics as a function of reverse micelle hydration.

Surprisingly, we observe similar relaxation components for all the interface samples we examined. In general, we find a subpicosecond component referred to as free water relaxation, an approxiamately 10 ps component, and an approximately 250 ps

component. These components vary to some extent from interface to interface. However, the greatest variation arises from the relative amplitudes associated with each component. These results are surprising because they suggest that modes of solvent relaxation are relatively constant from interface to interface. We are tempted to conclude that the distinct water classes we observed within cyclohexane/lecithin/water reverse micelles are prevalent at all lecithin interfaces. Unfortunately, the spherical reverse micelles and the vesicle samples did not allow us to observe dynamics as a function of hydration. Because of this we are unable to conclude that the separate time components correspond to distinct classes as we did for the cyclohexane/lecithin/water reverse micelles. However, these results may be indicating distinct water types do exist near all lecithin interfaces. It would be interesting to find if other interfaces comprised of different lipids behave similarly.

Even though similar dynamical components appear for all interfaces studied, we found that dynamics are sensitive to lipid structure and organization. The most dramatic example is the comparison of spherical reverse micelles prepared in benzene with the worm-like reverse micelles prepared in cyclohexane. The interiors of the two reverse micelles should consist of the same chemical components, namely, lecithin and water. Possibly because of the same chemical components, we observe the same types of relaxation in each reverse micelle. However, the relative amplitudes of each component are dramatically different between the two reverse micelles. We argue that this indicates dependence on reverse micelle structure. Another example of lipid structure affecting dynamics would be the effect of cholesterol incorporation into lecithin vesicles. In this case, cholesterol again has little effect on the different components, however,

dramatically reduces the overall solvent response. Again we observe the same possible modes of relaxation, but, their overall presence is reduced.

As a final comment, comparison of the dynamics observed with cyclohexane/lecihtin/water reverse micelles with those observed at a lecithin vesicle interface suggest that the solvation dynamics we measure may be limited to only a few solvent shells. If this is true, this would imply that processes occurring at lipid interfaces are also only sensitive to solvent motion within the first few surrounding solvent shells. This could prove to be an important finding for accurate modeling of lipid interface processes.

We end with a few final thoughts as to how these results could be built upon in future research. First, because of the limitations of our experimental setup, the dynamics we measured were limited to window of time between approximately 100 fs to 500 ps. Dynamics certainly occur on shorter and longer timescales. Inertial solvent motions typically occur on the sub-hundred femtosecond timescale in bulk solvents. By shortening the pulse width of the laser system, these experiments could be extended to include these motions. Understanding lipid inertial motion could prove to be very interesting because others have shown inertial motion accounts for a significant proportion of a solvent's overall response. It is also possible to extend the experiments to longer timescales by using TCSPC to measure TRES. Experiments by others have measured nanosecond dynamics within lipid bilayers using fluorescent probes. In addition, it may be possible to measure microsecond dynamics using phosphorescent probes. Being able to directly compare the results of our experiments with the experiments by others would be advantagous.

Second, an interesting set of experiments would be to attempt phospholipids other than lecithin. Biological membranes are composed of a variety of different phospholipids. We have chosen lecithin primarily for convenience. However, a variety of lipids are readily available that may induce dynamics different than observed for lecithin. Additionally, new types of water with different modes of relaxation are possible. In contrast to the zwitterionic lecithin headgroup, phospholipids may be purchased that are anionic or cationic headgroup functionality.

Third, while we have interrogated reverse micelles and vesicles, a variety of other lipid structures are possible. For example, lipid hexagonal and cubic phases are possible structures that would be interesting to interrogate. Unlike reverse micelles and vesicles, these structures are anisotropic, showing long range order. In addition, many of these structures are temperature dependent. Following the dynamics as a function of temperature could reveal how these structures evolve from one structure to another as temperature is changed.

Finally, we would like to reproduce the results presented in this work with other probes. As we have presented earlier, solvation dynamics experiments should be independent of the probe molecule used. Reproduction with a different probe would validate these results. In addition, probes with different fuctionality could be designed to better interrogate specific interfacial regions. For example, a probe molecule with greater hydrophilicity than C343 would have a greater propensity to extend out into the aqueous phase, probing regions separated from the lipid interface. It may also be possible to synthesize spacer groups that extend the probe into the aqueous phase at incremental distances.

The ultimate goal is to better model living processes. Because the systems we have interrogated represent model systems, an enormous amount of research still remains if we are ever going to be able to fully understand much more complex biological systems. We hope that this research will spawn further research to meet this goal.